

Combined Structure and Ligand Guided Protocols to Target the Gain-of-function Mutation of Gárdos Channel in Red Cell Deformability



By

Maham Ahmad

(NUST00000317722-MSBI-Fall19)

(MS Bioinformatics)

Supervised by:

Dr. Ishrat Jabeen

**Research Center for Modeling and Simulation
National University of Sciences and Technology
Islamabad, Pakistan.**

September 2021

Combined Structure and Ligand Guided Protocols to Target the Gain-of- function Mutation of Gárdos Channel in Red Cell Deformability

A thesis submitted in partial fulfilment of the requirement for
the degree of Master's in Bioinformatics



By

Maham Ahmad

(NUST00000317722-MSBI-Fall19)

Supervised by:

Dr. Ishrat Jabeen

Research Center for Modeling and Simulation
National University of Sciences and Technology
Islamabad, Pakistan.

September 2021

Dedication

I dedicate this work to my family for their constant

Love and support

Certificate of Originality

I hereby certified that this thesis is based on my own research and struggle. Furthermore, none of its contents have been plagiarized or submitted for a higher degree. Other people's contributions to this project are acknowledged and referenced.

Maham Ahmad

(NUST00000317722-MSBI-Fall21)

Acknowledgment

First and foremost, I would like to thank Allah, the Almighty, who gave me the ability and thinking power to accomplish this research work.

My sincere appreciation is towards my supervisor Dr. Ishrat Jabeen, to whom I relied upon ultimate guidance. Her dedication and constructive comments on my work helped me to provide the best version of myself. I am grateful for the contribution of her time and efforts that helped in achieving this output. She has been and always be a Mentor to me. Moreover, I thank my guidance committee members: Dr. Mehak Rafiq and Dr. Zamir Hussain who have been a constant support. Their encouragement is all that was needed for the completion of this task. I would like to thank my faculty members, fellow friends, and the lab assistants at RCMS, NUST.

I like to acknowledge two of the Ph.D. Scholars; Humaira Ismatulah and Sadaf Ijaz that were always there by my side. I owe big thanks to my research group that includes Maharij Jadoon, Aqsa Khalid, Fatima Iqbal, Awais Attique, Maria Ehsan, Syeda Aniqah Bukhari, Aiman Rauf, Ammara Naz, Rija Hussain, Umair Khan, and Rabia Gulzar for their constant support and help in achieving the goal.

I like to acknowledge my dear friends at NUST namely Maheera Amjad, Huzaifa Arshad, Ramsha Khalid and Abbas Khan for motivating me throughout my research phase. I'd want to express my sincere thanks to my parents and family for their unwavering support and prayers, which were a source of relief and comfort during this difficult research period.

Table of Contents

List of Abbreviations	VI
List of Tables	VIII
List of Figures	X
Abstract	XII
Chapter 1	1
1.1. Symptoms associated with HX	2
1.2. Distribution of Gárdos Channel	2
1.3. Physiological Effects of Calcium-Activated Potassium Channel (KCa)	2
1.4. Regulatory Factors of KCa3.1 Channel	3
1.5. KCa3.1 Channels and Thrombotic Disease	3
1.6. Structure and membrane topology of KCNN4	4
1.7. Gating mechanism of KCNN4	4
1.8. Normal, hyperactivated, and diseases Gárdos channel	7
1.9. Application of KCa3.1 Channel in Treatment	8
1.10. Challenges	9
1.11. Problem statement	9
1.12. Proposed Strategy	9
1.13. Novelty of work	9
1.14. Objectives	10
Chapter 2	11
2.1. Channel activity	11
2.1.1. Monovalent cations	12
2.1.2. Divalent cations	13
2.2. Structural analysis of Gárdos Channel	14
2.2.1. The architecture of Ca ²⁺ activated K ⁺ channel (free from Ca ²⁺)	15
2.2.2. The Ca ²⁺ sensor – Dynamic N-lobe of CaM	17
2.2.3. Transmembrane domain and ion-conducting pore region	19
2.2.4. KCNN4 – in Ca ²⁺ bound state	20
2.2.5. Channel activation – structural basis	21
2.3. Relation between KCNN4 wild type and R352H mutant	21
2.4. Relation between KCNN4 wild type and V282E/V282M mutant	22
2.5. Inhibitors of Gárdos Channel	23
Chapter 3	26
3.1. Collection of Datasets	26

3.2. Homology Modelling	26
3.3. Molecular Dynamic Simulation	27
3.4. Molecular docking	28
3.5. Common scaffold clustering	29
3.6. Physiochemical parameters calculation	31
3.7. GRIND (GRID independent descriptors)	31
Chapter 4	33
4.1. Data collection and refinement	33
4.2. Homology modeling of the mutated KCNN4 protein	33
4.3. Molecular dynamic simulation of the mutant KCNN4 protein	37
4.4. Molecular Docking	41
4.5. Common Scaffold Clustering (CSC)	42
4.5.1. Clustering for class 1 ligands	49
4.5.2. Clustering for class 2 ligands	50
4.5.3. Clustering for class 3 ligands	51
4.5.4. Clustering for class 4 ligands	51
4.6. Protein-ligand interaction analysis	52
4.7. GRIND	58
Chapter 5	69
Conclusion	71
References	72
Appendix	88

List of Abbreviations

KCNN4, KCa3.1, IKCa	Gárdos Channel, Intermediate Conductance Calcium channel
HX	Hereditary Xerocytosis
MCHC	Mean Corpuscular Hemoglobin Concentration
R352H	p.Arg352His
V282M	p.Val282Met
V282E	p.Val282Glu
DRY	Hydrophobic
O	Hydrogen Acceptor
NI	Hydrogen Donor
TIP	Shape Based feature
VSMC	Vascular smooth muscle cells
REST factor	Repressor element-1 silencing transcription
AP-1	Activator protein-1
EF-hands	Helix-loop-helix
CAMBD	Calmodulin binding domain
CaM	Calmodulin binding domain
WT	Wild Type
NHE	Na ⁺ /H ⁺ exchanger
NKCC	Na-K-Cl cotransporter
PTH	Parathyroid hormone
PGE-2	Prostaglandin E2
Cryo-EM	Cryo-electron microscopy

PDB	Protein databank
MMFF94X	Merck Molecular Force Field
MOE	Molecular Operating Environment
CSC	Common scaffold clustering
QSAR	Quantitative Structural Activity Relationship
GRIND	GRID Independent Descriptors
CLACC	Consistently large and auto cross-correlation
GOLD	Genetic optimization and ligand binding
HBA	Hydrogen Bond Acceptor
HBD	Hydrogen Bond Donor
PLS	Partial least square analysis

List of Tables

Table 1: Inhibitors of KCNN4 with specific activity values	24
Table 2: Different inhibitors of KCNN4 along with biological activity values in isotonic and saline solution. The displacement of ¹²⁵ I -Charybdotoxin is also represented [114]	25
Table 3: x, y, and z coordinated selected for specifying the binding pocket in three different positions in the mutated KCNN4 protein for the docking of ligands via GOLD software.....	29
Table 4: the number of ligands having the common scaffold i.e. belonging to the same class.....	30
Table 5: the total number of ligands and the number of ligands (best poses) clusters out in the same binding region of the Gárdos channel.....	30
Table 6: The top 6 models selected from the homology model based on the ERRAT score and Ramachandran plot statistics. The Ramachandran scores before and after energy minimizations are also provided.	34
Table 7: Ramachandran plot statistics and ERRAT score for the model D, after Molecular dynamic simulation protocol.	40
Table 8: The number of poses reduced depending upon the number of ligands in each cluster. The top 10 poses of each ligand were taken.	42
Table 9: 2D structure of ligands dataset. The common scaffold of each class with their SMILE is represented. All the ligands are separated into different classes. ...	43
Table 10: The best clusters chosen from class 1, with the maximum number of ligands and the ligands not in those clusters. All the best poses chosen from the cluster were separated for further analysis.....	50
Table 11: The best clusters chosen from class 2, with the maximum number of ligands and the ligands not in those clusters. All the best poses chosen from the cluster were separated for further analysis.....	50
Table 12: The best clusters chosen from class 3, with the maximum number of ligands and the ligands not in those clusters. All the best poses chosen from the cluster were separated for further analysis.....	51
Table 13: The best clusters chosen from class 4, with the maximum number of ligands and the ligands not in those clusters. All the best poses chosen from the cluster were separated for further analysis.....	52

Table 14: 25 among 51 ligands that showed the residual value >1 and < -1 . Among the 25 ligands, 5 ligands had residual value > 1.5 or < -1.5	65
Table 15: Two of the least active compounds with their pIC_{50} and $\log P$ (o/w) and a residual difference between the actual and predicted $pIC_{50} < -1.5$	68
Table 16: Active compounds with their pIC_{50} and $\log P$ (o/w) and a residual difference between the actual and predicted $pIC_{50} > 1.5$	68

List of Figures

Figure 1: Structure and membrane topology of KCNN4.	5
Figure 2: The cyro-EM of KCNN4 showing the two hotspots of mutations..	6
Figure 3: Schematic representation of the proposed mechanism observed in normal, active, and mutated RBCs	8
Figure 4: Ion transport pathway of potassium distribution in the red cells.	12
Figure 5: KCNN4 crystal structure representing the 4 subunits	15
Figure 6: Cyro-EM structure of KCNN4.	16
Figure 7: The S1-S6 helices for a single subunit of the KCNN4 channel.	16
Figure 8: The HA and HB helices of KCNN4. the terminal end of the HB helix is attached to the HC helix..	17
Figure 9: Cyro-EM structure of KCNN4 representing the CaM N-lobe and CaM C-lobe.	18
Figure 10: 90° rotation of Cyro-EM structure of KCNN.	18
Figure 11: Pore region of the KCNN4 channel.	20
Figure 12: Workflow of homology modeling of the mutated KCNN4 channel using Modeller 9.12 server.	27
Figure 13: Workflow of Molecular dynamic simulation to get a stabilized mutated KCNN4 protein using Schrodinger server.	28
Figure 14: General workflow of molecular docking protocol to generate the docked poses for mutated KCNN4 protein against 51 ligands.	29
Figure 15: General workflow of GRIND to extract 3D features from the mutated KCNN4 using the 51 ligands with their activity values.	32
Figure 16: Ramachandran plot for selected model D (model 62) among the 100 models before energy minimization.	35
Figure 17: Ramachandran plot for selected model D (model 62) among the 100 models, after energy minimization	36
Figure 18: (A) Representation of two mutations R352H and V282M. (B) A closer look at the R352H mutation. (C) A closer look at the V282M mutation	37
Figure 19: Output obtained after the Molecular Dynamic Simulation of the modeled mutant KCNN4 structure.	38
Figure 20: Output obtained after the Molecular Dynamic Simulation of the modeled mutant KCNN4 structure.	39

Figure 21: The homology modeled and simulated structure of mutant KCNN4.	40
Figure 22: Ramachandran plot for the mutated KCNN4 model 62 after MD simulation	41
Figure 23: Different classes interaction with the mutant KCNN4 structure..	56
Figure 24: PLIF results showing the most common interaction found between the ligands of different classes and the mutant KCNN4 structure.	57
Figure 25: PLIF results showing the most common interaction found between the complete dataset and the mutant KCNN4 structure.	58
Figure 26: Correlogram of GRIND model for the KCNN4 inhibitors explaining the contribution of DRY-O, O-NI, O-TIP, and NI-TIP towards activity in a positive manner.	59
Figure 27: The virtual receptor site (hotspot) of KCNN4 against the Gárdos43 (the most active compound in the dataset).	60
Figure 28: The common scaffold for class 1.	61
Figure 29: The virtual receptor site (hotspot) of KCNN4 against the Gárdos43 (the most active compound in the dataset).	61
Figure 30: The virtual receptor site (hotspot) of KCNN4 against the Gárdos43 (the most active compound in the dataset).	62
Figure 31: The virtual receptor site (hotspot) of KCNN4 against the Gárdos43	64
Figure 32: Actual vs predicted pIC ₅₀ for the GRIND model.	66
Figure 33: the graph constructed between pIC ₅₀ of the ligands and the logP (o/w) to link activity with lipophilicity.	67

Abstract

Hereditary Xerocytosis (HX) is an autosomal dominant, hereditary hemolytic anemia characterized by red cells dehydration. In HX patients, the erythrocytes exhibit abnormal intracellular cation content and water loss. These factors cause an elevated erythrocyte mean hemoglobin concentration (MCHC) and decreased erythrocyte osmotic fragility. HX is linked with gain-of-function mutations of the Gárdos Channel (KCNN4 or KCa3.1). Gárdos channel is an intermediate conductance Ca^{2+} dependent K^+ channel. It is Ca^{2+} sensitive and present in several cell types, including erythrocytes. The Gárdos channel is inactive under steady-state conditions. Under the external stimulus, intracellular Ca^{2+} increases and binds with Calmodulin molecules that are firmly attached to each of the four-channel subunits of KCNN4. In HX patients, even a ten times lesser concentration of calcium activates the channel and leads towards pathogenicity. The abnormal functioning of the Gárdos channel is due to three different types of mutations i.e. R352H (p.Arg352His); located in the calmodulin-binding domain within the long COOH-terminal cytoplasmic tail, V282M (p.Val282Met), and V282E (p.Val282Glu) in the pore region of the transmembrane. Numerous drugs such as Senicapoc and TRAM-34 have been designed to block the activity of the Gárdos channel, but none of them are completely efficient against all three mutations. Therefore, in the present project, a combined structure and ligand-guided protocol was opted to explore the binding hypothesis of KNCC4 which could facilitate the design optimization of the KNCC4 modulators. The protocol consists of modeling of mutant KCNN4, molecular dynamic simulation of mutant KCNN4, molecular docking, common scaffold clustering and GRIND analysis for the prediction of 3D features of the inhibitors of Gárdos Channel. The modeling of mutant KCNN4 structure introduced loops in the start (residue 1- 10) and end (residue 386 – 427) of the structure that were not present in the wild KCNN4. Therefore, those loops were spliced out. The docking of mutant KCNN4 with 51 ligands generated different conformations that were clustered using Common Scaffold Clustering. The clusters showed mainly pi-Hydrogen and Hydrogen-acceptor interaction with the Lysine at 309 position of the mutant protein. Moreover, the GRIND analysis generated features that were consistent with the docking output and complementary with the residues in the binding pocket. The features that contributed positively towards the biological activity of KCNN4 were Hydrophobic

– Hydrogen bond acceptor feature at a distance 9.60 – 10.00, Hydrogen – bond acceptor and Hydrogen bond donor feature at a distance of 8.40 – 8.80, Hydrogen-bond acceptor and shape based feature at a distance of 10.40 – 10.80, and Hydrogen-bond donor and shape based feature at a distance of 10.40 – 10.80 in the virtual receptor site. These features were complementary with the Glutamine353, Methionine302, Lysine360, Glutamine306 and Arginine359 residues in the actual receptor site. The predicted 3D features of the Gárdos Channel can help predict new drug-like compounds with optimized molecular properties.

Chapter 1

Introduction

Hemolytic diseases are mostly linked with the change in morphological appearances of the red blood cells. Among these red blood cells, the stomatocytes are the type having an appearance like a slit with a central zone of pallor on the dried smears. In the diseases referred to as "hemolytic anemia", mostly this slit-like shape is distorted with abnormal membrane permeability to the monovalent cation such as Na^+ and K^+ . These cations are responsible for osmotic stability of the cell which is an important component of the pathophysiology [1, 2]. The abnormal membrane transport was also first recognized in the hereditary stomatocytosis disease of humans. Among this disease set, Hereditary Xerocytosis (HX) is the most common and crucial variant. The variant is dominantly inherited like all other hereditary stomatocytosis diseases. It is characterized by red cell dehydration [3]. In HX patients, the erythrocytes exhibit abnormal intracellular cation content and water loss. These factors cause an elevated erythrocyte mean hemoglobin concentration (MCHC) and decreased erythrocyte osmotic fragility [4].

HX is linked with the gain-of-function mutations in the FAM38A gene encoding the mechanosensitive channel of the red cell membrane i.e., PIEZO1 [5, 6]. The PIEZO1 mutations slow down the inactivation of the channel and introduce a significant latency for its activation [7]. Deleterious mutations of the Gárdos Channel (KCNN4 or KCa3.1) are also associated with the disease. KCNN4 is an intermediate conductance Ca^{2+} dependent K^+ channel. It is Ca^{2+} sensitive, initially described in pancreatic cells but present in several cell types, including erythrocytes [8]. The Gárdos channel comprises 4 identical subunits; each subunit is encoded by a single gene, KCNN4, and consists of 6 transmembrane domains and a pore region between the 5th and 6th domain of transmembrane [8]. The Gárdos channel is inactive under steady-state conditions. Its function is not known in normal, mature erythrocytes. Under the external stimulus, intracellular Ca^{2+} increases and binds with Calmodulin molecules that are firmly attached to each of the four-channel subunits of KCNN4. In HX patients, even a ten times lesser concentration of calcium activates the channel and leads towards pathogenicity [9].

1.1. Symptoms associated with HX

Different researchers recognized and experimented on approximately 30 families with HX [10-13]. Patients carrying the disease showed anemia, moderate jaundice, gallstones, and a slight tendency to develop thrombosis in later life – only if splenectomy has been performed [1]. The disease can be manifested with a moderate to deliberate fatigue level. It is also followed by variable splenomegaly, transient perinatal edema, hyperbilirubinemia, and a systemic iron overload which is disproportionate to the degree of hemolysis and the transient frequency. Association of splenectomy was depicted in the patient suffering from HX caused due to PIEZO1, but no such associations are reported for the patient with mutations of KCNN4. In HX patients, there is variability in the cellular and clinical phenotype within the individuals of the family as well as among families carrying a different form of mutations [14-17].

1.2. Distribution of Gárdos Channel

Smooth muscle cells, T lymphocytes, macrophages, and other cells linked with thrombotic disorders all express KCNN4. It is also found in hematopoietic system cells, as well as salt and fluid-transporting organs (including colon, lung, and salivary glands). Erythrocytes, platelets, lymphocytes, mast cells, monocytes/macrophages, epithelial tissues (gastrointestinal, lung, endocrine glands, exocrine glands), vascular endothelial cells, vascular smooth muscle cells (VSMC), and fibroblasts are all known to express the KCa3.1 channel [13].

1.3. Physiological Effects of Calcium-Activated Potassium Channel (KCa)

KCa is a non-voltage-dependent calcium channel that is extremely sensitive to cytoplasmic calcium concentration levels, such as those caused by growth factors. The combination of intracellular Ca^{2+} and calmodulin activates it [18]. Calmodulin is responsible for KCa's calcium sensitivity. KCa is involved in the regulation of cell membrane potential as well as gene expression. The KCa3.1 channel serves various physiological functions including its involvement in erythrocyte volume regulation. K^{+} outflow is accompanied by water loss once the channel is activated, causing erythrocyte dehydration and shriveling [19]. The Ca^{2+} inflow of the cell is controlled by the KCa channel, which also regulates the Ca^{2+} signal transduction mechanism. The Gárdos channel is implicated in endothelial smooth muscle cell hyperpolarization, inducing

smooth muscle relaxation by mediating voltage-gated Ca^{2+} channel closure [20]. The KCa channel is also known to regulate T-lymphocyte and smooth muscle cell proliferation. The channel is associated with a variety of vascular disorders, including pulmonary hypertension, systemic hypertension, diabetes, and atherosclerosis. The secretion mechanism of epithelial cells in the digestive system, lungs, and secretory gland is regulated by the KCa channel. Furthermore, studies have revealed that KCNN4 is involved in cell cycle regulation [21].

1.4. Regulatory Factors of KCa3.1 Channel

Growth factors including FGF and transforming growth factor β (TGF- β) influence the expression of the Gárdos channel. Growth factors, for example, can regulate calcium signaling and KCNN4 activity in smooth muscle cells via a protein kinase phosphatase signaling pathway, resulting in changes in smooth muscle cell characteristics [22]. The Ras/MEK/ERK and JAK/STAT signaling pathways also regulate KCa. Furthermore, an increase in intracellular H^+ concentration can lower KCa channel activity without changing its single-channel conductance or inward rectification properties. With a rise in intracellular calcium concentration, the inhibitory action of H^+ did not vanish [23]. The transcriptional level of the KCa3.1 channel is inhibited by the repressor element-1 silencing transcription factor (REST) [24], whereas it is enhanced by the transcription factors activator protein-1 (AP-1) and Ikaros-2.

1.5. KCa3.1 Channels and Thrombotic Disease

KCa3.1 modulates cell activation, migration, and adhesion by regulating Ca^{2+} influx and membrane potential levels, and hence has a role in the incidence and progression of thrombotic disorders. By impacting vascular smooth muscle cells, T lymphocytes, and macrophages, the KCa3.1 channel may play a role in thrombotic diseases. The KCa3.1 channel can be blocked to slow the progression of arterial plaque and lessen the severity of vascular restenosis, making it a promising target for thrombotic disease treatment.

The abnormal functioning of the Gárdos channel might be caused by three different types of mutations i.e., R352H (p.Arg352His); located in the calmodulin-binding domain within the long COOH-terminal cytoplasmic tail, V282M (p.Val282Met), and V282E (p.Val282Glu) in the pore region of the transmembrane [9,

25, 26]. Apart from the R352H mutation, the V282M and V282E mutations also prolong the activation state of the channel. Numerous drugs such as Senicapoc and TRAM-34 have been designed to block the activity of the Gárdos channel, but none of them are completely efficient against all three mutations.

1.6. Structure and membrane topology of KCNN4

Gárdos initially described the KCNN4 channel in 1958 by visualizing the efflux of K^+ and increased intracellular Ca^{2+} [27]. Four decades later, the tetrameric membrane structure of KCNN4 was predicted using cloning and functional expression strategies. The KCNN4 is a tetramer with each subunit consisting of six transmembrane segments from S1-S6 and a pore region i.e., pore motif between the S5 and S6 transmembrane domain [28] as represented in Fig 1. The Ca^{2+} sensitivity is associated with the calmodulin that is bound to a domain; the Calmodulin binding domain (CAMBD) at the intracellular C-terminus (membrane-proximal region) of the channel. It is a Ca^{2+} sensor of the cell.

The work by Rapetti-Mauss *et al*, stated that the use of 2-microelectrode experiments on *Xenopus oocytes* and patch-clamp experimentation on HEK293 demonstrate that the mutated Gárdos channel exhibit a higher calcium sensitivity than the wild channel. Chronic hemolysis was the first human defect that was found to be associated with the KCNN4 Channel [9].

1.7. Gating mechanism of KCNN4

The structure of the Gárdos channel, coupled with Ca^{2+} concentration, plays a major role in the gating mechanism and channel activation. The CAMBD initiates the gating mechanism. Calmodulin (CAM) consists of two globular lobes (N- and C-lobe), each containing two pairs of helix-loop-helix (EF-hand) motifs (Fig. 1). The EF-hands are the binding sites for Ca^{2+} . So, typically, there are four binding sites for intracellular Ca^{2+} . Numbering these binding sites from I to IV from N-terminus, the III binding sites require calcium binding at high affinity to initiated conformational changes in the structure leading to gate activation [29, 30]

The structural homology model of the channel revealed that CaM C-lobe binds in a calcium-independent manner to a region on the c-terminal tail of the channel called the CAMBD1 (Fig. 1), while the N-lobe binds in a calcium-dependent manner, to the CAMBD2A (Fig. 1) of one subunit and CAMBD2B (Fig. 1) of the distal subunit. This

interaction introduces rotational changes in CAM and ultimately the S6 transmembrane leading towards a change in pore structure and opening of the gate [31]. The mutagenesis data also revealed certain residues present in the pore and transmembrane region could activate and close the channel. Among them, the F248 residue of the pore region (Fig. 1) interacts with the W216 residue of the S5 transmembrane to stabilize the closed conformation of KCNN4 (Fig. 1). Similarly, F248 may interact with residue G274; located near the gating hinge on the S6 helix (Fig. 1), to stabilize the open state of KCNN4 [32, 33]. Thus, techniques can be employed to maintain the open and closed conformation of mutated KCNN4 based on F248 residue interactions F248 with G274 and W216, respectively.

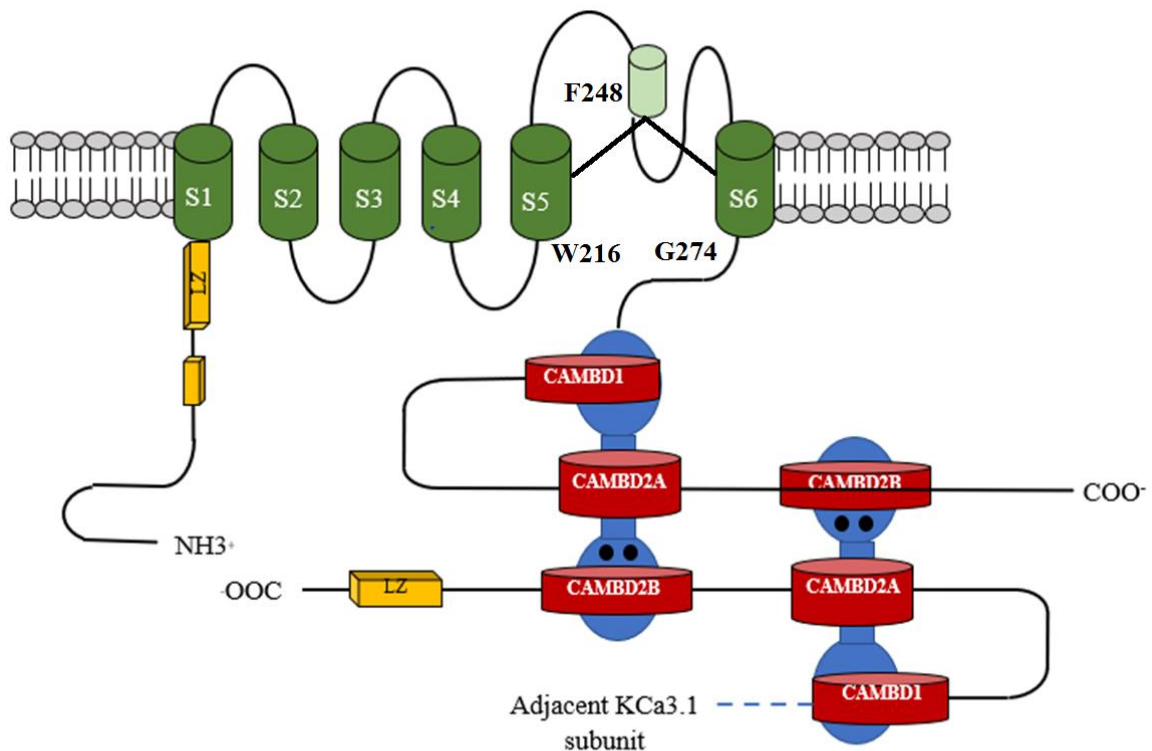


Figure 1: Structure and membrane topology of KCNN4. The protein consists of six transmembrane helices S1 - S6 with a pore region between S5 and S6. At the C-terminus of the S6 transmembrane domain, the Calmodulin Binding Domain is attached.

The different mutations of the Gárdos channel (Fig. 2), typically the R352H mutation likely removes a positive charge in the Calmodulin binding domain of KCNN4, and modifies interactions with the activating partner, causing a more active

channel. Experiments on HEK293 cell lines revealed an elevated current density of the mutated channel. These experiments demonstrated that p.Arg352His mutation is activated by a 10-fold lower Ca^{2+} concentration due to Ca^{2+} sensitivity, and thus conferring pathogenicity [35]. A study by Garneau *et al*, revealed the involvement of V282 in the gating process of KCNN4. It demonstrated that substitution of valine in the 282 positions by Glycine may be the reason for a more active Gárdos channel, conducting ions in the absence of Ca^{2+} . Thus, V282 plays an essential role in KCNN4 activity [32]. Also, the V282M mutant reveals a phenotype like the R352H which involves the constitutive KCNN4 channel activity at a resting calcium concentration of $0.2 \mu\text{M}$ [36]. Therefore, both mutants leak the potassium in resting conditions leading to cell dehydration. On the contrary, the potassium leak of the V282E mutant may be different as the channel activation is still calcium-sensitive as the one in the wild type (WT). Therefore, the cell dehydration would be consecutive to a high K^+ current only when the channel is active, however, the activation threshold will remain the same as WT [34].

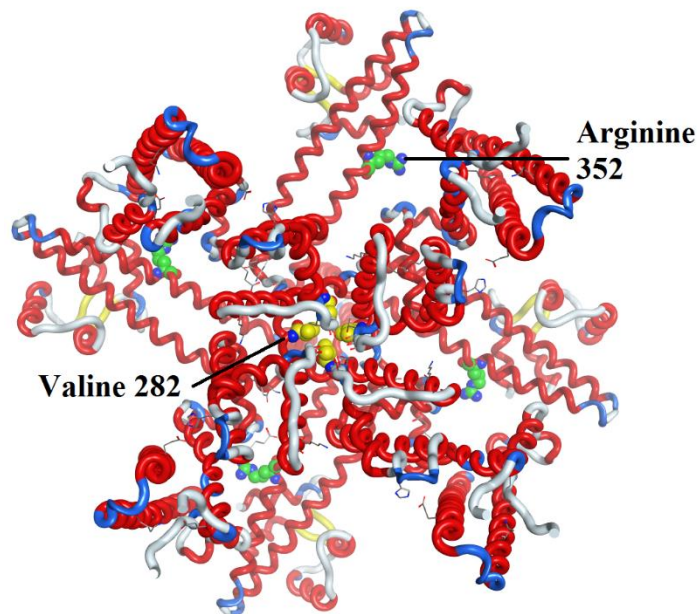


Figure 2: The cryo-EM of KCNN4 showing the two hotspots of mutations. First is the Valine on 282 position (yellow color) and the second is the Arginine at 352 position (green color).

1.8. Normal, hyperactivated, and diseases Gárdos channel

Under normal conditions, due to Ca^{2+} influx in the cell, the Gárdos channel activates and hyperpolarizes the membrane of red cells towards the K^+ equilibrium potential by the efflux of K^+ ions, thus amplifying the signal transduction (Fig. 3). Also, a more active Gárdos channel constantly leaks the K^+ ions and water, resulting in cell shrinkage as represented in Fig. 3. In the case of the mutated KCNN4, the K^+ leak is followed by cell shrinkage that leads to a K^+ influx through Na-K-Cl cotransporter (NKCC). The Na^+/H^+ exchanger (NHE) activity is enhanced which increases the NKCC-mediated Na^+ accumulation in the cell. Abnormal Na^+ concentration results in cell swelling, leading towards Na, K-ATPase activation, and energy consumption (decreased ATP and enhanced stimulation of glycolysis) [37, 38]. The research using flow cytometry and cell imaging technique revealed the Ca^{2+} overload in the cell, which might be due to the activation of the PIEZO1 channel (possibly activated due to cell swelling) or Ca^{2+} entry pathways [35]. This increased concentration further activates the KCNN4 and the cycle continues, leading towards a premature removal of RBS from the circulation (Fig. 3) [39]. In my opinion, controlling the Ca^{2+} concentration in the cell with mutated KCNN4 can help in reducing the cause.

During blood circulation, the red blood cells are in constant movement. This movement exerts mechanical stress on the membranes of RBCs. On-cell clamp experimentations help in understanding that local cell deformation can be a stimulating event leading towards the onset of the Gárdos channel. It suggested that the mechanosensory mechanism can help in the maintenance of erythrocyte volume and shape that would allow them to pass through the narrow capillaries of the microvasculature [40]. In the research done by Rapetti-Mauss *et al* [9] on *Xenopus oocytes*, the functional experiments showed that mutation associated with the residue 352 of the channel was normally triggered by the calcium influx, however, it permitted the increased efflux of potassium when compared to the WT channel. It also demonstrated that the channel was kept open for a prolonged period. It was hypothesized that the mutation that removed a positive charge from the Calmodulin Binding Domain may modify interaction with its activating partner that could result in a more active channel.\

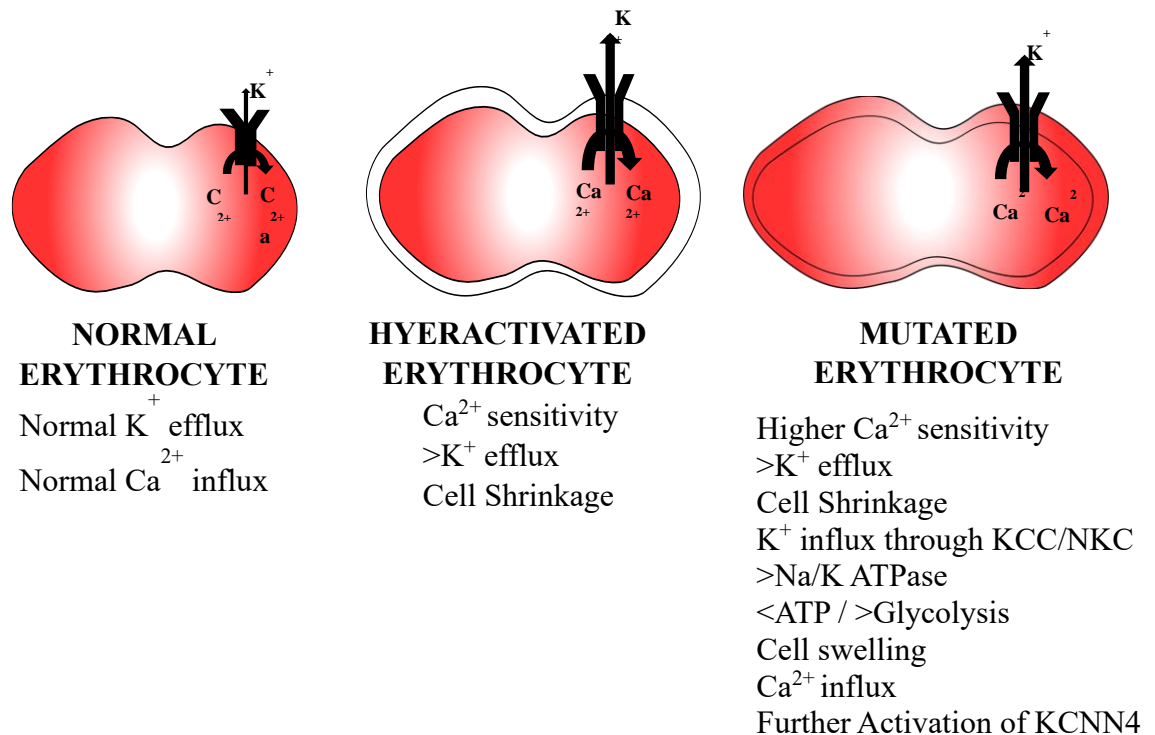


Figure 3: Schematic representation of the proposed mechanism observed in normal, active, and mutated RBCs represented as a, b and c respectively taken from [35]

1.9. Application of KCa3.1 Channel in Treatment

The Gárdos channel with the assistance of regulating cell membrane potential and calcium signal is involved in erythrocyte volume regulation, lymphocyte activation, macrophage migration, vascular smooth muscle cell and fibroblast proliferation, and other processes, leading towards a major role in the occurrence and development of various diseases. Blockage of the KCa3.1 channel leads towards the treatment of the disease. KCa3.1 channel blockers can prevent sickle cell dehydration [41]. Clotrimazole and its analogues TRAM34 and ICA-17043, which block KCa3.1, reduce cancer cell proliferation in vitro [42]. As a result, KCa3.1 channel blockers slow tumor development [43]. Drugs that block the KCa3.1 channel or gene knockouts of the KCa3.1 channel can alleviate renal fibrosis caused by bilateral ureteral obstruction [44]. KCa3.1 channel blockers could be utilized to treat chronic kidney disease caused by hypertension or diabetes [45]. TRAM-34, a KCa3.1 channel blocker developed by Wulff *et al.* [46] in 2000, has a substantial blocking effect and no clear adverse liver reaction. It's commonly employed in animal and cell research experiments. TRAM-34 has the benefit of being extremely selective. TRAM-34 does not alter the cell activity

of human T lymphocytes, VSMC, macrophages, or endothelial cells [47]. Its blocking effect on KCa3.1 channels is more than 1000 times that of other potassium, sodium, and calcium channels.

1.10. Challenges

Due to unavailability of X-ray crystal structure of the Gárdos channel till 2018, significant no computational analysis of structural features and predictive models were published. Additionally, no computational analysis on the mutations associated with the Gárdos channel was studied. Thus, in the present project, the mutant structure was modeled to probe the 3D structural features of the modulators of the mutant Gárdos channel.

1.11. Problem statement

Presence of certain hereditary mutations in the Gárdos channel, makes the channel less sensitive to Ca^{2+} therefore, these gain-of-function mutations in CAMBD of Gárdos channel, associated with Ca^{2+} influx, K^+ efflux, and dehydration can be controlled by either targeting the transmembrane domain and completely blocking the activation of the Gárdos channel, or modulating the mutant CAMBD and making it less sensitive to intracellular Ca^{2+} by various drug-like entities, thus maintaining a stable Ca^{2+} gradient inside and out of the cell. This could help avoid the premature death of red cells. Investigating the allosteric sites in the Calmodulin binding domain of mutated KCNN4 can also deliver requisite results.

1.12. Proposed Strategy

Modulation of the normal physiological function of KCNN4 by using combined ligand and structure-guided protocol could aid to probe the 3D structural features of the mutant KCNN4 that can help in the design/optimization of the new arsenal of the modulators of the KCNN4..

1.13. Novelty of work

The already designed modulators of KCNN4 are effective against one or two types of mutation. The drugs are not effective against all three types of mutations. Moreover, there is no *in-silico* analysis performed on the KCNN4 channel. The present research identifies certain structural 3D features of KCNN4 inhibitors that can open

new pathways for the computational analysis of the Gárdos channel and can help in strengthening the selectivity profile of the channel.

1.14. Objectives

Following are some objects of my research:

1. To evaluate the structural stability of mutant Calmodulin Binding domain of Gárdos channel as compared to wild type.
2. To probe the binding hypothesis of new therapeutic agents with the mutations at known binding sites of the Gárdos channels.
3. To predict 3D features against the inhibitors of mutant Gárdos channel by GRIND analysis.

Chapter 2

Literature review

Water and solute homeostasis are necessary for maintaining the integrity of the erythrocyte and is controlled via modulation of monovalent cation content. A variety of primary, inherited erythrocyte hydration disorders exist, that are characterized by abnormal permeability of sodium and potassium ions in the erythrocyte membrane, followed by the swelling or shrinkage of red cells [48]. They cause cell deformability, leading to premature cell death. Research present on the reduced erythrocyte deformability leads towards various diseases of hereditary hemolytic anemia such as sickle cell anemia, hereditary spherocytosis, hereditary elliptocytosis, hereditary xerocytosis, etc. [49]. The anemic group of channelopathies of this broader disease is referred to as HX. Among these, the Gárdos channelopathy; encoded by KCNN4, is of unique interest. Many recent studies presented its role in various physiological events, identifying it as an interesting therapeutic target in a wide range of human diseases [46, 49].

An erythrocyte's transmembrane ionic distribution with its environment is closely linked to its numerous functional features. Human erythrocytes' Na⁺/ K⁺-ATPase and Ca²⁺ -ATPase (Fig. 4) constitute the primary cation gradients across the membrane. The maintenance of these gradients, as well as their impact on cell physiology, has been intensively researched. In recent years, the Gárdos channel has gotten more attention. Medical, biological, and biophysical research has now reached a point where in-depth analysis and integration of these disparate discoveries is required for the channel's functionality.

2.1. Channel activity

Since the first reports of Ca²⁺-activated K⁺ permeability in erythrocytes [27], several "measures" have been proposed to describe K⁺ fluxes as being caused by the Gárdos channel. For example, the need for calcium at the intracellular face of the channel ((Ca²⁺)_i); a single-channel conductance of 20 pS (at 0 mV); high selectivity of K⁺ over Na⁺; evidence of open channel inward rectification; gating independence of membrane potential; inhibition either by specific drugs such as clotrimazole and charybdotoxin; or inhibition on pre-incubation of cells in the absence of external

potassium ($(K^+)o$). These identification criteria can and have been modulated through different physiological and experimental conditions.

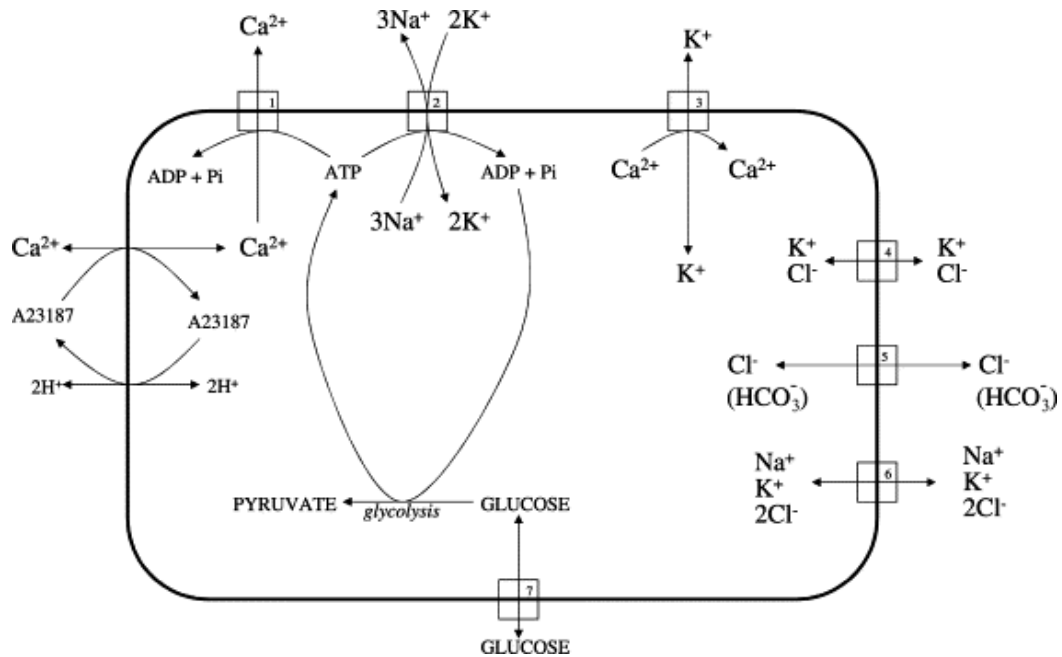


Figure 4: Ion transport pathway of potassium distribution in the red cells. The chemical potential set by the Na^+, K^+ - ATPase for the efflux of K^+ through Gárdos channel is powered by the ATP produced during glycolysis. Ca^{2+} gradient is also set up by the energy produced during the hydrolysis of ATP. Pathways in the figure are as [1] Ca^{2+} -ATPase; [2] Na^+, K^+ -ATPase; [3] Gárdos channel; [4] K^+/Cl^- co-transport; [5] Band 3 anion exchanger; [6] $Na^+/K^+/2Cl^-$ co-transporter; [7] glucose transporter.

2.1.1. Monovalent cations

Several studies have shown an inhibition of K^+ flux through $(Na^+)i$. The substitution of $(K^+)i$ for $(Na^+)i$ was shown by [50], which was more inhibited than if the replacement of the larger organic cation choline was used. This inhibition is highly dependent on voltage, with Na^+ implying to bind with several sites in the inner face of the channel [51]. The K^+ ion also interacts outside of the cells with the channel. The Ca^{2+} activated K^+ flux is not activated by the preincubation of erythrocytes in K^+ free medium [52, 53]. Closer examination indicates modulation of channel activity on both sides of the membrane by interactions between K^+ and H^+ . Heinz and Hoffman (1990) used a DIDS pH clamp to demonstrate that the decreasing pH of each side of the channel has an antagonistic effect of K^+ [52]. Despite contradictory data on the surface of the channels, several sites seem to be on the channel, whereby monovalent cations have a

secondary regulatory role [54]. This is not immediately justified, and it remains to be determined whether K^+ or any other ion contributes to the structural integrity of the various channel protein conformations.

2.1.2. Divalent cations

There has been extensive investigation into the role of Ca^{2+} in Gárdos as the primary regulator for channel activity. Because of the strong outward pumping activities of the Ca^{2+} -ATPase (transporter '1' in Fig. 4), the free $(Ca^{2+})_i$ is around 60 nM [55] in physiological conditions compared to the internal 'leakage' paths. The observation of the activity of Gárdos' channels in entire cells requires a disassociation from that of the ATPase of Ca^{2+} (as can be achieved by treatment with A23187).

For the Ca^{2+} channel activation, several authors have reported the IC_{50} values. Early studies in the equilibrium exchange conditions of red cell ghosts showed that Ca^{2+} had an IC_{50} of about 0.4 μM [50], the Ba^{2+} and Sr^{2+} showed a weak activation whereas the Mg^{2+} had an antagonist activity. Later work with the Ca^{2+} dye arsenazo III indicator revealed that the channel should be activated by 2–3 μM $(Ca^{2+})_i$ [56]. The patch clamping applied to red cell membranes indicates a similar level of activation of the efflux for the channel activity under equilibrium conditions [53] and a slightly higher (4.7 μM) value on physiological K^+ gradients [57]. In the latter report, Ca^{2+} depicted an increase in K^+_i permeability resulting in a prolonged channel opening frequency. It is estimated that the number of Ca^{2+} ions required for opening each channel is either 1 [58] or 2 [57].

In other studies, the lead compound showed an analogous role in the activation of K^+ influx in the erythrocytes [59-61]. Pb^{2+} allegedly enters the cells by anion exchange protein (AE1) (maybe as $PbCO_3$) and binds once inside to intracellular components like thiol groups, which therefore limits the capacity of the cell to extrude it using the pump Ca^{2+} [62-64]. There is still evidence of several coordination factors affecting the action of Ca^{2+} on the channel. Pellegrino and Pellegrini (1998) used patch-clamp experiments to indicate that an endogenous protein kinase (PKA) modulates Ca^{2+} channel sensitivity in human erythrocytes in a phosphorylation-promoting mixture of CaMP, MgATP, and theophylline [65]. A study of the erythrocyte chloride efflux also shows that intra-cellular regulatory mechanisms can affect the activity of the channel [66]. Using the chloride-fluorescent probe 6-methoxy-N-(3-sulfo-propyl) quinolinium

(SPQ) a significant decline in cellular chloride levels in the presence of the parathyroid hormone (PTH) was observed. PTH is believed to stimulate a substantial influx of calcium in red blood cells and its effects require the activation of PKA. Chloride efflux is very likely to be a passive consequence of K^+ efflux through the Gárdos channel under such conditions. The Gárdos channel has also been shown to be activated by prostaglandin E2 (PGE2), a hormone released by activated platelets [67]; the mechanism involves the activation of a Ca^{2+} influx pathway in the red cells.

This prostaglandin activity has an unclear physiological significance. The erythrocyte membrane does not stand large hydrostatic pressure gradients and as such, the activation of the Gárdos channel is synonymous with a decrease in cell volume. Li, Jungmann, Kiyatkin, and Low (1996) [67] postulate that the reduction of cell deformability in the site of activated platelets such as in clot formation promotes immobilization of erythrocytes. The time frame for sufficient change in cell morphology is one limitation of this proposal.

2.2. Structural analysis of Gárdos Channel

In 2018, work done by Chia-Hsueh Lee and Roderick MacKinnon helped in the demonstration of cryo-electron microscopy (cryo-EM) structures of a human SK4-CaM channel complex (KCNN4) in a closed and open state at a resolution of 3.4 – 3.5 Angstrom. In KCNN4, four Calmodulin (CaM) molecules were attached. (Fig. 5) The CaM had two distinct lobes. Each lobe of the CaM was associated with a distinct function. The C-lobe of CaM binds to the channel, whereas the N lobe was involved in the interaction between the S4-S5 linker in a calcium-dependent manner (Fig. 8). The S4-S5 linker is composed of two distinct helices. When the CaM molecule binds, these helices undergo conformational changes, leading towards an open state of the channel. The structure of KCNN4 published in 2018, revealed the basis for understanding the pharmacology of the KCNN4 channel [68].

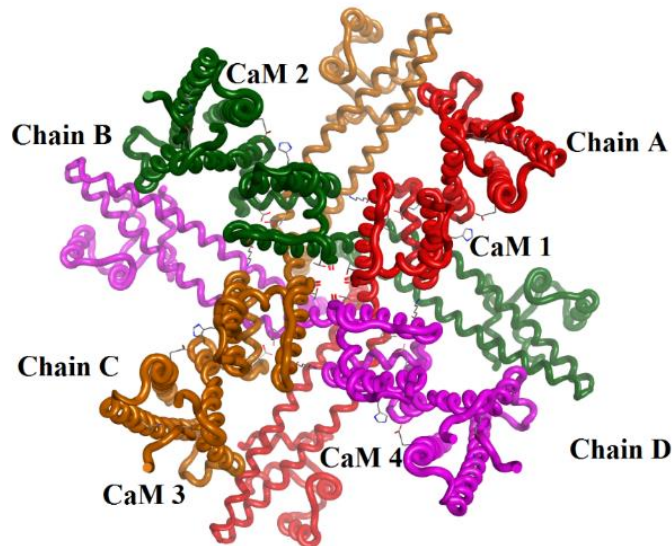


Figure 5: KCNN4 crystal structure representing the 4 subunits; 4 chains and 4 CaM domains. each chain is represented in a different color.

2.2.1. The architecture of Ca^{2+} activated K^+ channel (free from Ca^{2+})

In 2018, the research done by Chia-Hsueh Lee and Roderick MacKinnon determined the structure of Ca^{2+} activated K^+ channels in the absence of Ca^{2+} . The structure was determined using Cryo Electron microscopy at a resolution of 3.4 Å. The structure presented a four-fold symmetrical tetramer having a length of ~95 Å and an overall width of 120 Å when the protein was viewed from the plane of the membrane (Fig. 6). The pore of protein was formed with the transmembrane helices s5 and s6 whereas the surrounding region is embedded by the s1 – s4 transmembrane helices. The domain of s1 – s4 interacts with the pore domain of the same subunit (Fig. 7). The unwinding of the C-terminus of the S6 helices takes place at the inner leaflet of the membrane, allows the polypeptide chain to take a sharp turn. It is then followed by two other helices named HA and HB. These two helices are parallel to the membrane. At the terminal end of the HB helix, there is another helix named HC (Fig. 8) [68]. All the HC helices of the 4 subunits assemble in a coiled-coil confirmation to allow the trafficking and assembly of the channel [69, 70]. This coiled-coil conformation of the structure is the most flexible one and comprises 41 residues. In the research done by [71, 72], the researchers Chia-Hsueh Lee and Roderick MacKinnon too, in their study found that the peripheral ends of HA and HB helices form a binding site for the C-lobe of Calmodulin (CaM) molecules. The research by Halling *et al*, [73] suggested that approximately 2 – 8 calmodulin molecules may bind to one Gárdos channel. However,

the cryo-EM structure presented one CaM attached with each subunit, making a total of 4 CaM attachments to the whole subunit.

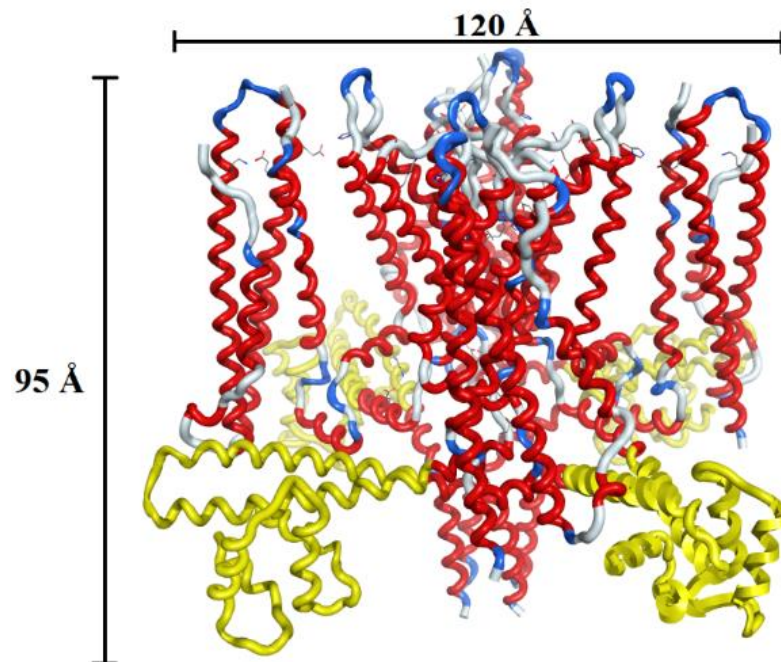


Figure 6: Cryo-EM structure of KCNN4. The CaM C and N-lobe for all 4 subunits are represented in yellow

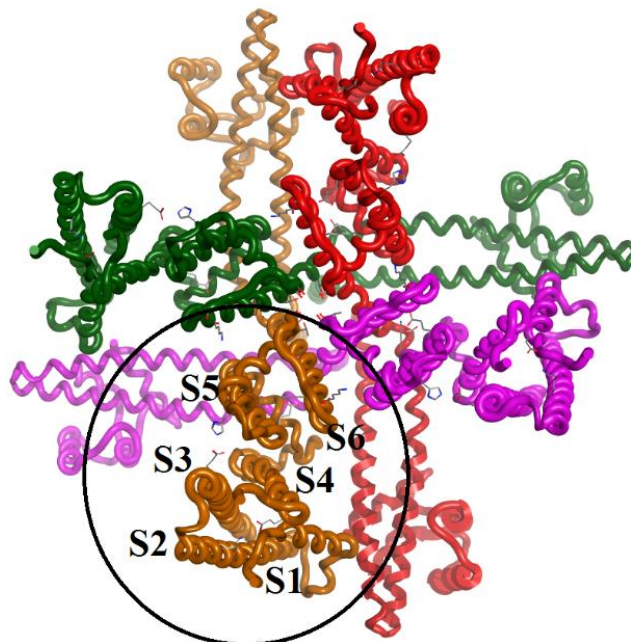


Figure 7: The S1-S6 helices for a single subunit of the KCNN4 channel. All the subunits are represented in different colors.

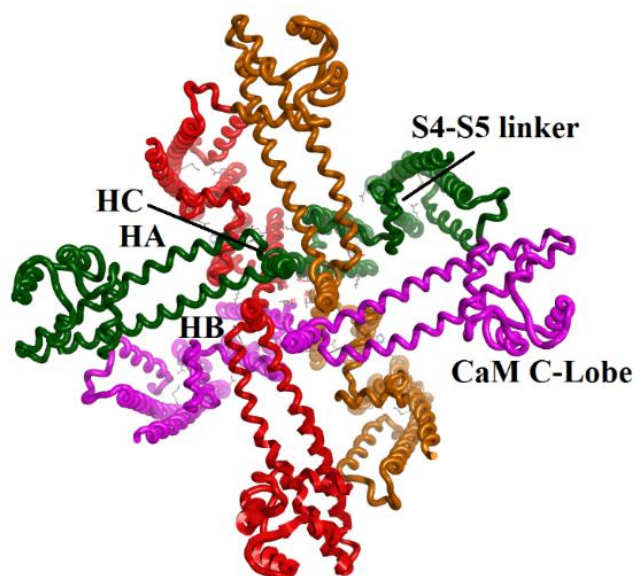


Figure 8: The HA and HB helices of KCNN4. the terminal end of the HB helix is attached to the HC helix. The S4-S5 linker is also represented.

2.2.2. The Ca^{2+} sensor – Dynamic N-lobe of CaM

The N-lobe of the CaM molecule exhibits a static disorder. It shows a high rate of mobility in the absence of Ca^{2+} ions. The CaM N-lobe density was improved by the researchers by performing various classifications and refinements resulting in 3 distinct conformations that best explained the structure with a low N-lobe density of the CaM. In all the three conformations, the C-lobe of the CaM molecule remains intact, whereas the N-lobe represented positional variance. The CaM could move from the peripheral region (Fig. 9 - 10, red) of the protein to the center of the Gárdos channel that consisted of coiled coils (Fig. 9 - 10, blue). Both the ends of CaM i.e., the N and C-lobes are connected by a linker. This linker can adopt alpha-helical or loop conformation, thus leading towards multiple conformations of the CaM molecule itself [74]. In the absence of Ca^{2+} , the -lobe of CaM undergoes large movements from the bottom S2 helix towards the bottom of the S4-S5 linker (Fig. 5), alternatively, the C-lobe keeps its interactions with the HA and HB helices.

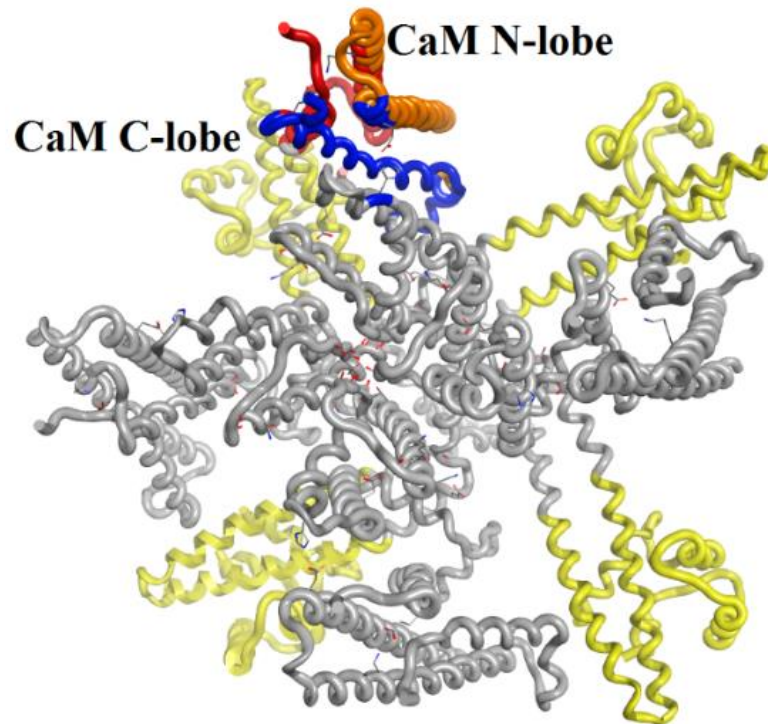


Figure 9: Cryo-EM structure of KCNN4 representing the CaM N-lobe and CaM C-lobe.

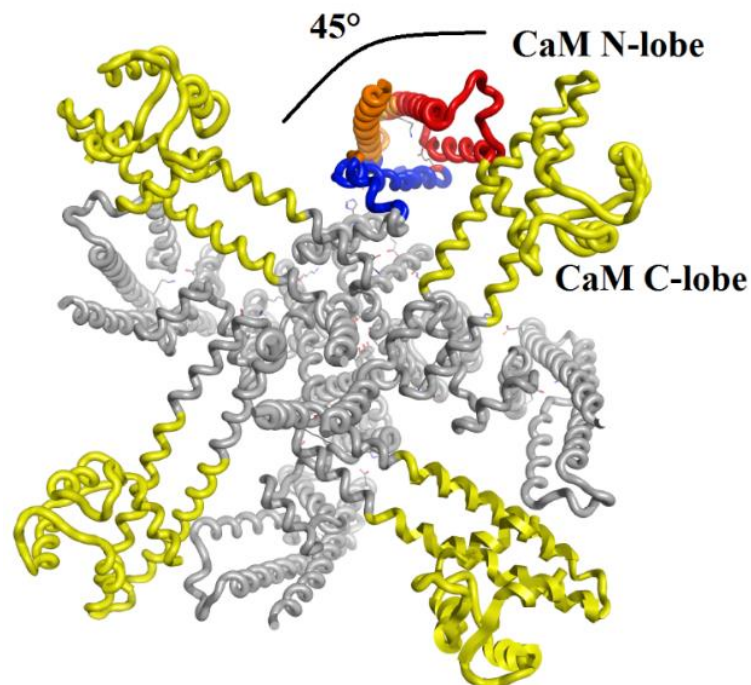


Figure 10: 90° rotation of Cryo-EM structure of KCNN. Different densities of CaM N-lobe are represented in (blue, orange, red) from 3 different classes after focused classification.

Several mutagenesis research depicted two different functions of C and N-lobe of CaM [75, 76]. The function of the C-lobe was to interact with the KCNN4 channel in the presence of calcium whereas the N-lobe was associated with the sensing of Calcium and the opening of the channel gates. The research of Chia-Hsueh Lee and Roderick MacKinnon about the 3D structure of the Gárdos channel supported these mutagenesis studies by showing the permanent bond C-lobe and dynamic N-lobe of CaM

2.2.3. Transmembrane domain and ion-conducting pore region

The S1 and S2 helices in the Gárdos Channel are relatively longer than the other channels [77]. Each of the helices is about 60 Å in length. The S1 and S2 helices of the Gárdos channel extend towards the cytoplasm, crossing the membrane boundary. Moreover, the S4-S5 linker of KNN4 consists of two alpha-helices named S45A and S45B [77-81]. In other channels such as voltage-gated channels, the S4-S5 linker is associated with the channel gating mechanism, but the KCNN4 is voltage-independent [77-81], thus the S4-S5 linker might confer the sensitivity of calcium to the CaM for gate opening. The S45B alpha helix is embedded between the HA and S6, causing lateral contacts with the pore region of the structure and the structural elements of the cytoplasm (they attach CaM to the channel). The different subunits of the structure are bound together with different interactions.

The hydrogen bonds are formed between the Lys197 on the S25B of one subunit and Glu295 on the HA on another subunit, followed by the bonds between Asn201 of S45B of one subunit and Arg287 on the S6 of the other subunit. These bonds help in attaching different subunits. Having a mutation at the Arg287 position might change the open probability of the channel in the absence of Ca^{2+} [82]. The inter-connectivity of different subunits by the interactions among the S4S5 linker with S6 transmembrane can be considered a foundation for high Ca^{2+} activation in the Gárdos channel [18, 83-86]. The Gárdos channel remains closed in the absence of Ca^{2+} . A constricted gate of radius less than 1 Å is formed by the Valine 282 in the S6 transmembrane of all 4 subunits (Fig. 11). The research conducted by Chia-Hsueh Lee and Roderick MacKinnon also validates these findings [33, 87-89]. Mutagenesis data also showed that the replacement of Val 282 by Gly produces a leaky channel in the absence of Ca^{2+} , causing current conductance [90]. The Val282→Glu and Val282→Met (14, 15, 46, 47)

mutations of the Gárdos channel involve those residues that are constricted in a narrow region in the pore of the structure.

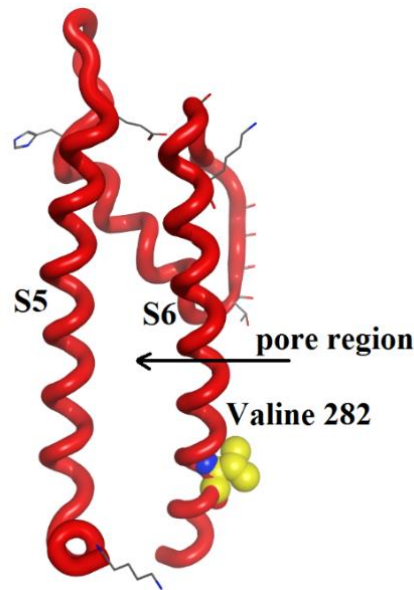


Figure 11: Pore region of the KCNN4 channel between the S5 and S6 transmembrane domain from where the efflux of K^+ and influx of Ca^{2+} occur.

2.2.4. KCNN4 – in Ca^{2+} bound state

The structure of KCNN4 in the presence of Ca^{2+} was published in 2018 by the research done by Chia-Hsueh Lee and Roderick MacKinnon. The structure was used the Cryo Electron microscopy at a resolution of 3.5 Å. In the presence of Ca^{2+} too, the four CaM molecules bind to the channel tetramer. (Fig. 5). In the presence of Ca^{2+} , the density of the N-lobe is improved as compared to the density in the absence of Ca^{2+} . The N-lobe of CaM firmly attaches to the channel in this state. The S1 and S2, having large lengths, interacts with the CaM molecule. This interaction alone is a justification for the large length of the S1 and S2 chains. In the presence of Ca^{2+} , the N-lobe of CaM interacts with HA and HC helices of the adjacent subunit of the Gárdos channel. The new interactions result in each CaM subunit interacting with all the three subunits. Moreover, in the Cryo-EM structure of the Gárdos channel, the S45A linker is recognized by the binding pocket of the CaM N-lobe making it a functional binding site for the CaM N-lobe.

2.2.5. Channel activation – structural basis

The S45A is not a canonical CaM binding motif [91]. However, the region is highly conserved. All the residues in S45A that face the N-lobe of CaM molecules i.e., Alanine, Serine, and Leucine are consistent against all the Ca²⁺ activated K⁺ channel family. It indicates the region is crucial in channel function. Upon binding of the N-lobe of CaM molecule, the S45A linked with it is displaced by 4 Å in the downward direction. This leads towards the movement of S4B4 in the outward direction, expanding the S6 helical bundle to the radius of 5 Å. It is followed by the expansion of the channel gate that is formed by the Valine at 282 position of pore region. However, the Valine still constricts the pore region at ~1.6 Å, not allowing the K⁺ ions to pass through them. The pore remains non-conductive while the channel tends to open at this point. Numerous studies validate that the maximum probability of the Gárdos channel to remain open is low i.e., between 0.1 to 0.3 at an extensive Ca²⁺ concentration. The researchers in 2018, identified another active state which is determined by the structure at a resolution of (4.7 Å). In active state II, a better rearrangement of the S45A, S45B, and S6 helices occurs. In this state, an additional displacement of 2 Å occurs with the S45A and S45B helices, dragging the S6 helix further away from the pore region. At this point, the channel gate at the Val 282 position opens to a remarkable radius of ~3.5 Å, allowing the flow of K⁺ ions. The binding of the CaM N-lobe with the S45A thus initiates the activation mechanism of the channel.

2.3. Relation between KCNN4 wild type and R352H mutant

Experimentation and studies of some researchers helped in elucidating the crucial role of R352 in channel activation through Calmodulin interaction. Firstly, the research by Schumacher *et al*, demonstrating the crystal structure of Calmodulin bound to the calmodulin-binding domain in KCNN2 (another calcium-dependent potassium channel), the residue Arginine at the 464 position in the calmodulin-binding domain was found to interact with glutamine at position 84, present in the C-lobe of calmodulin aiding in the calcium-independent interaction between the calmodulin molecule and the CaMBD [92]. Coinciding with this research, the Arg464 residue may correspond to the Arg352 in KCNN4.

Secondly, the research by Morales *et al*, presented a significant contribution in the gating mechanism of KCNN4 through the KCNN4-calmodulin interaction process. The research stated that during the gating process, the electrostatic interaction occurs

between the Arg352 of one monomer of KCNN4 and the Glu363 of the adjacent monomer of KCNN4. This interaction then contributes to the open probability of the Gárdos channel [93]. In the same model, it was also observed that substitution of Arg352 by Cysteine resulted in an increased deactivation time for the Gárdos channel. Thus, it may be possible that the substitution of mutant residue Histidine in place of Arg352 may change electrostatic interactions with Glu363, leading towards a change in kinetic properties of KCNN4 and thus a prolonged activation of Gárdos channel for p.Arg352His mutant.

2.4. Relation between KCNN4 wild type and V282E/V282M mutant

The HX mutations in the PIEZO1 and KCNN4 channels are referred to as the gain-of-function mutations as they are associated with a new molecular function and a new pattern of gene expression [94-99]. In the HEK-293 cells, the PIEZO1 mutant polypeptides showed delayed inactivation kinetics that was proposed to increase the entry and elevation of calcium [98, 100] causing a hyperactivated erythroid KCNN4. In the similar cell lines as well as the patient red cells, the KCNN4 mutants' polypeptides showed an increased current magnitude during the presence of intracellular Calcium ions [101, 102]. In the research done by [103-105], the V282M mutations were shown to exhibit hemolytic anemia with an occasional stomatocytosis. They also showed elevated resistance to the osmotic lysis, increase in the cell density higher sodium content, and reduced potassium levels, accompanied by a dramatically left-shift ektacytometry curve with lower D_{max} and O_{hyp} values, representing a decreased shear-stress deformability and severe cell dehydration. The V282M mutations also depicted an elevated baseline NP_o that was sensitive to the Senicapoc inhibitor. It had an increased senicapoc-sensitive baseline influx of $^{86}Rb^+$, and elevated net potassium efflux [101, 106].

The residue V282 in the KCNN4 channel is of unique interest. The residue has an isopropyl chain and each isopropyl chain in V282 of all subunits if KCNN4 forms a narrow construction of Gárdos inner pore [107]. In the V282E mutant, the senicapoc sensitivity is relatively less as compared to the V282M mutant [36]. The retention of sensitivity of senicapoc inhibition in KCNN4 mutant polypeptides can suggest senicapoc as an effective treatment for the gain-of-function phenotype linked with the KCNN4 mutants [78, 101].

2.5. Inhibitors of Gárdos Channel

Successful inhibitors of the Gárdos channel are designed that include Senicapoc and TRAM-34. Senicapoc shows a varying efficiency in blocking the KCNN4 mutants. It blocks the R352H and V282M with high activity i.e., IC_{50} of 0.3nM and 10nM, respectively. Whereas the modulator is less sensitive to V282E. it may be due to the presence of a long side chain in the region of V282E mutation [93]. The KCa3.1 channel is distinguished by its sensitivity to a scorpion toxin named charybdotoxin (ChTX). But the inhibitor also blocks other calcium-activated potassium channels such as KCa1.3 and KCa1.1. Therefore, it is problematic to use this blocker to any cell type that expresses the other two channels. Maurotoxin (MTX, IC_{50} 1 nM); another scorpion toxin, also blocks the KCNN4 channel. However, it shows higher affinity (IC_{50} 100 pM) for the Voltage-dependent calcium channel named Kv1.2 [108]. Effective experimentation was done by the group of George Chandy lead to the production of ChTX analog ChTX-Glu32. This blocker consists of negatively charged Glu32. The Glu-32 residue in the inhibitor is repelled by the negatively charged residues present in the outer vestibule of Kv1.3. This helps in providing a 30-fold greater selectivity on Kca3.1 over the Kv1.3 channel [109]. Apart from the peptide toxins, the KCNN4 channel is blocked by several old drugs. These include Antimalarial quinine, vasodilator cetiedil, L-type Ca channel blockers nifedipine, nitrendipine, and antimycotic clotrimazole [110]. The long-term usage of clotrimazole is not suitable due to its acute inhibition and chronic induction of human cytochrome P450-dependent enzymes [111, 112].

This leads to changes in cortisol level and liver damage of an organism. Therefore, a new inhibitor was constructed, using the clotrimazole as a template. A triarylmethane based KCNN4 blocker was designed. The blocker was free from cytochrome P450 inhibition and thus posed no threat to long-term usage. Wulff *et al.* identified TRAM-34. The compound has an inhibitory effect on KCNN4 with an IC_{50} value of 20nM. The research replaced the imidazole ring in clotrimazole systematically with a heteroaromatic ring system or other functional groups to design TRAM-34. The inhibitor, thus, does not affect the P450 enzyme CYP3A4. It has 200-500-fold selectivity over the Kv ion channels and 1000-fold selectivity over the KCa2.1 and KCa1.1 channel (Wulff *et al.*, 2000) In a self-directed mutagenesis study, it was revealed that both clotrimazole and TRAM-34 interact with the Val275 in S6 and

Thr250 in the pore loop and form an inner pore blocker for KCNN4 [113]. Other triarylmethane-like blockers of KCNN4 include 11-phenyl-diazepines and diphenylindanones [114]. Also, a distant class of KCNN4 blocker includes the Aromatically substituted sulfonamides such as (N-(4-methyl-2-oxazol-2yl-phenyl)-3-trifluoromethyl-benzenesulfonamide). The blocker inhibits the 86Rb flux through KCNN4 in the human red cells with an IC_{50} value $< 500nM$ (Wulff & Castle, 2010). Table 1 below represents different inhibitors with their IC_{50} values against the Gárdos channel.

Table 1: Inhibitors of KCNN4 with specific activity values

Drug	IC_{50} (nM)	Reference
Maurotoxin	1	[115]
Antimalarial quinine	100000	[116]
Vasodilator cetiedil	25000	[116]
L-type Ca channel blockers nifedipine	4000	[116]
Nitrendipine	1000	[116]
Antimycotic clotrimazole	70 – 250	[116]
TRAM-34	20	[117]
11-phenyl-diazepines	~90	[114]
Diphenylindanones	189	[114]
(N-(4-methyl-2-oxazol-2yl-phenyl)-3-trifluoromethyl-benzenesulfonamide)	<500	[118]

A study by Brugnara *et al*, revealed the interaction of clotrimazole (CLT) and related compounds with the KCNN4 channel in sickle cell anemia. The results revealed the complete blockage of KCNN4 in erythrocytes with an IC_{50} value of 29 ± 15 nM in an isotonic solution of 20nM salt and 51 ± 15 nM in saline solution. Also, the efflux of potassium was inhibited by the CLT interaction with KCNN4 as it displaced the bound 125I -Charybdotoxin (ligand of KCNN4) with an IC_{50} value of 12 ± 4 nM in an isotonic solution. Table 2 below represents different blockers of KCNN4 with relevant IC_{50} values in isotonic and saline solution [114].

Table 2: Different inhibitors of KCNN4 along with biological activity values in isotonic and saline solution. The displacement of ¹²⁵I -Charybdotoxin is also represented [114]

Drug	Low ionic strength		Normal saline		Displacement of specifically bound ¹²⁵ i -charybdotoxin	
	IC ₅₀ nM	Max inhibition (%)	IC ₅₀ nM	Max inhibition (%)	IC ₅₀ nM	Present displacement by 10 ⁻⁵ M
Imidazoles						
Clotrimazole	29	93.0	51	87.0	12.	98.0
Miconazole	100.0	49.0	100.	63.0	165.0	77.0
			0			
Econazole	575.0	31.0	270.	47.0	205.0	50.0
			0			
Triazoles						
Fluconazole	-	0	-	0	-	26.0
Nitroimidazole						
Metronidazole	850.0	28.0	440.	36.0	580.0	66.0
			0			
Ornidazole	-	11.0	-	21.0	-	-
Tinidazole	-	21.0	-	3.0	-	-
Charybdotoxi	0.08	95.50	1.2	52.0	0.03	100.0
n						

Therefore, effective modulators with low toxicity and high efficacy are required to block the pore region or make CAMBD less sensitive to Ca²⁺ and maintain a normal gradient of calcium inside and outside the cell.

Chapter 3

Methodology

3.1. Collection of Datasets

A dataset of 56 compounds was selected from the ChEMBL database [119] as well as from literature along with known IC_{50} in μM against the KCNN4 channel. After the removal of duplicates, 51 compounds were used which belong to different classes of a compound consisting of derivatives of clotrimazole, metronidazole, econazole, etc. (Appendix table). The selected compound was assembled into 3D and then energy minimized with a force field of Merck Molecular Force Field (MMFF94x) [120] through Molecular Operating Environment 2015 [121].

3.2. Homology Modelling

Wild type KCNN4 crystal structure was available on PDB [122] therefore, the structural model of mutated human KCNN4 was generated by using the KCNN4 (6CNM) [107] structure of humans as a template. UniProt server [123] was used to retrieve the primary sequence of Human KCNN4 (O15554) [84]. Mutated human KCNN4 Fasta sequence was generated manually by inducing mutation at the 282 and 352 positions in the amino acid sequence of the wild-type KCNN4 protein. At position 282 of the sequence retrieved from UniProt, the Valine was replaced with Methionine. Similarly, at position 352, Arginine was replaced with Histidine. The wild-type structure was also downloaded from the protein databank (PDB) having accession number 6CNM. An online server TCOFFEE [124] was used to perform multiple sequence alignment (MSA) of the wild-type sequence and the mutated sequence to check if the mutations were induced in respective positions. Modeller v9.21 [125] was used to generate a total of 100 models of mutated KCNN4. ERRAT score was calculated to validate these models by using the ERRAT server [126]. A model which had the best score of ERRAT was further verified by the Ramachandran plot [127]. SAVES v5.0 (an online server of UCLA) was used to calculate the ERRAT score and Ramachandran plot. The best model was energy minimized to account for no residues

in the disallowed region. The general workflow of homology modeling is shown in figure 12.

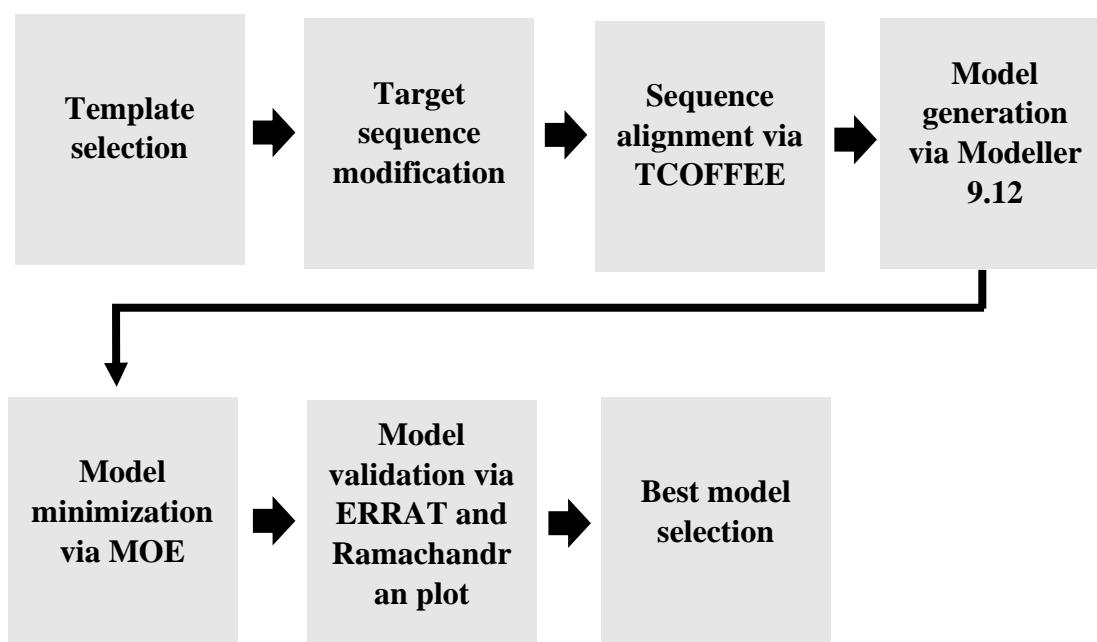


Figure 12: Workflow of homology modeling of the mutated KCNN4 channel using Modeller 9.12 server.

3.3. Molecular Dynamic Simulation

The mutant KCNN4 structure was subjected to Molecular Dynamic simulation to probe the stability of structure and validity of the homology model. For this, the Maestro package of the Schrodinger server [128] was used. The simulation was run for 300 nanoseconds with a TIP3P solvent model to get a stable structure. Figure 13 represents the protocol followed to perform an MD simulation of the mutated KCNN4 protein structure.

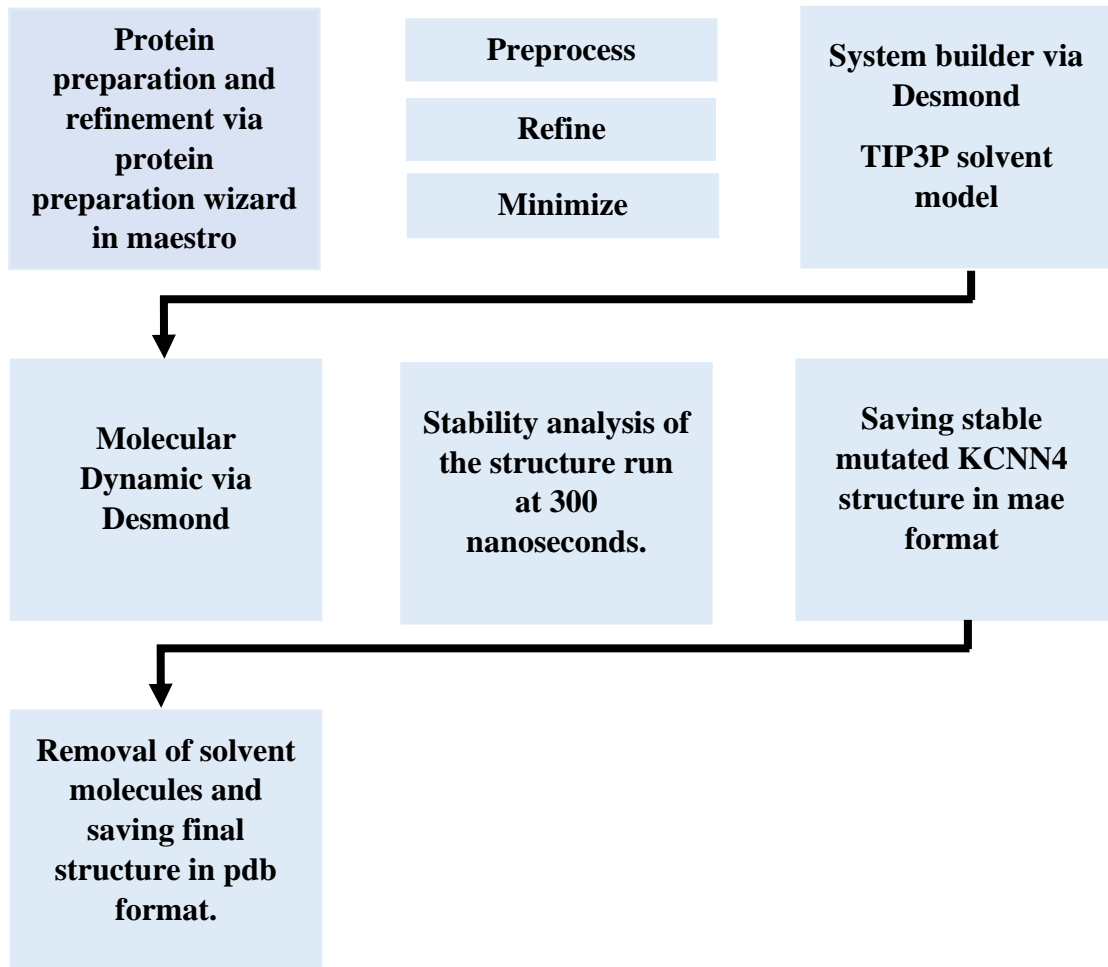


Figure 13: Workflow of Molecular dynamic simulation to get a stabilized mutated KCNN4 protein using Schrodinger server.

3.4. Molecular docking

The mutated KCNN4 protein structure after MD simulation was docked with ligand dataset at the calmodulin-binding domain where the R352H mutation was present. Docking simulations were executed through GOLD software (Genetic Optimization for Ligand Docking) 5.6.1 version [129]. Active binding sites were selected by using their coordinates i.e., x, y, and z nearby its point of center around a single residue. 30Å radius was set to obtain all the active site amino acid residues which were important. For each ligand, a sum of 100 genetic runs was performed by using GoldScore to rank the resulting poses of each ligand using the Gold Scoring function as:

$$\Delta G_{\text{(bind)}} = \Delta G_{\text{(hb_ext)}} + \Delta G_{\text{(vdw_ext)}} + \Delta G_{\text{(hb_int)}} + \Delta G_{\text{(vdw_int)}}$$

No constraints were applied, and all other parameters were set to default. However, the slow protocol was used because it gives high precision and more accuracy in results. Table 3 below shows the x, y, and z coordinates nearby the point of center around the residues CaMBD - R352H. Figure 14 represents a general workflow of docking for all three positions in the binding pocket of the mutated KCNN4 protein.

Table 3: x, y, and z coordinated selected for specifying the binding pocket in three different positions in the mutated KCNN4 protein for the docking of ligands via GOLD software.

Region	Coordinates around the residue		
	x	y	z
Calmodulin binding domain	-14.1468	-0.7	2.3730

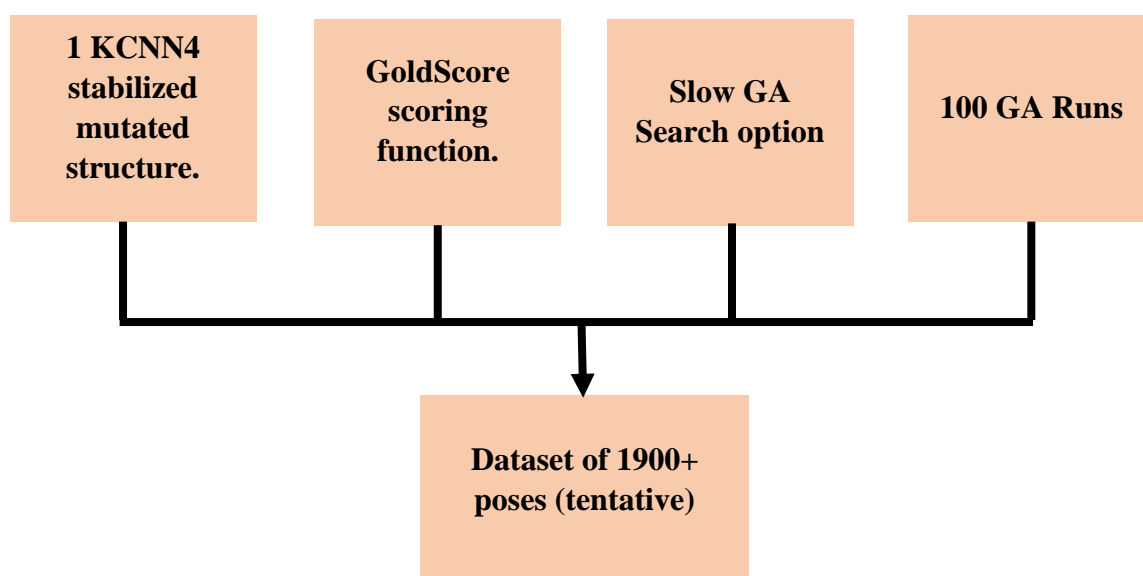


Figure 14: general workflow of molecular docking protocol to generate the docked poses for mutated KCNN4 protein against 51 ligands.

3.5. Common scaffold clustering

The 51-ligand dataset was manually checked for common scaffold and the MOE scaffold scripts were run to validate the scaffold. 51 ligands comprise of five different

classes namely, Class A, B, C, D and the miscellaneous class. Table 4 represents the number of ligands in each class.

Table 4: the number of ligands having the common scaffold i.e. belonging to the same class.

Class #	Number of ligands
1	23
2	14
3	6
4	5
Miscellaneous	3

Based upon these classes, the docking poses were classified into different classes and their RMSD from the common scaffold was calculated for the selection of the similarly docked poses within each class.

Clusters were made at 3.2Å using the "complete linkage – wards minimum variance" method. For each of the classes, the maximum number of ligands selected are provided in the table 5.

Table 5: the total number of ligands and the number of ligands (best poses) clusters out in the same binding region of the Gárdos channel

Class #	Total number of ligands	Ligands selected in the final cluster
1	23	21
2	14	9
3	6	5
4	5	4
Miscellaneous	3	-

The poses in these clusters with the best docking score were selected. Also, the ligands that were not in the poses were separated and their best-docked score was selected for further analysis.

3.6. Physicochemical parameters calculation

The qualities of a molecular structure are represented by the descriptors, which are the characteristic features of molecular structures. Using the MOE software, descriptors, such as logP(o/w) and molecular weight, were calculated for the entire dataset to see how these descriptors influenced biological activity. To assess the influence of these descriptors on the inhibitor's biological activity, a correlation graph was created between descriptors and pIC₅₀.

3.7. GRIND (GRID independent descriptors)

To compute GRID independent descriptors, selected molecular conformations of KCNN4 inhibitors were loaded into Pentacle v1.07 [130] along with their pIC₅₀ values. Four distinct probes were used to investigate the areas of molecular interactions. TIP refers to a shape-based probe, O stands for a hydrogen bond donor group within a molecule of carbonyl O, and hydrogen bond acceptors with the molecule of Amide N, which is represented by N1. The most essential and relevant molecular interacting fields (MIFs) were analyzed, and distances between nodes to nodes were determined using the AMANDA algorithm. Furthermore, each probe in the GRID is used to calculate the overall energy of interaction at each node by combining Lennard-Jones, electrostatic, and hydrogen bond interactions [131]:

$$E_{xyz} = \sum E_{lj} + \sum E_{el} + \sum E_{hb}$$

For MIF discretization, the AMANDA algorithm [132] is employed. By default, the probe cut-off settings for the MIF discretization were DRY = -0.5, N1 = -4.2, O = -2.6, and TIP = -0.75. Nodes that did not have default values were removed. The cut-off values for the deleted Nodes were exceeded. CLACC (Consistently large auto and cross-correlation) [133] was used for encoding because it produces a more consistent set of variables by changing the compound according to their moment of inertia rather than MACC[79] and picking those nodes for all the consistent compounds in a series.

The final Grind model was created as a set of correlograms that represented various regions such as node to node product and distances between nodes, and it was validated using the leave-one-out approach. The high-energy products for the same probes were represented by different correlograms. DRY–DRY, TIP–TIP, N1–N1, and O–O auto correlograms were obtained, as well as six cross correlograms: O–TIP, DRY–O, O–N1, DRY–TIP, DRY–N1, and N1–TIP. The predictive ability and PLS of the

QSAR model were used to evaluate the values of Q2 and R2. Figure 15 depicts the GRIND's workflow.

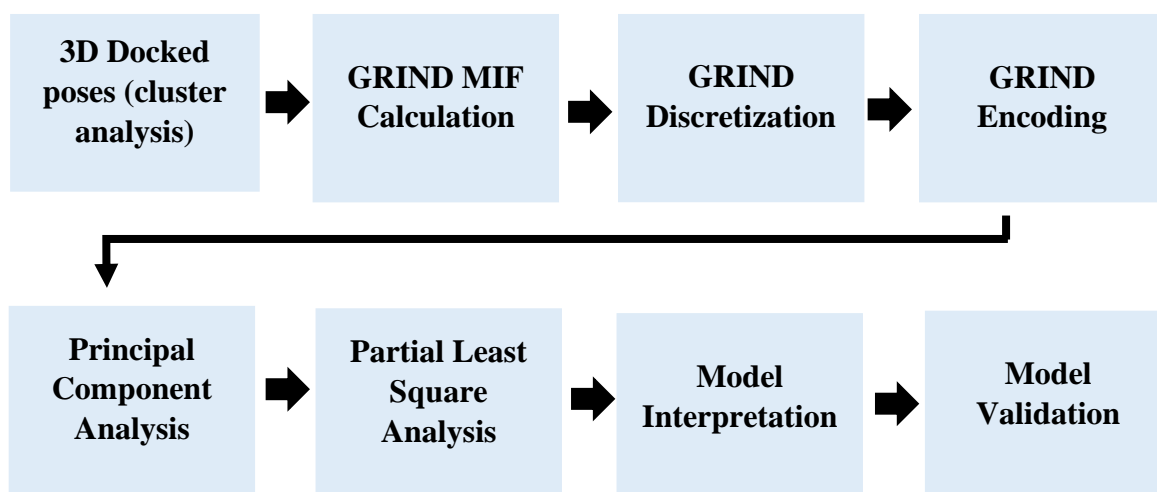


Figure 15: general workflow of GRIND to extract 3D features from the mutated KCNN4 using the 51 ligands with their activity values.

Chapter 4

Results

4.1. Data collection and refinement

The data of 51 ligands were collected from ChEMBL and was preprocessed into different classes based on the common scaffold. Four classes with some common scaffolds were made while one miscellaneous class consisted of three distinct ligands. The ligand classes with their common scaffold and number of ligands are represented in the table 9.

4.2. Homology modeling of the mutated KCNN4 protein

Homology modeling is a necessary step in the structural modeling of proteins that do not have crystal structures. The mutated Gárdos channel protein structure was not available in the protein database. Therefore, a mutated protein structure was modeled. The purpose of homology modeling is to predict a protein's secondary structure so that it can be studied further. 100 models of mutated KCNN4 were constructed using the Modeller software and the best one was selected among them. Before the final model was selected, it underwent a series of filters to account for any steric clashes among the protein residues. The ERRAT score and Ramachandran plot were used to analyze any steric clashes in side-chain amino acid residues. A higher ERRAT score leads towards a better model whereas the least ERRAT scores depict a bad model. Similarly, the model is acceptable and good if there are more residues in the favorable region and none or few residues in the unfavorable region. For the calculation of these two parameters, the SAVES server from UCLA was used. The results on this server were expressed as quality factors, which depict the atomic interactions of proteins; a greater quality factor indicates that the model's protein interactions are good. After the generation of 100 models, the top 6 models with the highest ERRAT scores were selected. The models were also checked for their residues in the disallowed region. For further improvements in the model, the top 6 models underwent energy minimization using the Amber99 force field in MOE software. The models showed improvement in their Ramachandran plot. Model D was selected with the highest ERRAT score and 0 residues in its generously allowed and disallowed

region after energy minimization. The table 6 shows the top 6 models selected along with their Ramachandran values before and after energy minimization.

Table 6: The top 6 models selected from the homology model based on the ERRAT score and Ramachandran plot statistics. The Ramachandran scores before and after energy minimizations are also provided.

Model	Model #	ERRAT Score	Ramachandran score before energy minimization				Ramachandran score after energy minimization			
			Core	All	Gen	Disall	Core	All	Gen	Disall
A	12	74.7396	92.6	6.6	0.5	0.3	73.3	25.7	1.1	0
B	51	75.7256	92.6	6.3	0.8	0.3	70.1	28.8	1.1	0
C	59	75.3213	92.3	6.9	0.8	0	70.6	28.3	0.5	0.5
D	62	78.4777	93.9	5.3	0.5	0.3	72.2	27.8	0	0
E	75	74.6667	92.6	6.9	0.3	0.3	74.0	24.3	0.5	0.5
F	96	73.8342	93.9	5.3	0.5	0.3	68	31	0.8	0.3

The Ramachandran plot for selected model **D** referred to as **model 62** among the 100 models is represented in the figure below before energy minimization (Fig. 16) and after energy minimization (Fig. 17).

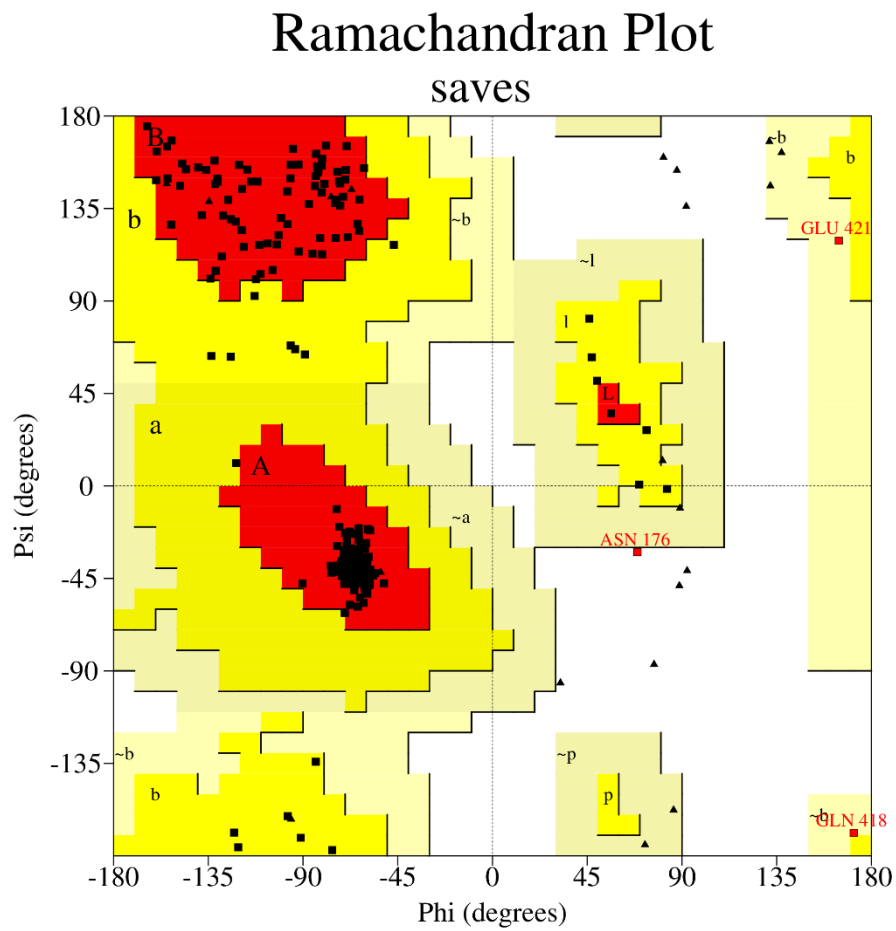


Figure 16: Ramachandran plot for selected model D (model 62) among the 100 models before energy minimization.

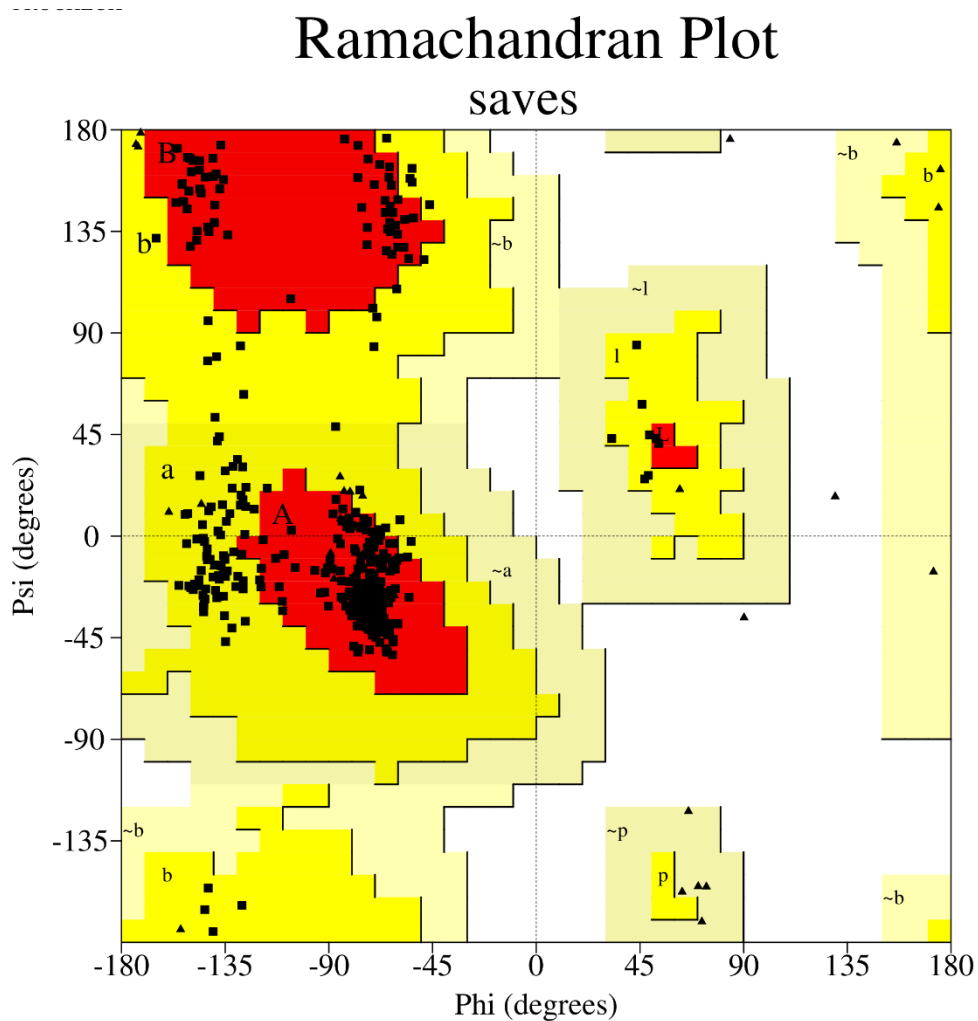


Figure 17: Ramachandran plot for selected model D (model 62) among the 100 models, after energy minimization

The 3D structure of protein both mutations i.e., V282M and R352H were also represented in the (Fig. 18A) with a closer view of R352H (Fig. 18B) and V282E (Fig. 18C).

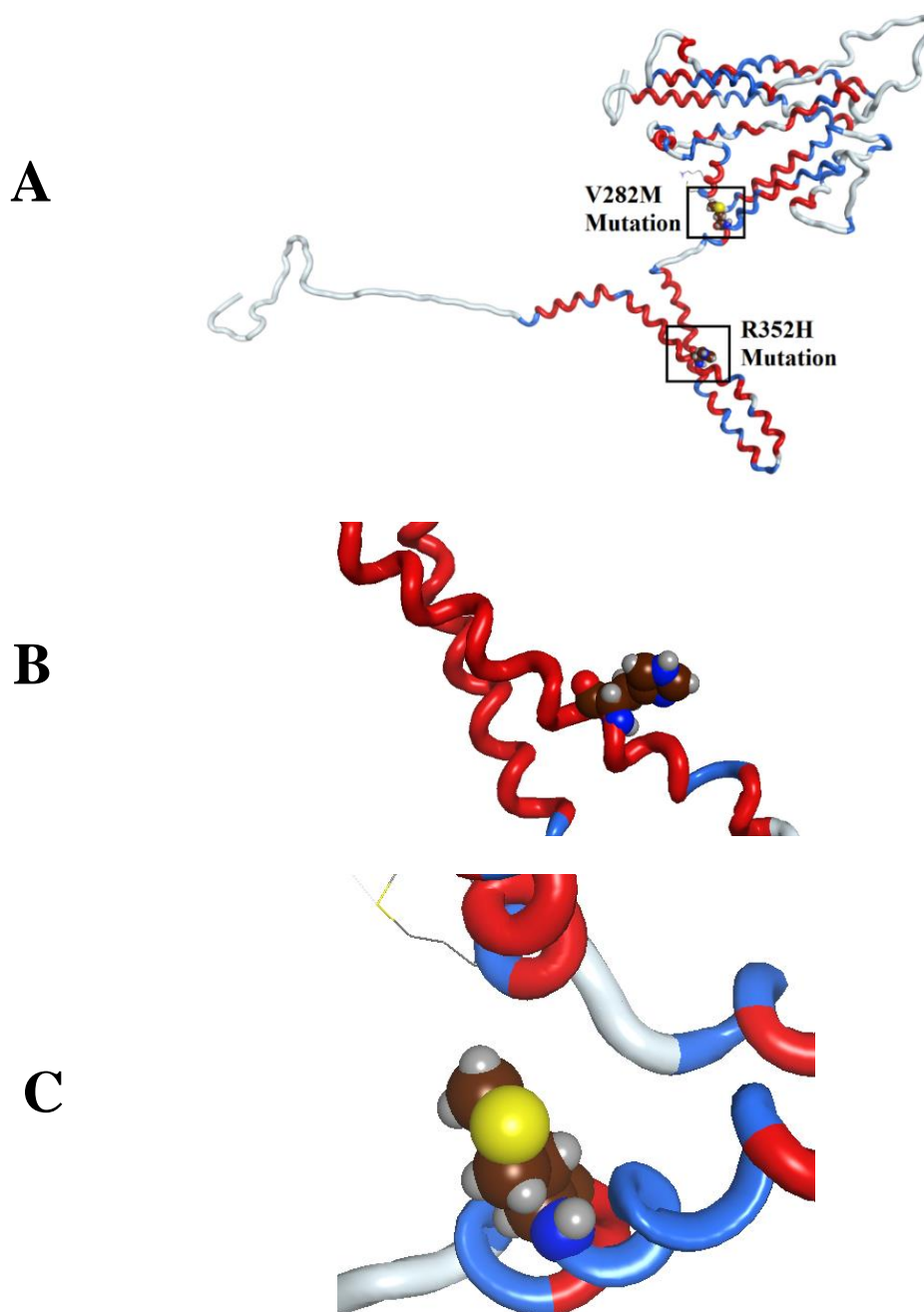


Figure 18: (A) Representation of two mutations R352H and V282M. The structure is a single subunit of KCNN4 mutated and modeled using Modeller. (B) A closer look at the R352H mutation; in which the Arginine was replaced with Histidine at position 352. (C) A closer look at the V282M mutation; in which the Valine was replaced with Methionine at position 282.

4.3. Molecular dynamic simulation of the mutant KCNN4 protein

The molecular dynamic simulation of mutant KCNN4 structure was done by simulating 300ns at a 7.4 pH value. The simulation took time due to the presence of

loops at the start and end of the structure that was modeled through the homology modeling by using 6CNM (PDB entry) as a template. The loops that were modeled in the mutated KCNN4 structure were not present in the original template. The structure was stabilized at 300ns due to the presence of loops. The figure 19 represents the RMSD values in association with the time frame required for the stabilization of the structure. The peaks are stable at 4.0A RMSD values.

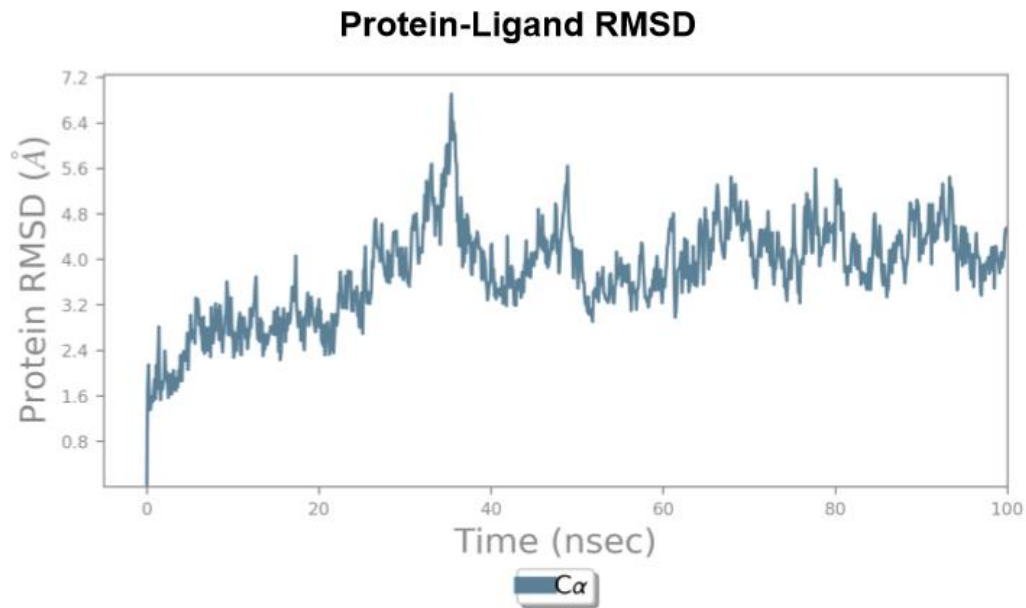


Figure 19: Output obtained after the Molecular Dynamic Simulation of the modeled mutant KCNN4 structure. The graph shows RMSD values (y-axis) vs time frame(ns) (x-axis) required for the stabilization of structure.

However, the RMSF versus residue Index graph showed high peaks at the start and end of the structure as represented in the figure 20. These peaks are due to the presence of long loops in the start and end of the mutated KCNN4 structure that wasn't present in the original template. The figure 21 shows a superimposed structural representation of mutated and wild type (6CNM – chain A) Gárdos channel. In total, the modeled structure had 3 loops.

1. From amino acid 1 – 10 (represented in yellow in figure 21)
2. From amino acid 123 – 141 (represented in green in the figure 21)
3. From amino acid 386 – 427 (represented in yellow in figure 21)

In the overall structure, the yellow loops (Fig. 21) amino acid 1- 10 and amino acid 386 – 427 were deleted from the mutated KCNN4 region while the green loop (Fig. 21)

amino acid 123 – 141 remained intact. Both the RMSF vs Residue index graph (Fig. 20) and the superimposed structural representation depict the reason for the extended stabilization time of mutant protein structure in MD simulation as well as the reason for the deletion of those loops to avoid further clashes.

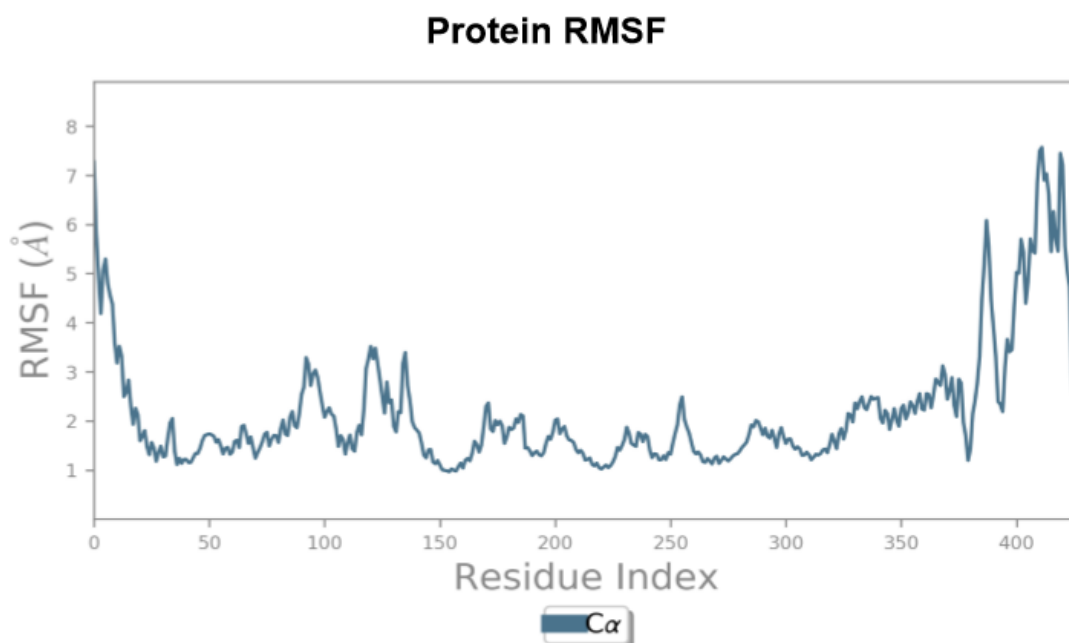


Figure 20: Output obtained after the Molecular Dynamic Simulation of the modeled mutant KCNN4 structure. The graph shows RMSF values (y-axis) vs Residue Index (x-axis) required for the stabilization of the structure.

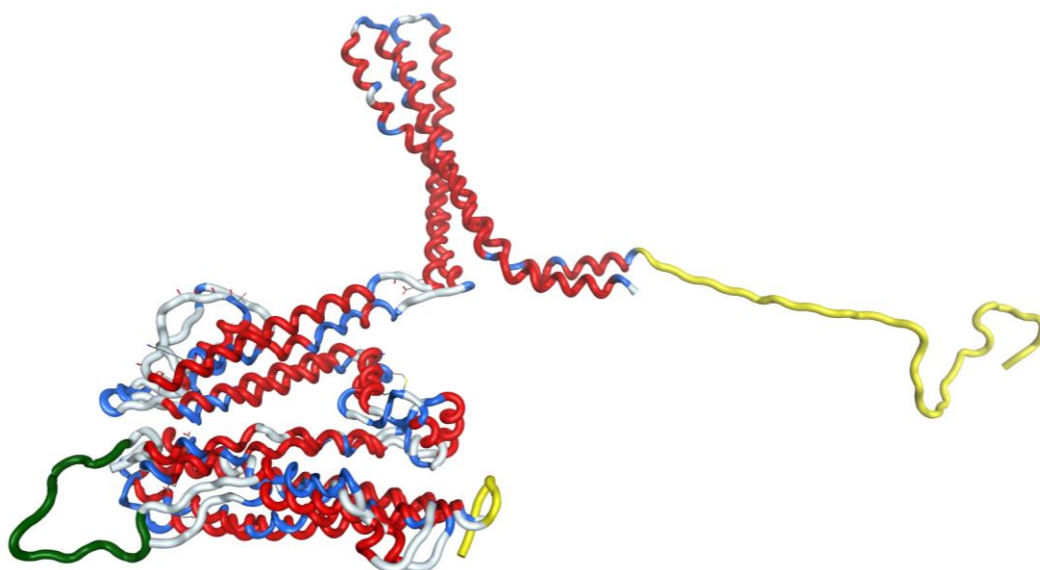


Figure 21: The homology modeled and simulated structure of mutant KCNN4. The yellow loops in the structure were removed, whereas the green loop was kept intact.

After the removal of loops, the protein structure was energy minimized. The model was checked once again in SAVES to evaluate the ERRAT score and Ramachandran plot analysis to view the residues in allowed, generously allowed, and disallowed regions. The ERRAT score calculated for the mutated KCNN4 model stabilized at 300ns was 76.1518 and the Ramachandran summary is provided in the table 7. The figure 22 represents the Ramachandran plot for the mutated KCNN4 model after MD simulation

Table 7: Ramachandran plot statistics and ERRAT score for the model D, after Molecular dynamic simulation protocol.

Model	ERRAT Score	Ramachandran score			
		Core	Allowed	Generous	Disallowed
Model after MD simulation at 300ns	76.15	85.2	13.6	0.6	0.6

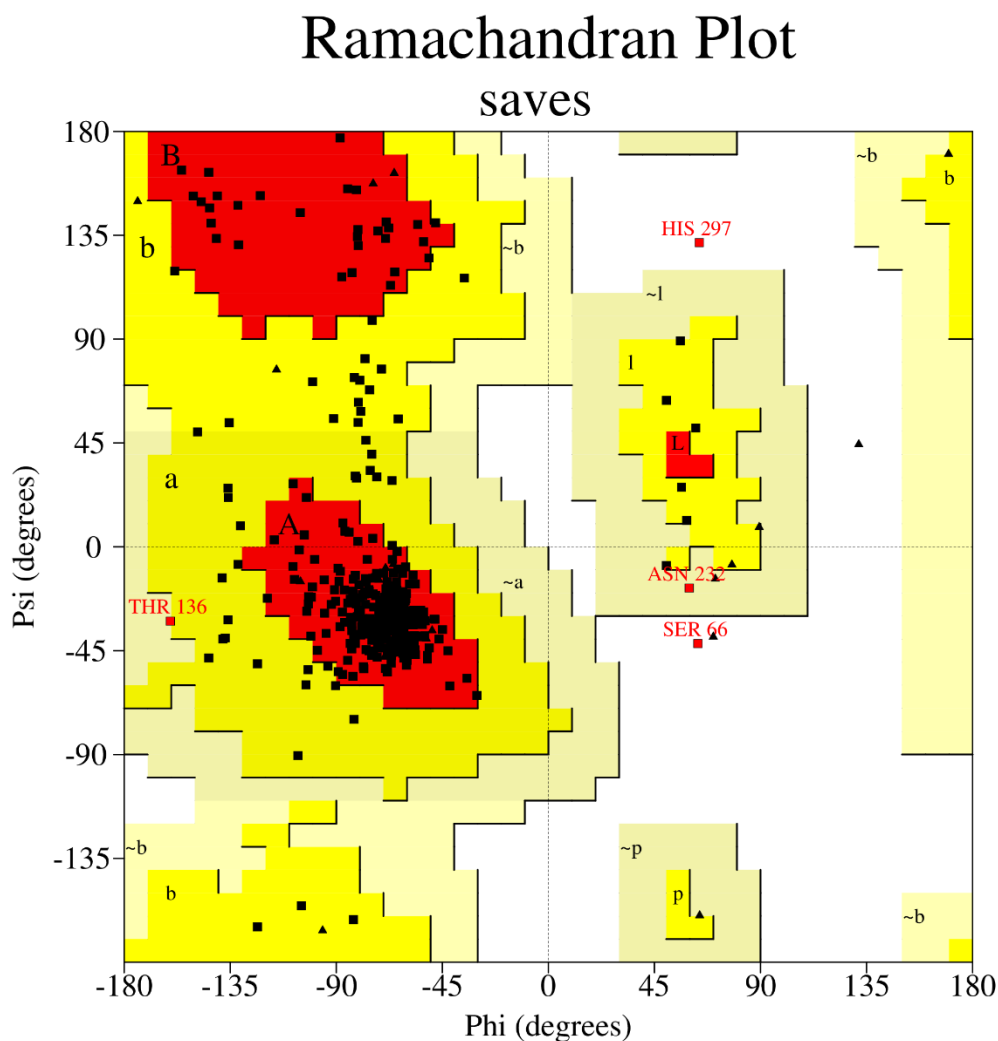


Figure 22: Ramachandran plot for the mutated KCNN4 model 62 after MD simulation

4.4. Molecular Docking

Molecular docking is the most effective approach in molecular modeling for modeling atomic-level interactions between proteins and ligands. It enables the understanding of fundamental biological processes by analyzing the behavior of chemical compounds in the target protein's binding region. The goal of molecular docking is to acquire the most probable confirmation of ligands for virtual screening (GRIND). Using a crystal structure (PDB ID: 6CNM) with a resolution power of 3.40 Å, a dataset of 51 ligands was docked into the binding pocket of the calmodulin-binding domain. All important amino acid residues were included in the binding site, which was kept at a radius of 30Å. The GOLD scoring function was used to rank each pose of docked ligands. The poses were assigned a gold fitness score. For 51 ligands, a

total of 4459 poses were generated. These poses were analyzed and sorted based on the highest gold fitness score value and the lowest values. One of the poses associated with ligand "Gárdos_6" had the lowest score i.e. 24.3500004 while the pose associated with "Gárdos_34" had the highest score i.e. 60.6166. these two values are the two extremes of the docked dataset. From the dataset of 4459 poses, the top 10 poses for each ligand were selected for the identification of final docked confirmation with the help of common scaffold clustering (CSC).

4.5. Common Scaffold Clustering (CSC)

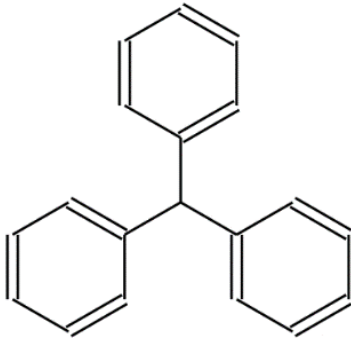
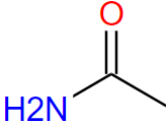
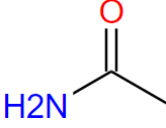
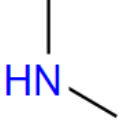
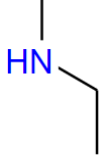
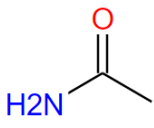
The dataset of 4459 poses was reduced to 510 poses for the top 10 poses of the 51 ligands. The 510 poses were further separated into 5 classes as represented in the table 8.

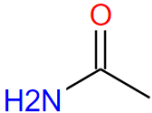
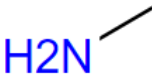
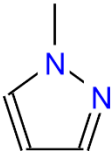
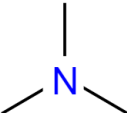
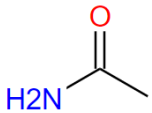
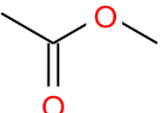
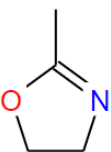
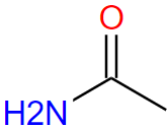
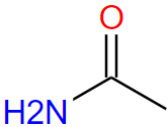
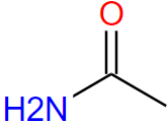
Table 8: The number of poses reduced depending upon the number of ligands in each cluster. The top 10 poses of each ligand were taken.

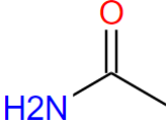
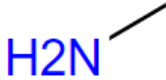
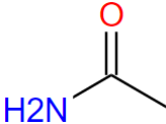
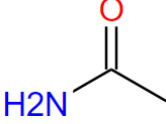
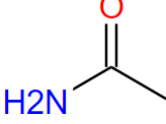
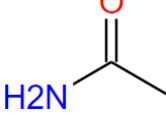
Class #	Number of ligands	Number of poses
1	23	230
2	14	140
3	6	50
4	5	50
Miscellaneous	3	30

The table 9 shows all the 51 ligands separated into different classes based on the common scaffold.

Table 9: 2D structure of ligands dataset. The common scaffold of each class with their SMILE is represented. All the ligands are separated into different classes.

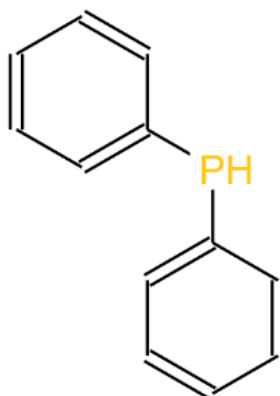
Class A				
Common scaffold				
				
Ligand Name	R1	R2	R3	R4
Gardos_1		P – Fluorine	-	P – Fluorine
Gardos_2		-	O - Fluorine	O - Fluorine
Gardos_3		-	-	-
Gardos_5		-	-	-
Gardos_6		-	-	(O, P) - Fluorine

Gardos_7		O - Fluorine	O - Fluorine	P - Fluorine
Gardos_8		-	-	-
Gardos_12		O - Chlorine	-	-
Gardos_13		-	-	-
Gardos_14		-	-	P - Fluorine
Gardos_21		-	-	-
Gardos_22		-	-	-
Gardos_26		-	-	(M, P) - Fluorine
Gardos_29		M - Fluorine	P - Fluorine	M - Fluorine
Gardos_30		P - Fluorine	P - Fluorine	P - Fluorine

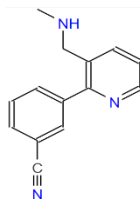
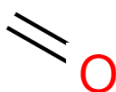
Gardos_37		O - Fluorine	P - Fluorine	P - Fluorine
Gardos_38		O - Chlorine	-	-
Gardos_39		M - Fluorine	-	M - Fluorine
Gardos_42		M - Fluorine	M - Fluorine	M - Fluorine
Gardos_43		O - Fluorine	-	P - Fluorine
Gardos_49		M - Fluorine	P - Fluorine	P - Fluorine

Class B

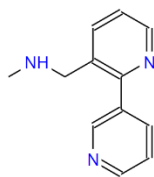
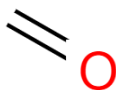
Common scaffold



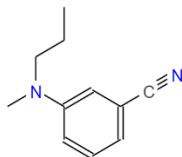
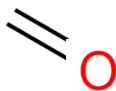
Gardos_11



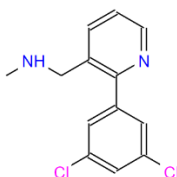
Gardos_15



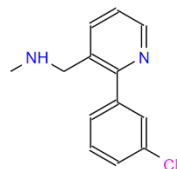
Gardos_16



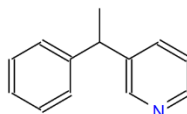
Gardos_19



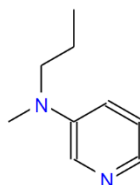
Gardos_20



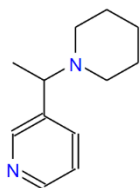
Gardos_34



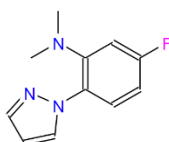
Gardos_35



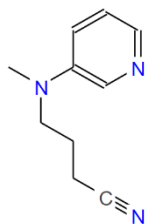
Gardos_40



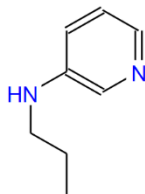
Gardos_44



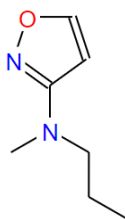
Gardos_45



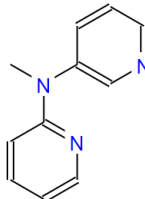
Gardos_46



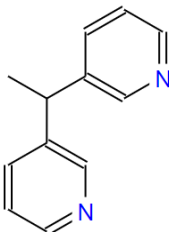
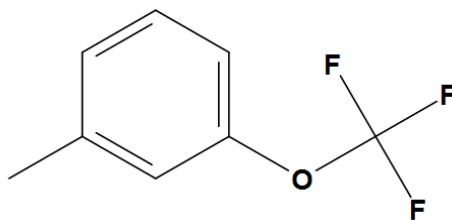
Gardos_47

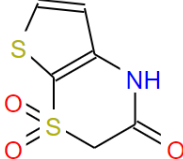
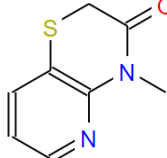
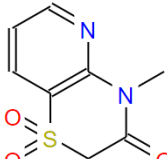
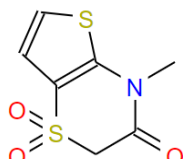
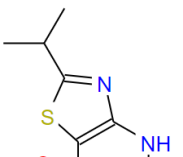
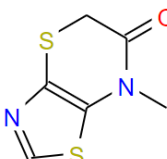


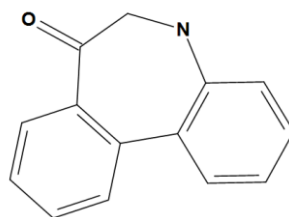
Gardos_48

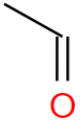
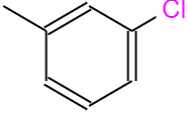
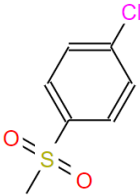
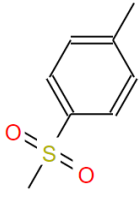
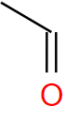
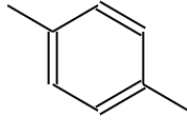
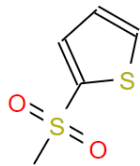


Gardos_51

**Class C****Common scaffold**

Gardos_4	P - Fluorine		
Gardos_9	-		
Gardos_23	P - Fluorine		
Gardos_24	P - Fluorine		CH3
Gardos_33	P - Fluorine		
Gardos_50	P - Fluorine		CH3

Class D**Common scaffold**

Gardos_27		
Gardos_28		-
Gardos_32		-
Gardos_36		
Gardos_41		-

After computing the common scaffold and dividing the dataset of 510 poses into 5 small datasets, the cluster optimization procedure was carried out. Clustering was done using the "complete linkage – wards minimum variance" method and the clusters were generated at an RMSD of 3.2Å.

4.5.1. Clustering for class 1 ligands

Class 1 consisted of twenty-three ligands with the common scaffold as "Triphenylmethane". The clustering was performed at 3.2Å to attain the maximum number of ligands having the same binding site. Among many clusters generated, 6 clusters with the maximum number of ligands were selected having the same binding site. From 23 ligands (230 poses), 21 ligands from 6 different clusters were selected as represented in the table 10.

Table 10: The best clusters chosen from class 1, with the maximum number of ligands and the ligands not in those clusters. All the best poses chosen from the cluster were separated for further analysis.

Cluster number	No. of ligands	Ligands selected	Remaining ligands
9	2	Gárdos_43	Gárdos_8, Gárdos_38
13	8	Gárdos_2, Gárdos_6, Gárdos_29, Gárdos_39,	
17	3	Gárdos_5, Gárdos_12,	
18	11	Gárdos_1, Gárdos_7, Gárdos_14, Gárdos_17, Gárdos_18, Gárdos_21, Gárdos_22, Gárdos_26, Gárdos_30, Gárdos_42, Gárdos_49	
20	7	Gárdos_37,	
25	3	Gárdos_3, Gárdos_13,	

4.5.2. Clustering for class 2 ligands

Class 2 consisted of fourteen ligands with the common scaffold as "Diphenylphosphine". The clustering was performed at 3.2A to attain the maximum number of ligands having the same binding site. Among many clusters generated, 2 clusters with the maximum number of ligands were selected having the same binding site. From 14 ligands (140 poses), 9 ligands from 2 different clusters were selected as represented in the table 11.

Table 11: The best clusters chosen from class 2, with the maximum number of ligands and the ligands not in those clusters. All the best poses chosen from the cluster were separated for further analysis.

Cluster number	No. of ligands	Ligands selected	Remaining ligands
----------------	----------------	------------------	-------------------

24	8	Gárdos_16, Gárdos_20, Gárdos_35, Gárdos_34, Gárdos_45, Gárdos_48, Gárdos_51, Gárdos_47	Gárdos_11, Gárdos_15, Gárdos_19, Gárdos_40, Gárdos_46
16	1	Gárdos_44	

4.5.3. Clustering for class 3 ligands

Class 3 consisted of six ligands with the common scaffold as "(Trifluoromethoxy)benzene". The clustering was performed at 3.2A to attain the maximum number of ligands having the same binding site. Among many clusters generated, 5 clusters with the maximum number of ligands were selected having the same binding site. From 6 ligands (60 poses), 5 ligands from 5 different clusters were selected as represented in the table 12.

Table 12: The best clusters chosen from class 3, with the maximum number of ligands and the ligands not in those clusters. All the best poses chosen from the cluster were separated for further analysis.

Cluster number	No. of ligands	Ligands selected	Remaining ligands
1	1	Gárdos_50	Gárdos_24
2	2	Gárdos_33	
4	2	Gárdos_23	
11	2	Gárdos_9	
6	1	Gárdos_4	

4.5.4. Clustering for class 4 ligands

Class 4 consisted of five ligands with the common scaffold as "5,6-Dihydro-7H-dibenzo[b,d]azepin-7-one". The clustering was performed at 3.2A to attain the maximum number of ligands having the same binding site. Among many clusters generated, 4 clusters with the maximum number of ligands were selected having the same binding site. From 5 ligands (50 poses), 4 ligands from 4 different clusters were selected as represented in the table 13.

Table 13: The best clusters chosen from class 4, with the maximum number of ligands and the ligands not in those clusters. All the best poses chosen from the cluster were separated for further analysis.

Cluster number	No. of ligands	Ligands selected	Remaining ligands
6	1	Gárdos_32	Gárdos_27
7	1	Gárdos_36	
20	1	Gárdos_28	
21	1	Gárdos_41	

After the cluster analysis, the dataset now has the requisite clusters with the best poses. A single cluster had several poses for the same ligand, therefore the pose with the highest gold fitness score was selected for the specific ligands. A dataset was retrieved having 1 best pose of each ligand among the selected clusters. Along with that, the best pose for the remaining ligands (not included in the clusters) was also separated based on a good gold fitness score. The pose with the highest docked score of the miscellaneous class was also separated.

4.6. Protein-ligand interaction analysis

The interaction analysis of the best poses (clusters) of each ligand was done with the mutated protein structure with the help of the protein-ligand interaction fingerprint (PLIF) scheme. For this purpose, the MOE software was used. PLIF helps in the calculation of single interacting residues and the binding pattern of data. PLIF explains numerous interactions such as HBD (Sidechain Hydrogen Bond Donor), HBA (Sidechain Hydrogen Bond Acceptor), SAC (Surface Contact), HBd (Hydrogen Bond donor for the backbone), and HBa (Hydrogen Bond Acceptor for the backbone).

Interaction analysis was performed between clusters of all classes and the common interactions were checked out. The figures 23 show the interaction of the clusters of different classes and figure 24 shows the ratio of all interactions with specific residues in the vicinity.

The figure 23A show the interaction pattern of class 1 ligands. All of the 21/23 ligands clustered out, show the same interaction with the protein residues.

The interacting residues in class 1 include:

- Gln306, Gln353, and Met302 representing Hydrogen-donor interactions
- Leu356 and Val282 representing pi-Hydrogen interactions
- Lys357 representing pi-cation interactions
- Lys360 and Lys309 representing dual interactions i.e. Hydrogen-acceptor and pi-hydrogen interactions

The most common interactions among the class1 ligands were the Lys309 (21 interactions among 21 ligands). The PLIF results in Fig 24A below shows the number of interactions that occurred between the 21 ligands of class 1.

The figure 23B shows the interaction pattern of class 2 ligands. All of the 9/14 ligands clustered out, show the same interaction with the protein residues.

The interacting residues in class 2 include:

- Gln353 and Met302 representing Hydrogen-donor interactions
- Lys360, Lys309, and Val282 representing pi-Hydrogen interactions

The most common interaction among the class1 ligands was the Lys09 (9 interactions among 9 ligands). The PLIF results in Fig 24B shows the number of interactions that occurred between the 9 ligands of class 2.

The figure 23C shows the interaction pattern of class 3 ligands. All of the 5/6 ligands clustered out, show the same interaction with the protein residues.

The interacting residues in class 3 include:

- Ala346 representing Hydrogen-donor interactions
- Gln320 and Thr270 representing Hydrogen-acceptor interactions
- Lys312 representing dual interactions i.e. Hydrogen-acceptor and pi-hydrogen interactions
- Arg317 representing dual interactions i.e. Hydrogen-acceptor and pi-cation interactions

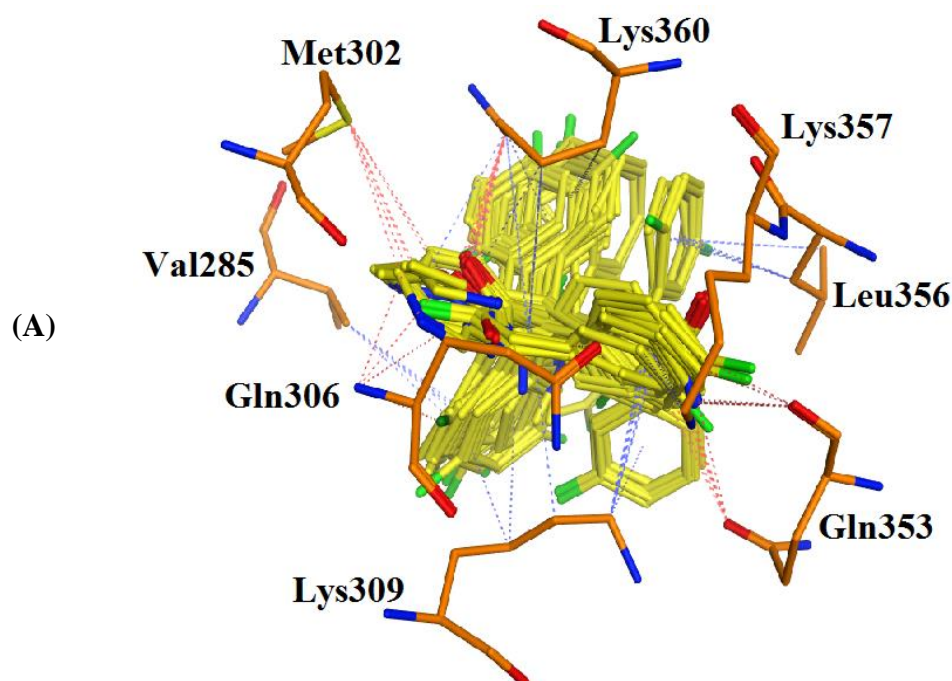
The most common interaction among the class3 ligands was the Gln320 (3 interactions for 6 ligands). The PLIF results in Fig 24C below shows the number of interactions that occurred between the 6 ligands of class 3.

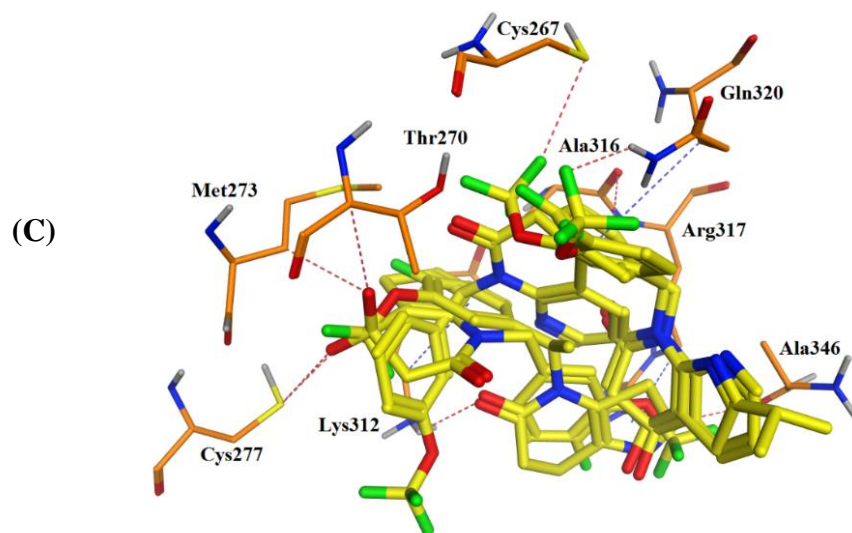
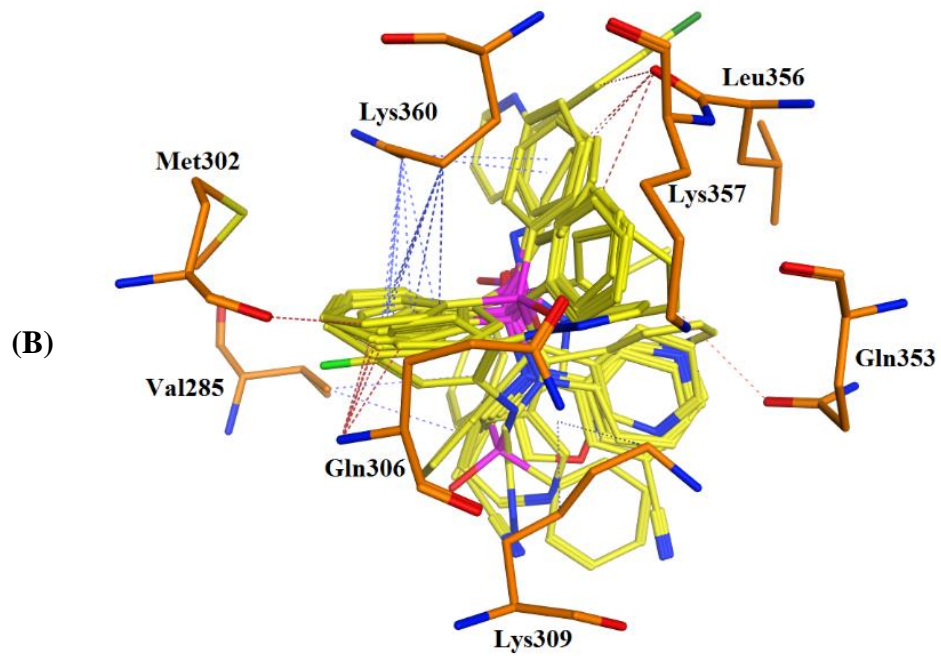
The figure 23D shows the interaction pattern of class 4 ligands. All of the 4/6 ligands clustered out, show the same interaction with the protein residues.

The interacting residues in class 4 include:

- Gln306 representing Hydrogen-donor interactions
- Leu356 representing pi-Hydrogen interactions
- Lys309 representing dual interactions i.e. Hydrogen-acceptor and pi-Hydrogen interactions
- Lys360 representing dual interactions i.e. Hydrogen-acceptor and pi-hydrogens.

The most common interaction among the class4 ligands was the Lys309 (4 interactions for the 4 ligands). The PLIF results in Fig 24D below shows the number of interactions that occurred between the 4 ligands of class 4.





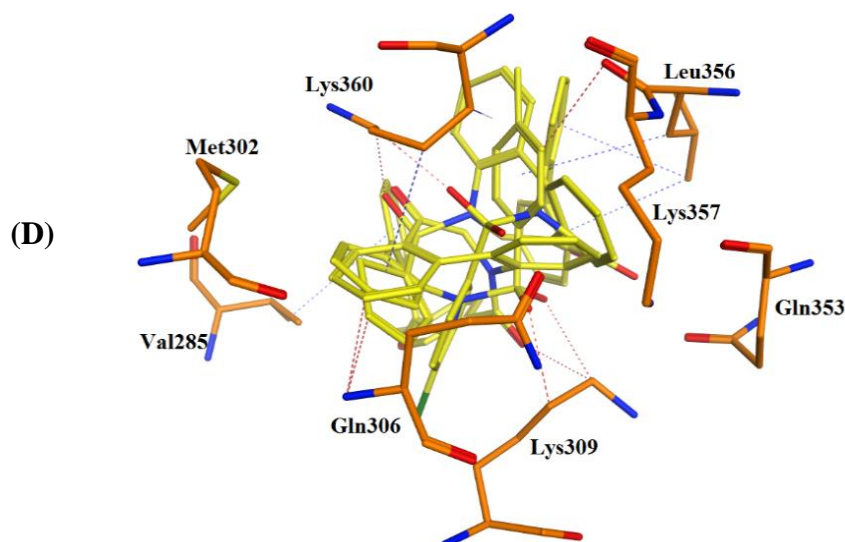
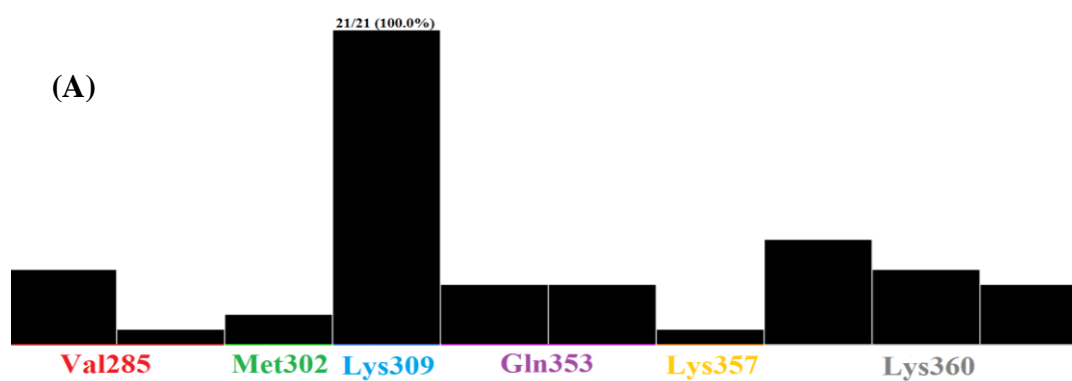


Figure 23: Different classes interaction with the mutant KCNN4 structure. The hydrogen bond interaction is represented in red color whereas the blue color depicts pi-pi interaction. (A) Interaction of Class 1 ligands with the mutant KCNN4 structure. (B) Interaction of Class 2 ligands with the mutant KCNN4 structure. (C) Interaction of Class 3 ligands with the mutant KCNN4 structure. (D) Interaction of Class 4 ligands with the mutant KCNN4 structure.



(B)

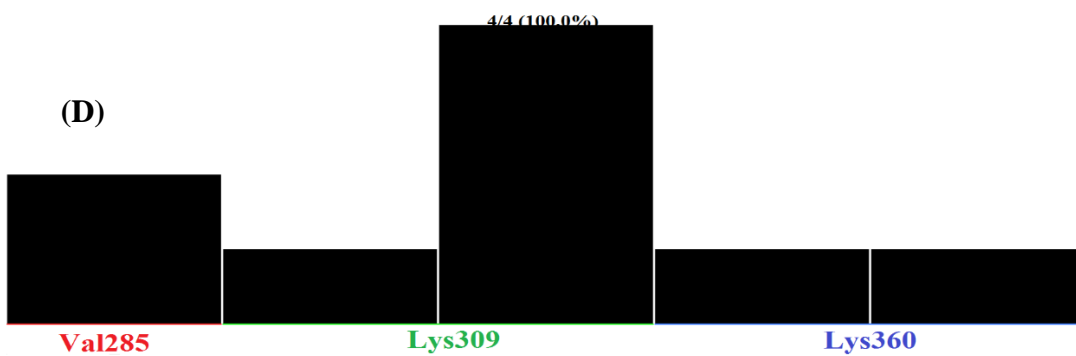
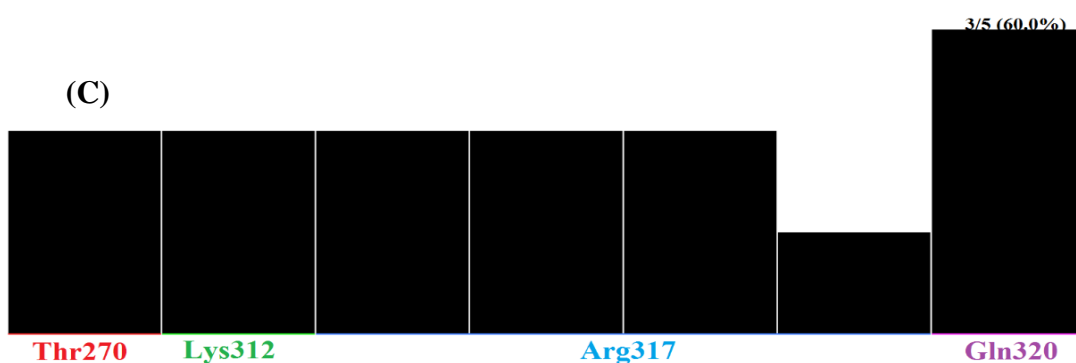
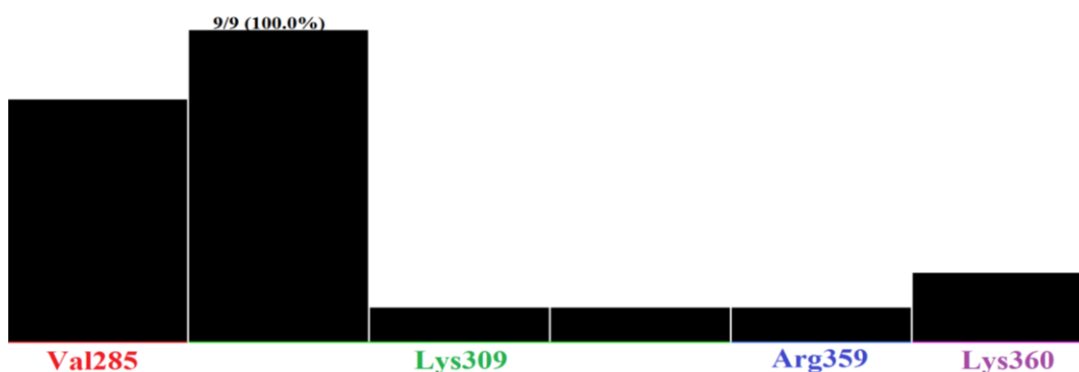


Figure 24: PLIF results showing the most common interaction found between the ligands of different classes and the mutant KCNN4 structure. (A) Class 1 major interactions. (B) Class 2 major interactions (C) Class 3 major interactions. (D) Class 4 major interactions

The overall summary of all the interactions among various classes is represented in the figure 25 where the highest number of interacting residue among all ligands with the mutated protein structure is Lysine at 309 position.

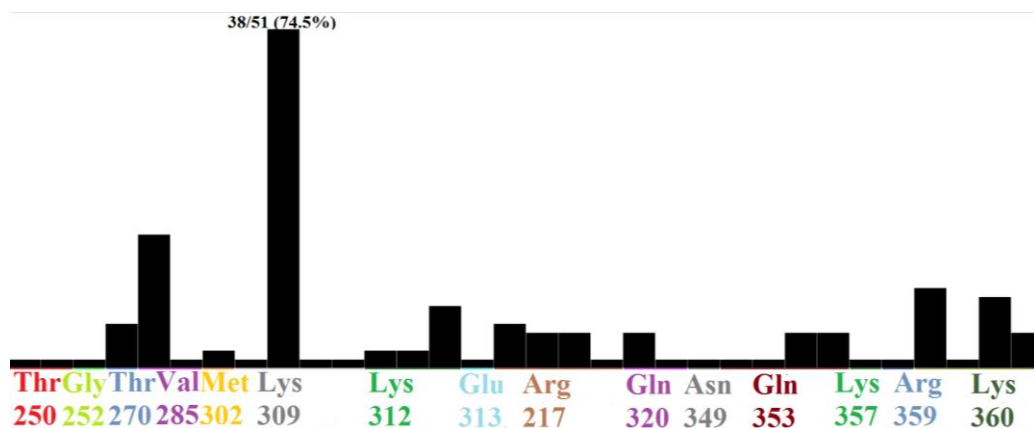


Figure 25: PLIF results showing the most common interaction found between the complete dataset and the mutant KCNN4 structure. The most consistent interaction was with the residue Lys309 of the mutant structure.

4.7. GRIND

The molecular confirmations obtained from docking, as well as their inhibitory activity (pIC_{50}) values, were used to create a 3D-QSAR model using special alignment independent GRIND descriptors in the pentacle v 1.07 software package. The research used the leave-one-out (LOO) cross-validation method to create a partial least square model to correlate inhibitory potencies with the 3D structural features of our training set. The model appeared reasonable and had significant statistical parameter values ($q^2 = 0.36$, $R^2 = 0.62$), but I refined it further using the fractional factorial design (FFD) variable selection algorithm, which eliminated inconsistencies. I attained q^2 of 0.57 and R^2 of 0.73 after applying one FFD, with a standard error of prediction of 0.77 for the final model i.e. 3. For all 51 inhibitors in the training set, the difference between actual and predicted activity values was less than 1 log unit. The coefficient correlogram of chosen GRIND descriptors produced by the PLS model indicated the direct/inverse relationship between biological activities and essential 3D structural features of drugs in our training set. The correlogram is shown in the figure 26, and the circled peaks contribute favorably to the biological activity of KCNN4 inhibitors, whereas three of the factors contribute negatively. Our compounds with activity values (pIC_{50}) equal to

or less than 7.02 were classified as actives and compounds with activity values less than 6.4 as inactive by the GRIND model.

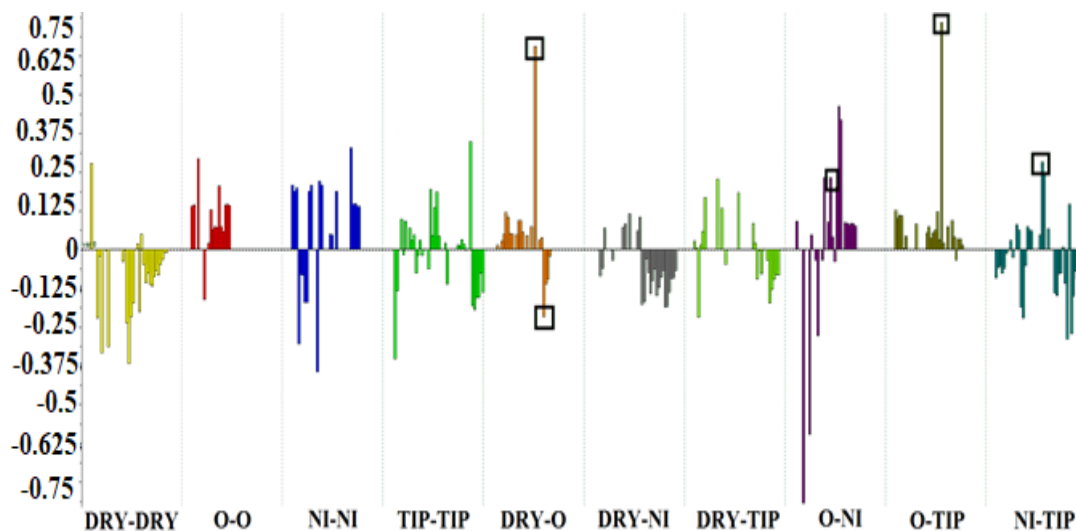


Figure 26: Correlogram of GRIND model for the KCNN4 inhibitors explaining the contribution of DRY-O, O-NI, O-TIP, and NI-TIP towards activity in a positive manner.

The peaks of the correlogram were effective in distinguishing the difference between the actives and inactive. 5 among 10 features depicted the biological properties of the residues in the molecules and the mutual distance between them.

In the correlogram, the DRY – O peak elucidates the link between one hydrophobic and one hydrogen bond acceptor with a mutual distance of 9.60 – 10.00 in the KCNN4 inhibitor's virtual receptor site as represented in the figure 27. The distance was validated by the presence of Glutamine353; acting as a hydrogen bond acceptor (O) and Methionine302; acting as a hydrophobic residue (DRY) at the same distance around the common scaffold as predicted by the pentacle i.e. between 9.60 – 10.00.

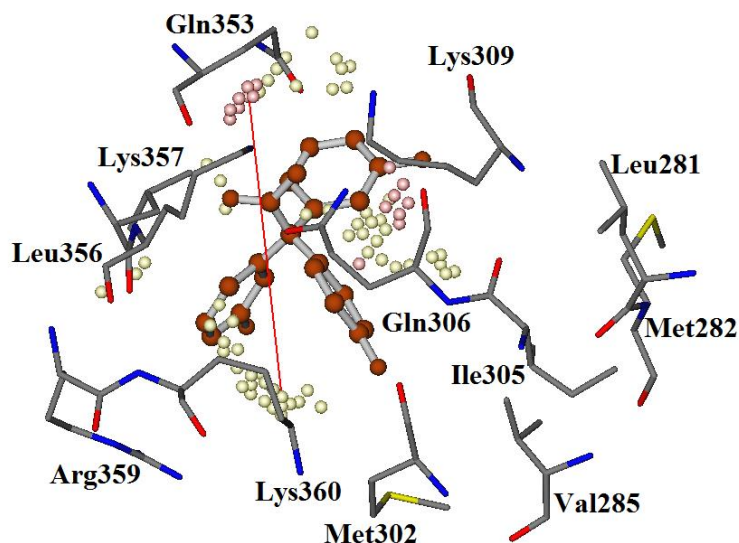


Figure 27: The virtual receptor site (hotspot) of KCNN4 against the Gárdos43 (the most active compound in the dataset). The virtual site is consistent with the actual receptor site where the presence of Lys360 and Gln353 at a certain distance complements the hydrophobic and hydrogen bond acceptor regions in the virtual receptor site respectively.

The distance feature is evident in most of the highly active drugs ($IC_{50} = 15 - 66$ nM) that belonged to class 1 of ligands having a specific common scaffold as presented in the figure 36. The distance feature is not present in the least active compounds ($IC_{50} = 1750 - 33000$) and the active compounds belonging to the other class of ligands. Some of the ligands belonging to class 1 of active compounds were not recognized by the DRY – NI feature. It is hypothesized that the presence of fluorine at diverse positions i.e., ortho, meta, and para of the benzene ring in the common scaffold (Fig. 28), maybe a distinguishing factor to exclude other ligands of class 1 from this feature. However, the presence of Glu353 (hydrogen bond acceptor) and Met302 (hydrophobic residue) also strengthens and complements the accuracy of the GRIND model and validates the results of docking.

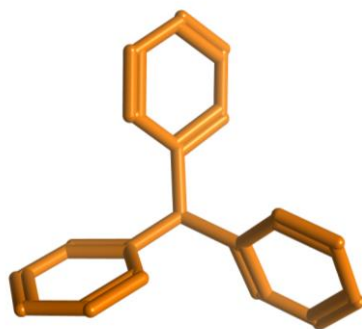


Figure 28: The common scaffold for class 1.

In the correlogram, the O – NI peak elucidates the link between one hydrogen-bond acceptor and one hydrogen bond donor that contributes in a positive manner towards the biological activity for the KCNN4 inhibitors. The mutual distance elucidated between these two features was estimated to be in a range of 8.40 – 8.80 in the KCNN4 inhibitor's virtual receptor site as represented in the figure 29. The distance was validated by the presence of Glutamine306; acting as a hydrogen bond acceptor (NI) and Lysine360; acting as a hydrogen bond donor (O) present at the same distance around the common scaffold as predicted by the pentacle i.e. between 8.40 – 8.80.

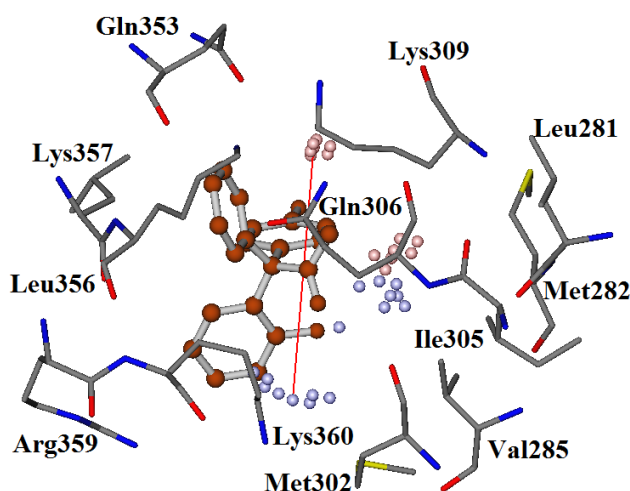


Figure 29: The virtual receptor site (hotspot) of KCNN4 against the Gárdos43 (the most active compound in the dataset). The virtual site is consistent with the actual receptor site where the presence of Lys360 and Gln306 at a certain distance complements the hydrogen bond donor and hydrogen bond acceptor regions in the virtual receptor site respectively.

The distance feature is evident in almost all the highly active drugs of class 1 ($IC_{50} = 9 - 39$ nM). The distance is not present in the least active compounds ($IC_{50} = 1750 - 33000$), compounds that belong to other classes, or some actives of class 1 having a Chloride or Nitrogen atom attached to the benzene ring.

However, the presence of Gln306 (hydrogen bond acceptor) and Lys360 (hydrogen bond donor) also strengthens and complements the accuracy of the GRIND model and validates the results of docking.

In the correlogram, the O – TIP peak elucidates the link between one hydrogen bond acceptor and one shape-based feature that contributes in a positive manner towards the biological activity for the KCNN4 inhibitors. The mutual distance elucidated between these two features was estimated to be in a range of 10.40 – 10.80 in the KCNN4 inhibitor's virtual receptor site as represented in the figure 30. The distance was validated by the presence of Glutamine306; acting as a hydrogen bond acceptor (O) and Arginine359; acting as a shape-based residue (TIP) present at the edges of the inhibitor of KCNN4 at the same distance around the common scaffold as predicted by the pentacle i.e. between 10.40 – 10.80.

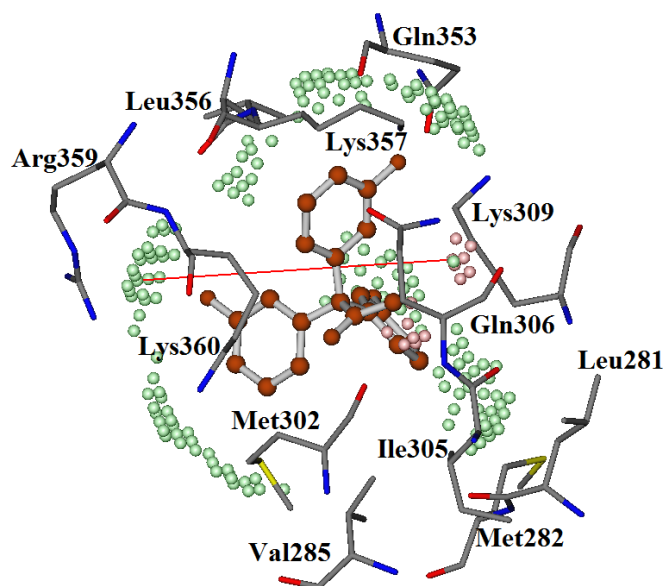


Figure 30: The virtual receptor site (hotspot) of KCNN4 against the Gárdos43 (the most active compound in the dataset). The virtual site is consistent with the actual receptor site where the presence of Gln306 and Arg359 at a certain distance

complements the hydrogen bond acceptor and shape-based regions in the virtual receptor site respectively.

The distance feature is evident in some of the highly active drugs ($IC_{50} = 10 - 40$ nM) belonging to class 1 of the ligands. The distance is not present in the least active compounds ($IC_{50} = 1750 - 33000$) and other active compounds of class 1. It was hypothesized that the position of fluorine at diverse positions i.e. ortho, para, and meta, plays a crucial role in the determining of O – TIP feature.

However, the presence of Gln306 (hydrogen bond acceptor) and Arg359 (shape-based residue) also strengthens and complements the accuracy of the GRIND model and validates the results of docking.

In the correlogram, the NI – TIP peak elucidates the link between one hydrogen bond donor and one shape-based feature that contributes in a positive manner towards the biological activity for the KCNN4 inhibitors. The mutual distance elucidated between these two features was estimated to be in a range of 10.40 – 10.80 in the KCNN4 inhibitor's virtual receptor site as represented in the figure 31. The distance was validated by the presence of Glutamine306; acting as a hydrogen bond donor (NI) and Arginine359; acting as a shape-based residue (TIP) present at the edges of the inhibitor of KCNN4 at the same distance around the common scaffold as predicted by the pentacle i.e. between 10.40 – 10.80.

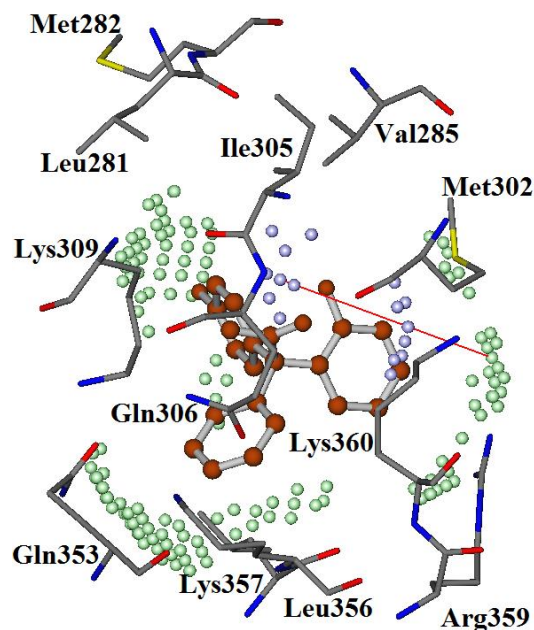


Figure 31: The virtual receptor site (hotspot) of KCNN4 against the Gárdos43 (the most active compound in the dataset). The virtual site is consistent with the actual receptor site where the presence of Gln306 and Arg359 at a certain distance complements the hydrogen-bond donor and shape-based regions in the virtual receptor site respectively.

The distance feature is evident in some of the highly active drugs ($IC_{50} = 9 - 51$ nM) belonging to class 1 of the ligands. The distance is not present in the least active compounds ($IC_{50} = 1750 - 33000$) and other active compounds of class 1.

However, the presence of Gln306 (hydrogen bond donor) and Arg359 (shape-based residue) also strengthens and complements the accuracy of the GRIND model and validates the results of docking.

The difference between actual and predicted values of the 51 ligands was calculated to obtain residual values. The difference was less than 1 log unit. All the ligands having difference > 1 and difference < -1 were separated. 15 ligands had a difference > 1 while 10 ligands had a difference < -1 . The table 14 shows these 25 ligands with their residual values.

Table 14: 25 among 51 ligands that showed the residual value >1 and < -1. Among the 25 ligands, 5 ligands had residual value > 1.5 or < -1.5

Ligand Name	Exp Values	Pred Values	Res Values	Difference (1 to -1)	Difference (1.5 to -1.5)
Gárdos_29	7.82	6.21	1.60	Difference > 1	Difference > 1.5
Gárdos_38	7.69	6.11	1.58		
Gárdos_12	7.69	6.11	1.58		
Gárdos_39	7.52	6.16	1.35		
Gárdos_6	7.46	6.12	1.34		
Gárdos_2	7.52	6.20	1.32		
Gárdos_24	7.40	6.14	1.26		
Gárdos_4	7.31	6.09	1.21		
Gárdos_25	7.38	6.18	1.20		
Gárdos_23	7.30	6.14	1.16		
Gárdos_9	7.28	6.12	1.16		
Gárdos_50	7.22	6.12	1.09		
Gárdos_8	7.15	6.12	1.03		
Gárdos_31	7.18	6.15	1.026		
Gárdos_44	5.10	6.23	-1.12	Difference < -1	
Gárdos_48	5.00	6.14	-1.14		
Gárdos_10	5.00	6.16	-1.16		
Gárdos_35	4.85	6.05	-1.20		
Gárdos_19	4.88	6.13	-1.25		
Gárdos_11	5.11351	6.37727	-1.26376		
Gárdos_46	4.85387	6.13314	-1.27927		
Gárdos_36	4.79588	6.19199	-1.39611		

Gárdos_47	4.74473	6.17414	-1.42941	
Gárdos_45	4.50864	6.08786	-1.57922	Difference < -
Gárdos_15	4.48149	6.17238	-1.69089	1.5

A graph was plotted between the actual and predicted pIC_{50} values, with actual values on the y-axis and predicted values on the x-axis to check the outliers i.e. the ligands with high residual values. The plot helps in easy identification of the outliers as attached in the figure 32.

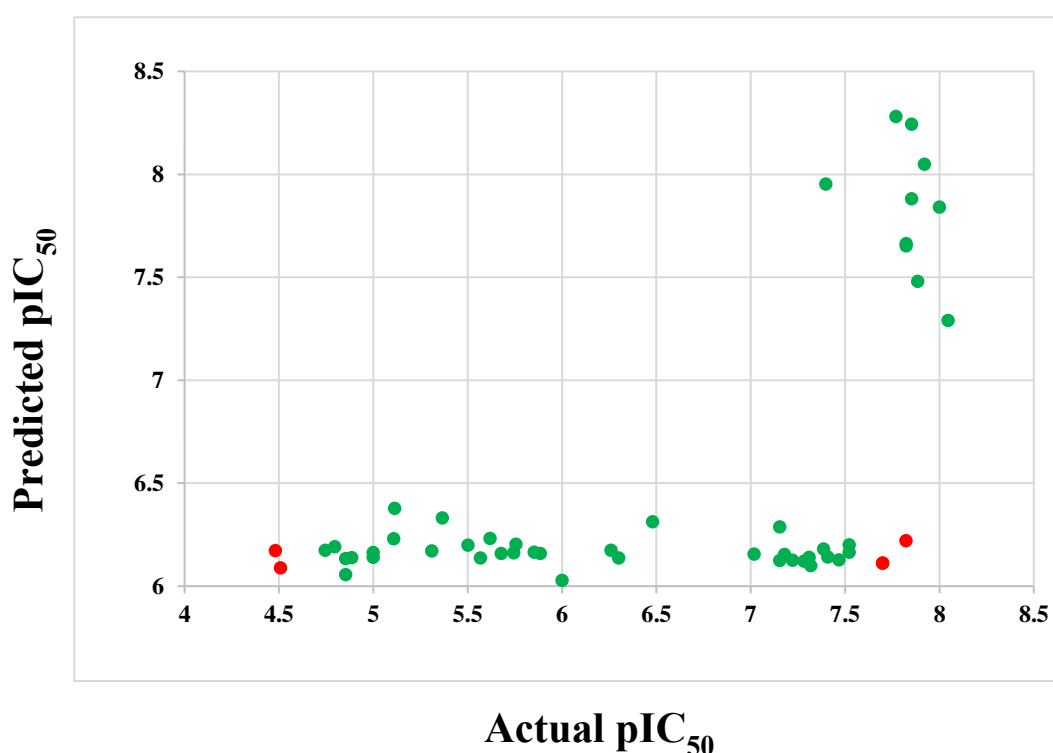


Figure 32: Actual vs predicted pIC_{50} for the GRIND model. The red dots in the plot shows ligands having residual > 1.5 and < -1.5 , and the green dots show ligands having residual values between 1 to -1

The behavior of 5 outliers having residual values > 1.5 and < -1.5 were checked. The outliers with residual value > 1.5 were **Gárdos_12**, **Gárdos_29**, and **Gárdos_38** whereas the ones with residual value < -1.5 were **Gárdos_15** and **Gárdos_45**.

The graph of pIC_{50} vs $\log P$ (o/w) was plotted to check the behavior of lipophilicity on activity for these 5 outliers (Fig. 33).

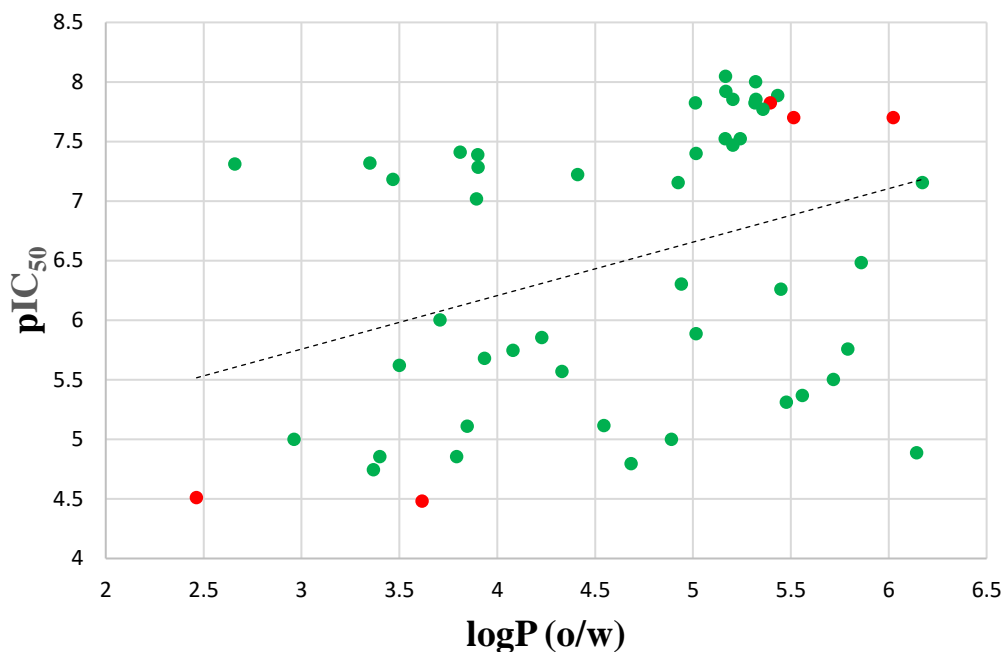
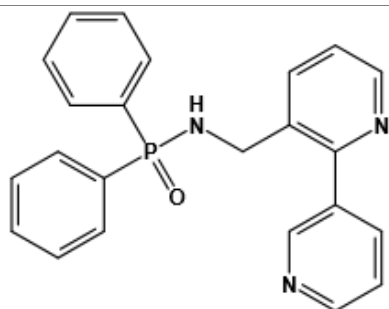


Figure 33: the graph constructed between pIC₅₀ of the ligands and the logP (o/w) to link activity with lipophilicity. The red dots represent those ligands having residual values > 1.5 and < -1.5.

Gárdos_15 and **Gárdos_45** were visualized to identify the structures that lead towards a constant activity but different lipophilicity. It might be possible that certain atoms in the **Gárdos_15** and **Gárdos_45** ligands enhance or reduce the permeability of the ligands into the membrane. The table 15 represents both ligands and their structure. It can be hypothesized that the more nitrobenzene in the structure, the more is the hydrophobicity of the ligands. Two nitrobenzenes in **Gárdos_15** lead towards a greater value of logP (o/w). It makes the ligand more hydrophobic than the **Gárdos_45**. The hydrophobic nature of the ligand aids towards easy transport of the ligand through the membrane; a better transport. Therefore, the difference in logP (o/w) can be attributed to the presence of nitrobenzene in **Gárdos_15** that is absent in **Gárdos_45**, thus making **Gárdos_45** less hydrophobic.

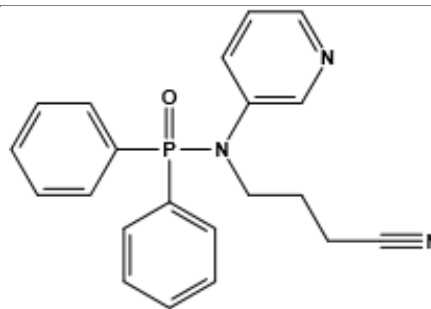
Table 15: Two of the least active compounds with their pIC₅₀ and logP (o/w) and a residual difference between the actual and predicted pIC₅₀ < -1.5



Gárdos_15

pIC₅₀ = 4.4814858

logP(o/w) = 3.6159999



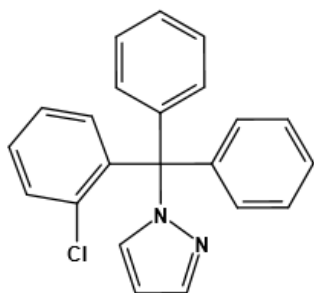
Gárdos_45

pIC₅₀ = 4.5086384

logP(o/w) = 2.464

Gárdos_12, **Gárdos_29**, and **Gárdos_38** were visualized to identify the structures that lead towards a constant activity but different lipophilicity. **Gárdos_29** slightly differed in the activity, although **Gárdos_12** and **Gárdos_38** had the same activity values. The structure of all three ligands with logP (o/w) and pIC₅₀ are represented in the table 16.

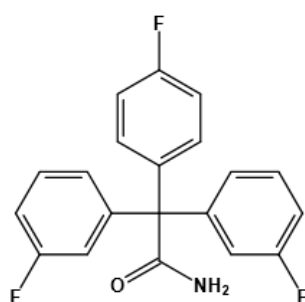
Table 16: Active compounds with their pIC₅₀ and logP (o/w) and a residual difference between the actual and predicted pIC₅₀ > 1.5



Gárdos 12

pIC₅₀ = 7.70

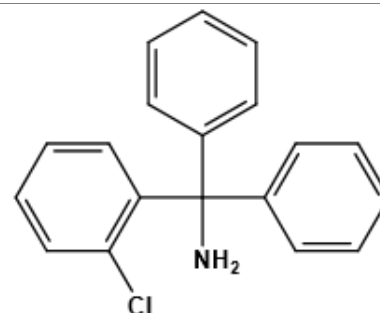
logP(o/w) = 6.02



Gárdos 29

pIC₅₀ = 7.82

logP(o/w) = 5.40



Gárdos 38

pIC₅₀ = 7.70

logP(o/w) = 5.51

The higher logP is for **Gárdos_12** as compared to **Gárdos_29** and **Gárdos_38**. It can be hypothesized that the presence of 1,2 di-nitro pentene along with a halogen group; specifically, chlorine, aids towards better lipophilicity. The 1,2 di-nitro pentene.

The group is not present in **Gárdos_29** and **Gárdos_38**. Even though the chloride group is present in **Gárdos_38**, but it alone cannot help in enhanced permeability of the ligand. Also, there is a slight difference in the lipophilicity of the three compounds, therefore, it might be possible that the attachment of the halogen group with the ligands at any position is a contributing factor towards the enhanced lipophilicity and greater transport (permeability) of the ligand across the bio membrane.

Chapter 5

Discussion

There is no solution to stop the spread of hereditary diseases, however, the treatment of such diseases is possible by the administration of different drugs and other therapeutic procedures. The mutations of the Gárdos channel are one among many disorders that lead towards the dehydration of red blood cells causing a subtype of anemia known as Hereditary Xerocytosis. The disease is treated with several inhibitors such as antimycotic clotrimazole [116] and TRAM-34 [117]. However, their inability to target all the three mutations i.e., R352H, V282E, and V282M [102], causes a hindrance in their selectivity profile. Moreover, most of the research done on Gárdos Channel was in-vitro and in-vivo. The structure of the Gárdos channel was published in 2018 [107]. There were structural limitations for employing computational research on the Gárdos channel and there was no mutant structure available for the channel. Due to the lack of sufficient data, and a limited number of ligand dataset; obtained from ChEMBL, the present research, with the use of the existing structure, modeled the mutant structure for the Gárdos channel consisting of the most common mutations known as R352H and the V282M. The publication of cyro-EM structure of Gárdos channel facilitated the way towards predictions. And predictions are always recommended for experimentation to reduce the time and cost for experimentation. Therefore, present research opened new avenues for the *in-silico* analysis of these mutant structures.

The present research predicted the 3D features for the inhibitors of the Gárdos Channel. The 3D features are the principal component for computational drug design. The previous efforts done by researchers were wholly based on personal experience, knowledge, and experimentation [34, 96, 102, 103]. The predicted feature design can help in improving the properties of the drug. Also, these predictions can aid in the design of new compounds/drug-like entities. It can also enhance the properties of the drug. The recent research added value by predicting the activity of drugs based on several interactions and lipophilicity patterns. Same interactions were found around all the ligands and the GRIND analysis too provided features that were consistent with the

docking output. The research can likely aid in the development of potential drug targets that can be elective against all the three types of mutations and open further avenues in drug discovery against the Gárdos channel, aiding in the control of different diseases associated with it such as sickle cell anemia [134], hereditary spherocytosis [135], and hereditary elliptocytosis [136].

Conclusion

The present research utilized a computational drug design approach to construct the mutant 3D structure of the KCNN4 channel. The hereditary mutations in the Gárdos channel make the channel less sensitive to Ca^{2+} , allowing a lesser concentration of Ca^{2+} to open the channel and lead towards the pathogenicity. The mutant 3D structure of this channel was modeled using a homology model to open new avenues towards drug discovery. The molecular docking of the small dataset of inhibitors against the KCNN4 channel helped in attaining the best conformations of the Gárdos channel that were able to differentiate the highly active compounds/inhibitors with the least active compounds/inhibitors. Also, it predicted the best interaction between the ligands dataset and the mutant protein structure, making **Lys 309** an important residue in the protein that facilitates maximum interactions with the ligand dataset. The model for the mutated Gárdos channel was constructed against the dataset of 51 inhibitors to extract the features that had a positive and negative impact on the activity of the inhibitors. Four features represented by correlogram DRY-O, O-NI, O-TIP, and NI-TIP impacted the activity in a positive manner. These features are **Hydrophobic and Hydrogen bond acceptor** feature at a distance **9.60 – 10.00**, **Hydrogen – bond acceptor** and **Hydrogen bond donor** feature at a distance of **8.40 – 8.80**, **Hydrogen- bond acceptor** and **shape-based** feature at a distance of **10.40 – 10.80**, and **Hydrogen- bond donor** and **shape-based feature** at a distance of **10.40 – 10.80** in the virtual receptor site. These features were complementary with the **Glutamine 353**, **Methionine 302**, **Lysine 360**, **Glutamine 306** and **Arginine 359** residues in the actual receptor site. The GRIND model, predicted in this research, can be of particular importance since it can help in the development of new drugs/compounds based on these features. Therefore, the present research can be an asset in the *in-silico* analysis of the KCNN4 channel, the mutations associated with it, and the design of new drugs that can treat the diseases associated with KCNN4.

References

- [1] G. W. Stewart, "3 The membrane defect in hereditary stomatocytosis," *Baillière's clinical haematology*, vol. 6, no. 2, pp. 371-399, 1993.
- [2] S. E. Lux, "Disorders of the red cell membrane," *Principles practise of Haematology*, pp. 1701-1818, 1995.
- [3] K. M. McGrath, M. Collecutt, A. Gordon, R. Sawers, and B. Faragher, "Dehydrated hereditary stomatocytosis-a report of two families and a review of the literature," *Pathology*, vol. 16, no. 2, pp. 146-150, 1984.
- [4] N. Archer, B. E. Shmukler, I. Andolfo, D. H. Vandorpe, R. Gnanasambandam, J. M. Higgins, A. Rivera, M. D. Fleming, F. Sachs, and P. A. Gottlieb, "Hereditary xerocytosis revisited," *American journal of hematology*, vol. 89, no. 12, pp. 1142, 2014.
- [5] R. Zarychanski, V. P. Schulz, B. L. Houston, Y. Maksimova, D. S. Houston, B. Smith, J. Rinehart, and P. G. Gallagher, "Mutations in the mechanotransduction protein PIEZO1 are associated with hereditary xerocytosis," *Blood*, vol. 120, no. 9, pp. 1908-1915, 2012.
- [6] I. Andolfo, S. L. Alper, L. De Franceschi, C. Auriemma, R. Russo, L. De Falco, F. Vallefucio, M. R. Esposito, D. H. Vandorpe, and B. E. J. B. Shmukler, *The Journal of the American Society of Hematology*, "Multiple clinical forms of dehydrated hereditary stomatocytosis arise from mutations in PIEZO1," vol. 121, no. 19, pp. 3925-3935, 2013.
- [7] C. Bae, P. A. Gottlieb, and F. Sachs, "Human PIEZO1: removing inactivation," *Biophysical journal*, vol. 105, no. 4, pp. 880-886, 2013.
- [8] A. D. Maher, and P. W. Kuchel, "The Gárdos channel: a review of the Ca^{2+} - activated K^{+} channel in human erythrocytes," *The international journal of biochemistry & cell biology*, vol. 35, no. 8, pp. 1182-1197, 2003.
- [9] R. Rapetti-Mauss, C. Lacoste, V. Picard, C. Guitton, E. Lombard, M. Loosveld, V. Nivaggioni, N. Dasilva, D. Salgado, and J.-P. J. B. Desvignes, *The Journal of the American Society of Hematology*, "A mutation in the Gárdos channel is associated with hereditary xerocytosis," vol. 126, no. 11, pp. 1273-1280, 2015.

- [10] D. R. Miller, F. R. Rickles, M. A. Lichtman, P. L. La Celle, J. Bates, and R. I. Weed, "A new variant of hereditary hemolytic anemia with stomatocytosis and erythrocyte cation abnormality," *Blood*, vol. 38, no. 2, pp. 184-204, 1971.
- [11] B. E. Glader, N. Fortier, M. M. Albala, and D. G. Nathan, "Congenital hemolytic anemia associated with dehydrated erythrocytes and increased potassium loss," *New England Journal of Medicine*, vol. 291, no. 10, pp. 491-496, 1974.
- [12] G. R. Nolan, "Hereditary xerocytosis a case history and review of the literature," *Pathology*, vol. 16, no. 2, pp. 151-154, 1984.
- [13] J. S. Wiley, "Inherited red cell dehydration: a hemolytic syndrome in search of a name," Taylor & Francis, 1984.
- [14] I. Andolfo, R. Russo, A. Gambale, and A. J. A. j. o. h. Iolascon, "Hereditary stomatocytosis: an underdiagnosed condition," vol. 93, no. 1, pp. 107-121, 2018.
- [15] I. Andolfo, R. Russo, B. E. Rosato, F. Manna, A. Gambale, C. Brugnara, and A. J. A. j. o. h. Iolascon, "Genotype-phenotype correlation and risk stratification in a cohort of 123 hereditary stomatocytosis patients," vol. 93, no. 12, pp. 1509-1517, 2018.
- [16] A. Caulier, R. Rapetti-Mauss, H. Guizouarn, V. Picard, L. Garçon, and C. J. I. j. o. l. h. Badens, "Primary red cell hydration disorders: pathogenesis and diagnosis," vol. 40, pp. 68-73, 2018.
- [17] V. Picard, C. Guitton, I. Thuret, C. Rose, L. Bendelac, K. Ghazal, P. Aguilar-Martinez, C. Badens, C. Barro, and C. Bénéteau, "Clinical and biological features in PIEZO1-hereditary xerocytosis and Gárdos channelopathy: a retrospective series of 126 patients," *Haematologica*, vol. 104, no. 8, pp. 1554, 2019.
- [18] T. M. Ishii, C. Silvia, B. Hirschberg, C. T. Bond, J. P. Adelman, and J. Maylie, "A human intermediate conductance calcium-activated potassium channel," *Proceedings of the National Academy of Sciences*, vol. 94, no. 21, pp. 11651-11656, 1997.
- [19] K. I. Ataga, W. R. Smith, L. M. De Castro, P. Swerdlow, Y. Sauntharajah, O. Castro, E. Vichinsky, A. Kutlar, E. P. Orringer, and G. C. Rigdon, "Efficacy and safety of the Gárdos channel blocker, senicapoc (ICA-17043),

- in patients with sickle cell anemia,” *Blood*, vol. 111, no. 8, pp. 3991-3997, 2008.
- [20] S. Brähler, A. Kaistha, V. J. Schmidt, S. E. Wölfle, C. Busch, B. P. Kaistha, M. Kacik, A.-L. Hasenau, I. Grgic, and H. Si, “Genetic deficit of SK3 and IK1 channels disrupts the endothelium-derived hyperpolarizing factor vasodilator pathway and causes hypertension,” *Circulation*, vol. 119, no. 17, pp. 2323-2332, 2009.
- [21] H. Lallet-Daher, M. Roudbaraki, A. Bavencoffe, P. Mariot, F. Gackiere, G. Bidaux, R. Urbain, P. Gosset, P. Delcourt, and L. Fleurisse, “Intermediate-conductance Ca²⁺-activated K⁺ channels (IK Ca1) regulate human prostate cancer cell proliferation through a close control of calcium entry,” *Oncogene*, vol. 28, no. 15, pp. 1792-1806, 2009.
- [22] T. L. Peña, S. H. Chen, S. F. Konieczny, and S. G. Rane, “Ras/MEK/ERK up-regulation of the fibroblast KCaChannel FIK is a common mechanism for basic fibroblast growth factor and transforming growth factor- β suppression of myogenesis,” *Journal of Biological Chemistry*, vol. 275, no. 18, pp. 13677-13682, 2000.
- [23] A. C. Gerlach, C. A. Syme, L. Giltinan, J. P. Adelman, and D. C. Devor, “ATP-dependent activation of the intermediate conductance, Ca²⁺-activated K⁺ channel, hIK1, is conferred by a C-terminal domain,” *Journal of Biological Chemistry*, vol. 276, no. 14, pp. 10963-10970, 2001.
- [24] A. Cheong, A. J. Bingham, J. Li, B. Kumar, P. Sukumar, C. Munsch, N. J. Buckley, C. B. Neylon, K. E. Porter, and D. J. Beech, “Downregulated REST transcription factor is a switch enabling critical potassium channel expression and cell proliferation,” *Molecular cell*, vol. 20, no. 1, pp. 45-52, 2005.
- [25] I. Andolfo, R. Russo, F. Manna, B. E. Shmukler, A. Gambale, G. Vitiello, G. De Rosa, C. Brugnara, S. L. Alper, and L. M. J. A. j. o. h. Snyder, “Novel Gárdos channel mutations linked to dehydrated hereditary stomatocytosis (xerocytosis),” vol. 90, no. 10, pp. 921-926, 2015.
- [26] E. Glogowska, K. Lezon-Geyda, Y. Maksimova, V. P. Schulz, and P. G. Gallagher, “Mutations in the Gárdos channel (KCNN4) are associated with hereditary xerocytosis,” *Blood*, vol. 126, no. 11, pp. 1281-1284, 2015.

- [27] G. Gárdos, “The function of calcium in the potassium permeability of human erythrocytes,” *Biochimica et biophysica acta*, vol. 30, no. 3, pp. 653-654, 1958.
- [28] C. M. Fanger, S. Ghanshani, N. J. Logsdon, H. Rauer, K. Kalman, J. Zhou, K. Beckingham, K. G. Chandy, M. D. Cahalan, and J. Aiyar, “Calmodulin mediates calcium-dependent activation of the intermediate conductance KCa channel, IKCa1,” *Journal of Biological Chemistry*, vol. 274, no. 9, pp. 5746-5754, 1999.
- [29] R. Gilli, D. Lafitte, C. Lopez, M.-C. Kilhoffer, A. Makarov, C. Briand, and J. Haiech, “Thermodynamic analysis of calcium and magnesium binding to calmodulin,” *Biochemistry*, vol. 37, no. 16, pp. 5450-5456, 1998.
- [30] M.-C. Kilhoffer, T. J. Lukas, D. M. Watterson, and J. Haiech, “The heterodimer calmodulin: myosin light-chain kinase as a prototype vertebrate calcium signal transduction complex,” *Biochimica et Biophysica Acta -Protein Structure Molecular Enzymology*, vol. 1160, no. 1, pp. 8-15, 1992.
- [31] P. Morales, L. Garneau, H. Klein, M.-F. Lavoie, L. Parent, and R. J. J. o. G. P. Sauvé, “Contribution of the KCa3. 1 channel–calmodulin interactions to the regulation of the KCa3. 1 gating process,” vol. 142, no. 1, pp. 37-60, 2013.
- [32] L. Garneau, H. Klein, U. Banderali, A. Longprá-Lauzon, L. Parent, and R. J. J. o. B. C. Sauvá, “Hydrophobic interactions as key determinants to the KCa3. 1 channel closed configuration: An analysis of KCa3. 1 mutants constitutively active in zero Ca²⁺,” vol. 284, no. 1, pp. 389-403, 2009.
- [33] H. Klein, L. Garneau, U. Banderali, M. Simoes, L. Parent, and R. Sauvé, “Structural determinants of the closed KCa3. 1 channel pore in relation to channel gating: results from a substituted cysteine accessibility analysis,” *The Journal of general physiology*, vol. 129, no. 4, pp. 299-315, 2007.
- [34] L. Sforza, A. Megaro, M. Pessia, F. Franciolini, and L. Catacuzzeno, “Structure, gating and basic functions of the Ca²⁺ -activated K channel of intermediate conductance,” *Current neuropharmacology*, vol. 16, no. 5, pp. 608-617, 2018.
- [35] E. Fermo, A. Bogdanova, P. Petkova-Kirova, A. Zaninoni, A. P. Marcello, A. Makhro, P. Hänggi, L. Hertz, J. Danielczok, and C. Vercellati, “‘Gárdos Channelopathy’: a variant of hereditary Stomatocytosis with complex molecular regulation,” *Scientific reports*, vol. 7, no. 1, pp. 1-13, 2017.

- [36] R. Rapetti-Mauss, O. Soriani, H. Vinti, C. Badens, and H. J. H. Guizouarn, "Senicapoc: a potent candidate for the treatment of a subset of hereditary xerocytosis caused by mutations in the Gárdos channel," vol. 101, no. 11, pp. e431, 2016.
- [37] G. Blanco, and R. W. Mercer, "Isozymes of the Na-K-ATPase: heterogeneity in structure, diversity in function," *American Journal of Physiology-Renal Physiology*, vol. 275, no. 5, pp. F633-F650, 1998.
- [38] J. F. Hoffman, A. Wickrema, O. Potapova, M. Milanick, and D. R. Yingst, "Na pump isoforms in human erythroid progenitor cells and mature erythrocytes," *Proceedings of the National Academy of Sciences*, vol. 99, no. 22, pp. 14572-14577, 2002.
- [39] A. Bogdanova, and H. U. Lutz, "Mechanisms tagging senescent red blood cells for clearance in healthy humans," *Frontiers in physiology*, vol. 4, pp. 387, 2013.
- [40] A. Dyrda, U. Cytlak, A. Ciuraszkiewicz, A. Lipinska, A. Cuff, G. Bouyer, S. Egée, P. Bennekou, V. L. Lew, and S. L. Thomas, "Local membrane deformations activate Ca²⁺-dependent K⁺ and anionic currents in intact human red blood cells," *PLoS ONE*, vol. 5, no. 2, pp. e9447, 2010.
- [41] C. Brugnara, and L. de Franceschi, "[Clinical trials of new therapeutic pharmacology for sickle cell disease]," *Sante*, vol. 16, no. 4, pp. 263-8, Oct-Dec, 2006.
- [42] C.-C. Chou, C. A. Lunn, and N. J. Murgolo, "KCa3. 1: target and marker for cancer, autoimmune disorder and vascular inflammation?," *Expert review of molecular diagnostics*, vol. 8, no. 2, pp. 179-187, 2008.
- [43] H. Jäger, T. Dreker, A. Buck, K. Giehl, T. Gress, and S. Grissmer, "Blockage of intermediate-conductance Ca²⁺-activated K⁺ channels inhibit human pancreatic cancer cell growth in vitro," *Molecular pharmacology*, vol. 65, no. 3, pp. 630-638, 2004.
- [44] I. Grgic, E. Kiss, B. P. Kaistha, C. Busch, M. Kloss, J. Sautter, A. Müller, A. Kaistha, C. Schmidt, and G. Raman, "Renal fibrosis is attenuated by targeted disruption of KCa3. 1 potassium channels," *Proceedings of the National Academy of Sciences*, vol. 106, no. 34, pp. 14518-14523, 2009.

- [45] C. Huang, C. A. Pollock, and X.-M. Chen, "KCa_{3.1}: a new player in progressive kidney disease," *Current opinion in nephrology and hypertension*, vol. 24, no. 1, pp. 61-66, 2015.
- [46] H. Wulff, and N. A. J. E. r. o. c. p. Castle, "Therapeutic potential of KCa_{3.1} blockers: recent advances and promising trends," vol. 3, no. 3, pp. 385-396, 2010.
- [47] K. Toyama, H. Wulff, K. G. Chandy, P. Azam, G. Raman, T. Saito, Y. Fujiwara, D. L. Mattson, S. Das, and J. E. Melvin, "The intermediate-conductance calcium-activated potassium channel KCa_{3.1} contributes to atherogenesis in mice and humans," *The Journal of clinical investigation*, vol. 118, no. 9, pp. 3025-3037, 2008.
- [48] J. Rinehart, E. E. Gulcicek, C. H. Joiner, R. P. Lifton, and P. G. Gallagher, "Determinants of erythrocyte hydration in current opinion in hematology," *Current opinion in hematology*, vol. 17, no. 3, pp. 191, 2010.
- [49] H. Wulff, and R. Köhler, "Endothelial Small-Conductance and Intermediate-Conductance KCa Channels: An Update on Their Pharmacology and Usefulness as Cardiovascular Targets," vol. 61, no. 2, pp. 102-112, 2013.
- [50] T. Simons, "Calcium-dependent potassium exchange in human red cell ghosts," *The Journal of physiology*, vol. 256, no. 1, pp. 227-244, 1976.
- [51] P. Stampe, and B. Vestergaard-Bogind, "Ca²⁺-activated K⁺ conductance of the human red cell membrane: voltage-dependent Na⁺ block of outward-going currents," *The Journal of membrane biology*, vol. 112, no. 1, pp. 9-14, 1989.
- [52] A. Heinz, and H. Passow, "Role of external potassium in the calcium-induced potassium efflux from human red blood cell ghosts," *The Journal of membrane biology*, vol. 57, no. 2, pp. 119-131, 1980.
- [53] R. Grygorczyk, W. Schwarz, and H. Passow, "Ca²⁺-activated K⁺ channels in human red cells. Comparison of single-channel currents with ion fluxes," *Biophysical journal*, vol. 45, no. 4, pp. 693-698, 1984.
- [54] B. Vestergaard-Bogind, P. Stampe, and P. Christophersen, "Voltage dependence of the Ca²⁺-activated K⁺ conductance of human red cell membranes is strongly dependent on the extracellular K⁺ concentration," *The Journal of membrane biology*, vol. 95, no. 2, pp. 121-130, 1987.
- [55] H. Gilboa, B. E. Chapman, and P. W. Kuchel, "19F NMR magnetization transfer between 5-FBAPTA and its complexes. An alternative means for

- measuring free Ca^{2+} concentration, and detection of complexes with protein in erythrocytes,” *NMR in Biomedicine*, vol. 7, no. 7, pp. 330-338, 1994.
- [56] D. R. Yingst, and J. F. Hoffman, “Ca-induced K transport in human red blood cell ghosts containing arsenazo III. Transmembrane interactions of Na, K, and Ca and the relationship to the functioning Na-K pump,” *The Journal of general physiology*, vol. 83, no. 1, pp. 19-45, 1984.
- [57] T. Leinders, R. G. Kleef, and H. P. Vijverberg, “Single Ca^{2+} -activated K^{+} channels in human erythrocytes: Ca^{2+} dependence of opening frequency but not of open lifetimes,” *Biochimica et Biophysica Acta -Biomembranes*, vol. 1112, no. 1, pp. 67-74, 1992.
- [58] R. Grygorczyk, and W. Schwarz, “Properties of the Ca^{2+} -activated K^{+} conductance of human red cells as revealed by the patch-clamp technique,” *Cell calcium*, vol. 4, no. 5-6, pp. 499-510, 1983.
- [59] S. L. Ørskov, *Untersuchungen über den Einfluß von Kohlensäure und Blei auf die Permeabilität der Blutkörperchen für Kalium und Rubidium*, 1935.
- [60] J. R. Riordan, and H. Passow, “Effects of calcium and lead on potassium permeability of human erythrocyte ghosts,” *Biochimica et Biophysica Acta - Biomembranes*, vol. 249, no. 2, pp. 601-605, 1971.
- [61] T. Simons, “Influence of lead ions on cation permeability in human red cell ghosts,” *The Journal of membrane biology*, vol. 84, no. 1, pp. 61-71, 1985.
- [62] T. Simons, “Passive transport and binding of lead by human red blood cells,” *The Journal of Physiology*, vol. 378, no. 1, pp. 267-286, 1986.
- [63] T. Simons, “The role of anion transport in the passive movement of lead across the human red cell membrane,” *The Journal of physiology*, vol. 378, no. 1, pp. 287-312, 1986.
- [64] B. Lal, G. Goldstein, and J. P. Bressler, “Role of anion exchange and thiol groups in the regulation of potassium efflux by lead in human erythrocytes,” *Journal of cellular physiology*, vol. 167, no. 2, pp. 222-228, 1996.
- [65] B. Del Carlo, M. Pellegrini, and M. Pellegrino, “Modulation of Ca^{2+} -activated K^{+} channels of human erythrocytes by endogenous protein kinase C,” *Biochimica et Biophysica Acta -Biomembranes*, vol. 1612, no. 1, pp. 107-116, 2003.
- [66] L. Soldati, D. Adamo, R. Spaventa, G. Bianchi, and G. Vezzoli, “Chloride fluxes activated by parathyroid hormone in human erythrocytes,” *Biochemical*

- and Biophysical Research Communications*, vol. 269, no. 2, pp. 470-473, 2000.
- [67] Q. Li, V. Jungmann, A. Kiyatkin, and P. S. Low, "Prostaglandin E2 stimulates a Ca²⁺-dependent K⁺ channel in human erythrocytes and alters cell volume and filterability," *Journal of Biological Chemistry*, vol. 271, no. 31, pp. 18651-18656, 1996.
- [68] C.-H. Lee, and R. J. S. MacKinnon, "Activation mechanism of a human SK-calmodulin channel complex elucidated by cryo-EM structures," vol. 360, no. 6388, pp. 508-513, 2018.
- [69] C. A. Syme, K. L. Hamilton, H. M. Jones, A. C. Gerlach, L. Giltinan, G. D. Papworth, S. C. Watkins, N. A. Bradbury, and D. C. Devor, "Trafficking of the Ca²⁺-activated K⁺ channel, hK1, is dependent upon a C-terminal leucine zipper," *Journal of Biological Chemistry*, vol. 278, no. 10, pp. 8476-8486, 2003.
- [70] D. Tuteja, S. Rafizadeh, V. Timofeyev, S. Wang, Z. Zhang, N. Li, R. K. Mateo, A. Singapuri, J. N. Young, A. A. Knowlton, and N. Chiamvimonvat, "Cardiac small conductance Ca²⁺-activated K⁺ channel subunits form heteromultimers via the coiled-coil domains in the C termini of the channels," *Circulation research*, vol. 107, no. 7, pp. 851-859, 2010.
- [71] R. Wissmann, W. Bildl, H. Neumann, A. F. Rivard, N. Klöcker, D. Weitz, U. Schulte, J. P. Adelman, D. Bentrop, and B. Fakler, "A helical region in the C terminus of small-conductance Ca²⁺-activated K⁺ channels controls assembly with apo-calmodulin," *Journal of Biological Chemistry*, vol. 277, no. 6, pp. 4558-4564, 2002.
- [72] M. A. Schumacher, A. F. Rivard, H. P. Bächinger, and J. P. Adelman, "Structure of the gating domain of a Ca²⁺-activated K⁺ channel complexed with Ca²⁺/calmodulin," *Nature*, vol. 410, no. 6832, pp. 1120-1124, 2001.
- [73] D. B. Halling, S. A. Kenrick, A. F. Riggs, and R. W. Aldrich, "Calcium-dependent stoichiometries of the KCa²⁺. 2 (SK) intracellular domain/calmodulin complex in solution," *Journal of General Physiology*, vol. 143, no. 2, pp. 231-252, 2014.
- [74] H. Tidow, and P. Nissen, "Structural diversity of calmodulin binding to its target sites," *The FEBS journal*, vol. 280, no. 21, pp. 5551-5565, 2013.

- [75] J. E. Keen, R. Khawaled, D. L. Farrens, T. Neelands, A. Rivard, C. T. Bond, A. Janowsky, B. Fakler, J. P. Adelman, and J. Maylie, “Domains responsible for constitutive and Ca²⁺-dependent interactions between calmodulin and small conductance Ca²⁺-activated potassium channels,” *Journal of Neuroscience*, vol. 19, no. 20, pp. 8830-8838, 1999.
- [76] W. Li, D. B. Halling, A. W. Hall, and R. W. Aldrich, “EF hands at the N-lobe of calmodulin are required for both SK channel gating and stable SK–calmodulin interaction,” *Journal of General Physiology*, vol. 134, no. 4, pp. 281-293, 2009.
- [77] X. Tao, R. K. Hite, and R. MacKinnon, “Cryo-EM structure of the open high-conductance Ca²⁺-activated K⁺ channel,” *Nature*, vol. 541, no. 7635, pp. 46-51, 2017.
- [78] J. R. Whicher, and R. MacKinnon, “Structure of the voltage-gated K⁺ channel Eag1 reveals an alternative voltage sensing mechanism,” *Science*, vol. 353, no. 6300, pp. 664-669, 2016.
- [79] W. Wang, and R. MacKinnon, “Cryo-EM structure of the open human ether-à-go-go-related K⁺ channel hERG,” *Cell*, vol. 169, no. 3, pp. 422-430. e10, 2017.
- [80] R. K. Hite, and R. MacKinnon, “Structural Titration of Slo2.2, a Na(+)-Dependent K(+) Channel,” *Cell*, vol. 168, no. 3, pp. 390-399.e11, Jan 26, 2017.
- [81] C. H. Lee, and R. MacKinnon, “Structures of the Human HCN1 Hyperpolarization-Activated Channel,” *Cell*, vol. 168, no. 1-2, pp. 111-120.e11, Jan 12, 2017.
- [82] W. Li, and R. W. Aldrich, “Electrostatic influences of charged inner pore residues on the conductance and gating of small conductance Ca²⁺ activated K⁺ channels,” *Proceedings of the National Academy of Sciences*, vol. 108, no. 15, pp. 5946-5953, 2011.
- [83] X.-M. Xia, B. Fakler, A. Rivard, G. Wayman, T. Johnson-Pais, J. Keen, T. Ishii, B. Hirschberg, C. Bond, and S. Lutsenko, “Mechanism of calcium gating in small-conductance calcium-activated potassium channels,” *Nature*, vol. 395, no. 6701, pp. 503-507, 1998.
- [84] W. J. Joiner, L.-Y. Wang, M. D. Tang, and L. K. Kaczmarek, “hSK4, a member of a novel subfamily of calcium-activated potassium channels,”

- Proceedings of the National Academy of Sciences*, vol. 94, no. 20, pp. 11013-11018, 1997.
- [85] N. J. Logsdon, J. Kang, J. A. Togo, E. P. Christian, and J. Aiyar, “A novel gene, hKCa4, encodes the calcium-activated potassium channel in human T lymphocytes,” *Journal of Biological Chemistry*, vol. 272, no. 52, pp. 32723-32726, 1997.
- [86] M. Köhler, B. Hirschberg, C. Bond, J. M. Kinzie, N. Marrion, J. Maylie, and J. Adelman, “Small-conductance, calcium-activated potassium channels from mammalian brain,” *Science*, vol. 273, no. 5282, pp. 1709-1714, 1996.
- [87] M. Simoes, L. Garneau, H. Klein, U. Banderali, F. Hobeila, B. Roux, L. Parent, and R. Sauvé, “Cysteine mutagenesis and computer modeling of the S6 region of an intermediate conductance IKCa channel,” *The Journal of general physiology*, vol. 120, no. 1, pp. 99-116, 2002.
- [88] A. Bruening-Wright, M. A. Schumacher, J. P. Adelman, and J. Maylie, “Localization of the activation gate for small conductance Ca²⁺-activated K⁺ channels,” *Journal of Neuroscience*, vol. 22, no. 15, pp. 6499-6506, 2002.
- [89] A. Bruening-Wright, W.-S. Lee, J. P. Adelman, and J. Maylie, “Evidence for a deep pore activation gate in small conductance Ca²⁺-activated K⁺ channels,” *The Journal of general physiology*, vol. 130, no. 6, pp. 601-610, 2007.
- [90] L. Garneau, H. Klein, U. Banderali, A. Longprá-Lauzon, L. Parent, and R. Sauvé, “Hydrophobic interactions as key determinants to the KCa3. 1 channel closed configuration: An analysis of KCa3. 1 mutants constitutively active in zero Ca²⁺,” *Journal of Biological Chemistry*, vol. 284, no. 1, pp. 389-403, 2009.
- [91] K. Mruk, B. M. Farley, A. W. Ritacco, and W. R. Kobertz, “Calmodulation meta-analysis: predicting calmodulin binding via canonical motif clustering,” *Journal of General Physiology*, vol. 144, no. 1, pp. 105-114, 2014.
- [92] M. A. Schumacher, A. F. Rivard, H. P. Bächinger, and J. P. Adelman, “Structure of the gating domain of a Ca²⁺-activated K⁺ channel complexed with Ca²⁺/calmodulin,” *Nature*, vol. 410, no. 6832, pp. 1120-1124, 2001/04/01, 2001.
- [93] P. Morales, L. Garneau, H. Klein, M.-F. Lavoie, L. Parent, and R. Sauvé, “Contribution of the KCa3. 1 channel–calmodulin interactions to the

- regulation of the KCa_{3.1} gating process,” *Journal of General Physiology*, vol. 142, no. 1, pp. 37-60, 2013.
- [94] J. Albuissou, S. E. Murthy, M. Bandell, B. Coste, H. Louis-dit-Picard, J. Mathur, M. Fénéant-Thibault, G. Tertian, J.-P. de Jaureguiberry, P.-Y. Syfuss, S. Cahalan, L. Garçon, F. Toutain, P. Simon Rohrlich, J. Delaunay, V. Picard, X. Jeunemaitre, and A. Patapoutian, “Dehydrated hereditary stomatocytosis linked to gain-of-function mutations in mechanically activated PIEZO1 ion channels,” *Nature Communications*, vol. 4, no. 1, pp. 1884, 2013/05/21, 2013.
- [95] I. Andolfo, S. L. Alper, L. De Franceschi, C. Auriemma, R. Russo, L. De Falco, F. Vallefucio, M. R. Esposito, D. H. Vandorpe, B. E. Shmukler, R. Narayan, D. Montanaro, M. D’Armiento, A. Vetro, I. Limongelli, O. Zuffardi, B. E. Glader, S. L. Schrier, C. Brugnara, G. W. Stewart, J. Delaunay, and A. Iolascon, “Multiple clinical forms of dehydrated hereditary stomatocytosis arise from mutations in PIEZO1,” *Blood*, vol. 121, no. 19, pp. 3925-3935, 2013.
- [96] I. Andolfo, R. Russo, F. Manna, B. E. Shmukler, A. Gambale, G. Vitiello, G. De Rosa, C. Brugnara, S. L. Alper, L. M. Snyder, and A. Iolascon, “Novel Gárdos channel mutations linked to dehydrated hereditary stomatocytosis (xerocytosis),” *American Journal of Hematology*, vol. 90, no. 10, pp. 921-926, 2015.
- [97] C. Bae, R. Gnanasambandam, C. Nicolai, F. Sachs, and P. A. Gottlieb, “Xerocytosis is caused by mutations that alter the kinetics of the mechanosensitive channel PIEZO1,” *Proceedings of the National Academy of Sciences*, vol. 110, no. 12, pp. E1162, 2013.
- [98] E. Glogowska, E. R. Schneider, Y. Maksimova, V. P. Schulz, K. Lezon-Geyda, J. Wu, K. Radhakrishnan, S. B. Keel, D. Mahoney, A. M. Freidmann, R. A. Altura, E. O. Gracheva, S. N. Bagriantsev, T. A. Kalfa, and P. G. Gallagher, “Novel mechanisms of PIEZO1 dysfunction in hereditary xerocytosis,” *Blood*, vol. 130, no. 16, pp. 1845-1856, 2017.
- [99] R.-M. Raphael, S. Olivier, V. Henri, B. Catherine, and G. Hélène, “Senicapoc: a potent candidate for the treatment of a subset of hereditary xerocytosis caused by mutations in the Gárdos channel,” *Haematologica*, vol. 101, no. 11, pp. e431-e435, 11/01, 2016.

- [100] S. Ma, S. Cahalan, R. Lohia, G. LaMonte, W. Zeng, S. Murthy, E. Paytas, N. D. Grubaugh, R. Gamini, and L. Berry, “Common Piezo1 allele in African populations causes xerocytosis and attenuates Plasmodium infection,” *bioRxiv*, pp. 159830, 2017.
- [101] A. Rivera, D. H. Vandorpe, B. E. Shmukler, D. R. Gallagher, C. C. Fikry, F. A. Kuypers, C. Brugnara, L. M. Snyder, and S. L. Alper, “Erythrocytes from hereditary xerocytosis patients heterozygous for KCNN4 V282M exhibit increased spontaneous Gárdos channel-like activity inhibited by senicapoc,” *American journal of hematology*, vol. 92, no. 6, pp. E108-E110, 2017.
- [102] R. Rapetti-Mauss, C. Lacoste, V. Picard, C. Guitton, E. Lombard, M. Loosveld, V. Nivaggioni, N. Dasilva, D. Salgado, and J.-P. Desvignes, “A mutation in the Gárdos channel is associated with hereditary xerocytosis,” *Blood, The Journal of the American Society of Hematology*, vol. 126, no. 11, pp. 1273-1280, 2015.
- [103] I. Andolfo, R. Russo, A. Gambale, and A. Iolascon, “Hereditary stomatocytosis: An underdiagnosed condition,” *American Journal of Hematology*, vol. 93, no. 1, pp. 107-121, 2018.
- [104] I. Andolfo, R. Russo, B. E. Rosato, F. Manna, A. Gambale, C. Brugnara, and A. Iolascon, “Genotype-phenotype correlation and risk stratification in a cohort of 123 hereditary stomatocytosis patients,” *American journal of hematology*, vol. 93, no. 12, pp. 1509-1517, 2018.
- [105] A. Caulier, R. Rapetti-Mauss, H. Guizouarn, V. Picard, L. Garçon, and C. Badens, “Primary red cell hydration disorders: pathogenesis and diagnosis,” *International journal of laboratory hematology*, vol. 40, pp. 68-73, 2018.
- [106] R. Rapetti-Mauss, O. Soriani, H. Vinti, C. Badens, and H. Guizouarn, “Senicapoc: a potent candidate for the treatment of a subset of hereditary xerocytosis caused by mutations in the Gárdos channel,” *Haematologica*, vol. 101, no. 11, pp. e431, 2016.
- [107] C.-H. Lee, and R. MacKinnon, “Activation mechanism of a human SK-calmodulin channel complex elucidated by cryo-EM structures,” *Science*, vol. 360, no. 6388, pp. 508-513, 2018.
- [108] R. Kharrat, K. Mabrouk, M. Crest, H. Darbon, R. Oughideni, Martin-Eauclaire, Marie-France, G. Jacquet, M. El Ayeb, J. Van Rietschoten, and H. Rochat, “Chemical synthesis and characterization of maurotoxin, a short

- scorpion toxin with four disulfide bridges that acts on K⁺ channels,” *European journal of biochemistry*, vol. 242, no. 3, pp. 491-498, 1996.
- [109] H. Rauer, M. D. Lanigan, M. W. Pennington, J. Aiyar, S. Ghanshani, M. D. Cahalan, R. S. Norton, and K. G. Chandy, “Structure-guided transformation of charybdotoxin yields an analog that selectively targets Ca²⁺-activated over voltage-gated K⁺ channels,” *Journal of Biological Chemistry*, vol. 275, no. 2, pp. 1201-1208, 2000.
- [110] H. Wulff, A. Kolski-Andreaco, A. Sankaranarayanan, J.-M. Sabatier, and V. Shakkottai, “Modulators of small-and intermediate-conductance calcium-activated potassium channels and their therapeutic indications,” *Current medicinal chemistry*, vol. 14, no. 13, pp. 1437-1457, 2007.
- [111] S. Suzuki, N. Kurata, Y. Nishimura, H. Yasuhara, and T. Satoh, “Effects of imidazole antimycotics on the liver microsomal cytochrome P450 isoforms in rats: comparison of in vitro and in vivo studies,” *European journal of drug metabolism and pharmacokinetics*, vol. 25, no. 2, pp. 121-126, 2000.
- [112] G. Luo, M. Cunningham, S. Kim, T. Burn, J. Lin, M. Sinz, G. Hamilton, C. Rizzo, S. Jolley, and D. Gilbert, “CYP3A4 induction by drugs: correlation between a pregnane X receptor reporter gene assay and CYP3A4 expression in human hepatocytes,” *Drug Metabolism and Disposition*, vol. 30, no. 7, pp. 795-804, 2002.
- [113] H. Wulff, G. A. Gutman, M. D. Cahalan, and K. G. Chandy, “Delineation of the clotrimazole/TRAM-34 binding site on the intermediate conductance calcium-activated potassium channel, IKCa1,” *Journal of Biological Chemistry*, vol. 276, no. 34, pp. 32040-32045, 2001.
- [114] C. Brugnara, L. de Franceschi, and S. L. Alper, “Inhibition of Ca(2+)-dependent K⁺ transport and cell dehydration in sickle erythrocytes by clotrimazole and other imidazole derivatives,” *J Clin Invest*, vol. 92, no. 1, pp. 520-6, Jul, 1993.
- [115] R. Kharrat, K. Mabrouk, M. Crest, H. Darbon, R. Oughideni, M. F. Martin-Eauclaire, G. Jacquet, M. el Ayeb, J. Van Rietschoten, H. Rochat, and J. M. Sabatier, “Chemical synthesis and characterization of maurotoxin, a short scorpion toxin with four disulfide bridges that acts on K⁺ channels,” *Eur J Biochem*, vol. 242, no. 3, pp. 491-8, Dec 15, 1996.

- [116] H. Wulff, A. Kolski-Andreaco, A. Sankaranarayanan, J. M. Sabatier, and V. Shakkottai, "Modulators of small- and intermediate-conductance calcium-activated potassium channels and their therapeutic indications," *Curr Med Chem*, vol. 14, no. 13, pp. 1437-57, 2007.
- [117] H. Wulff, M. J. Miller, W. Hansel, S. Grissmer, M. D. Cahalan, and K. G. Chandy, "Design of a potent and selective inhibitor of the intermediate-conductance Ca²⁺-activated K⁺ channel, IKCa1: a potential immunosuppressant," *Proc Natl Acad Sci U S A*, vol. 97, no. 14, pp. 8151-6, Jul 5, 2000.
- [118] H. Wulff, and N. A. Castle, "Therapeutic potential of KCa3. 1 blockers: recent advances and promising trends," *Expert review of clinical pharmacology*, vol. 3, no. 3, pp. 385-396, 2010.
- [119] A. Gaulton, A. Hersey, M. Nowotka, A. P. Bento, J. Chambers, D. Mendez, P. Mutowo, F. Atkinson, L. J. Bellis, E. Cibrián-Uhalte, M. Davies, N. Dedman, A. Karlsson, M. P. Magariños, J. P. Overington, G. Papadatos, I. Smit, and A. R. Leach, "The ChEMBL database in 2017," *Nucleic Acids Res*, vol. 45, no. D1, pp. D945-d954, Jan 4, 2017.
- [120] P. E. Gil, W. Murray, and M. H. Wright, *Practical Optimization*: ACADEMIC PRESS, INC, 1981.
- [121] C. C. G. Inc, "Molecular operating environment (MOE)," Chemical Computing Group Inc. 1010 Sherbooke St. West, Suite# 910, Montreal ..., 2016.
- [122] H. M. Berman, J. Westbrook, Z. Feng, G. Gilliland, T. N. Bhat, H. Weissig, I. N. Shindyalov, and P. E. Bourne, "The Protein Data Bank," *Nucleic Acids Research*, vol. 28, no. 1, pp. 235-242, 2000.
- [123] "UniProt: the universal protein knowledgebase in 2021," *Nucleic Acids Research*, vol. 49, no. D1, pp. D480-D489, 2021.
- [124] C. Notredame, D. G. Higgins, and J. Heringa, "T-Coffee: A novel method for fast and accurate multiple sequence alignment," *Journal of molecular biology*, vol. 302, no. 1, pp. 205-217, 2000.
- [125] B. Webb, and A. Sali, "Comparative protein structure modeling using MODELLER," *Current protocols in bioinformatics*, vol. 54, no. 1, pp. 5.6. 1-5.6. 37, 2016.

- [126] C. Colovos, and T. O. Yeates, "Verification of protein structures: patterns of nonbonded atomic interactions," *Protein science*, vol. 2, no. 9, pp. 1511-1519, 1993.
- [127] J. W. Gooch, "Ramachandran Plot," *Encyclopedic Dictionary of Polymers*, J. W. Gooch, ed., pp. 919-919, New York, NY: Springer New York, 2011.
- [128] S. Release, "Maestro, Schrödinger, LLC, New York, NY, 2020," *Schrödinger Release*, vol. 1, 2020.
- [129] M. L. Verdonk, G. Chessari, J. C. Cole, M. J. Hartshorn, C. W. Murray, J. W. M. Nissink, R. D. Taylor, and R. Taylor, "Modeling water molecules in protein– ligand docking using GOLD," *Journal of medicinal chemistry*, vol. 48, no. 20, pp. 6504-6515, 2005.
- [130] Á. Durán Alcaide, *Development of high-performance algorithms for a new generation of versatile molecular descriptors. The Pentacle software*: Universitat Pompeu Fabra, 2010.
- [131] S. Mukhtar, Y. S. Kiani, and I. Jabeen, "Molecular docking simulations and GRID-independent molecular descriptor (GRIND) analysis to probe stereoselective interactions of CYP3A4 inhibitors," *Medicinal Chemistry Research*, vol. 26, no. 10, pp. 2322-2335, 2017.
- [132] A. Duran, G. C. Martínez, and M. Pastor, "Development and validation of AMANDA, a new algorithm for selecting highly relevant regions in molecular interaction fields," *Journal of chemical information and modeling*, vol. 48, no. 9, pp. 1813-1823, 2008.
- [133] Á. Durán, and M. Pastor, "An advanced tool for computing and handling GRid-INdependent," *Descriptors. User Manual Version*, vol. 1, 2011.
- [134] J. F. Hoffman, W. Joiner, K. Nehrke, O. Potapova, K. Foye, and A. Wickrema, "The hSK4 (KCNN4) isoform is the Ca²⁺-activated K⁺ channel (Gárdos channel) in human red blood cells," *Proceedings of the National Academy of Sciences*, vol. 100, no. 12, pp. 7366-7371, 2003.
- [135] M. Mariani, W. Barcellini, C. Vercellati, A. P. Marcello, E. Fermo, P. Pedotti, C. Boschetti, and A. Zanella, "Clinical and hematologic features of 300 patients affected by hereditary spherocytosis grouped according to the type of the membrane protein defect," *haematologica*, vol. 93, no. 9, pp. 1310-1317, 2008.

- [136] M. Salomao, K. Chen, J. Villalobos, N. Mohandas, X. An, and J. A. Chasis, “Hereditary spherocytosis and hereditary elliptocytosis: aberrant protein sorting during erythroblast enucleation,” *Blood, The Journal of the American Society of Hematology*, vol. 116, no. 2, pp. 267-269, 2010.

Appendix

Dataset of Gárdos Channel

Molecule ChEMBL ID	Molecular Formula	SMILES	IC50 (nM)
Gárdos_1	C20H15F2NO	<chem>NC(=O)C(c1ccccc1)(c1ccc(F)cc1)c1ccc(F)cc1</chem>	12
Gárdos_2	C20H15F2NO	<chem>NC(=O)C(c1ccccc1)(c1ccccc1F)c1ccccc1F</chem>	30
Gárdos_3	C20H19N	<chem>CNC(c1ccccc1)(c1ccccc1)c1ccccc1</chem>	550
Gárdos_4	C14H9F4NO4S2	<chem>O=C1CS(=O)(=O)c2sccc2N1Cc1ccc(F)c(OC(F)(F)F)c1</chem>	48
Gárdos_5	C21H21N	<chem>CCNC(c1ccccc1)(c1ccccc1)c1ccccc1</chem>	1750
Gárdos_6	C20H15F2NO	<chem>NC(=O)C(c1ccccc1)(c1ccccc1)c1ccc(F)cc1F</chem>	34
Gárdos_7	C20H14F3NO	<chem>NC(=O)C(c1ccc(F)cc1)(c1ccccc1F)c1ccc(cc1)F</chem>	15
Gárdos_8	C19H17N	<chem>NC(c1ccccc1)(c1ccccc1)c1ccccc1</chem>	70
Gárdos_9	C15H11F3N2O2S	<chem>O=C1CSc2ccnc2N1Cc1ccc(OC(F)(F)F)c1</chem>	52
Gárdos_10	C21H18O5	<chem>O=c1ccc2c(OCCCCO)c3ccccc3)c3ccoc3cc2o1</chem>	10000
Gárdos_11	C25H20N3OP	<chem>N#Cc1ccc(-c2ncccc2CNP(=O)(c2ccccc2)c2ccccc2)c1</chem>	7700
Gárdos_12	C22H17ClN2	<chem>Clc1ccccc1C(c1ccccc1)(c1ccccc1)n1cccn1</chem>	20
Gárdos_13	C21H21N	<chem>CN(C)C(c1ccccc1)(c1ccccc1)c1ccccc1</chem>	3150
Gárdos_14	C20H16FNO	<chem>NC(=O)C(c1ccccc1)(c1ccccc1)c1ccc(F)cc1</chem>	40
Gárdos_15	C23H20N3OP	<chem>O=P(NCc1ccnc1-c1ccnc1)(c1ccccc1)c1ccccc1</chem>	33000
Gárdos_16	C22H21N2OP	<chem>CCCN(c1cccc(C#N)c1)P(=O)(c1ccccc1)c1ccccc1</chem>	2700
Gárdos_17	C20H16FNO	<chem>NC(=O)C(c1ccccc1)(c1ccccc1)c1ccccc1F</chem>	15
Gárdos_18	C22H17ClN2	<chem>Clc1ccccc1C(c1ccccc1)(c1ccccc1)n1ccnc1</chem>	70
Gárdos_19	C24H19Cl2N2OP	<chem>O=P(NCc1ccnc1-c1cc(Cl)cc(Cl)c1)(c1ccccc1)c1ccccc1</chem>	13000
Gárdos_20	C24H20ClN2OP	<chem>O=P(NCc1ccnc1-c1cccc(Cl)c1)(c1ccccc1)c1ccccc1</chem>	4900
Gárdos_21	C21H18O2	<chem>COC(=O)C(c1ccccc1)(c1ccccc1)c1ccccc1</chem>	330
Gárdos_22	C22H19NO	<chem>c1ccc(C(C2=NCCO2)(c2ccccc2)c2ccccc2)cc1</chem>	4300

Gárdos_23	C15H10F4N2O4S	O=C1CS(=O)(=O)c2cccnc2N1Cc1ccc(F)c(OC(F)(F)F)c1	49
Gárdos_24	C15H11F4NO4S2	CC(c1ccc(F)c(OC(F)(F)F)c1)N1C(=O)CS(=O)(=O)c2ccsc21	39
Gárdos_25	C16H13F3N2OS	CC(c1cccc(C(F)(F)F)c1)N1C(=O)CSc2ccnc21	41
Gárdos_26	C20H15F2NO	NC(=O)C(c1ccccc1)(c1ccccc1)c1ccc(F)c(F)c1	14
Gárdos_27	C21H14ClNO2	O=C1CN(C(=O)c2cccc(Cl)c2)c2ccccc2-c2ccccc21	1300
Gárdos_28	C20H14ClNO3S	O=C1CN(S(=O)(=O)c2ccc(Cl)cc2)c2ccc cc2-c2ccccc21	1400
Gárdos_29	C20H14F3NO	NC(=O)C(c1ccc(F)cc1)(c1ccccc(F)c1)c1ccc(F)c1	15
Gárdos_30	C20H14F3NO	NC(=O)C(c1ccc(F)cc1)(c1ccc(F)cc1)c1ccc(F)cc1	14
Gárdos_31	C16H12ClF3N2O2S	O=C1CSc2ccc(CO)nc2N1Cc1ccc(Cl)c(C(F)(F)F)c1	66
Gárdos_32	C21H17NO3S	Cc1ccc(S(=O)(=O)N2CC(=O)c3ccccc3-c3ccccc32)cc1	2100
Gárdos_33	C16H14F4N2O4S2	CC(C)c1nc2c(s1)S(=O)(=O)CC(=O)N2Cc1ccc(F)c(OC(F)(F)F)c1	96
Gárdos_34	C24H20NOP	O=P(c1ccccc1)(c1ccccc1)C(c1ccccc1)c1ccnc1	500
Gárdos_35	C20H21N2OP	CCCN(c1ccnc1)P(=O)(c1ccccc1)c1ccccc1	14000
Gárdos_36	C22H17NO2	Cc1ccc(C(=O)N2CC(=O)c3ccccc3-c3ccccc32)cc1	16000
Gárdos_37	C20H14F3NO	NC(=O)C(c1ccc(F)cc1)(c1ccc(F)cc1)c1ccc(F)c1	10
Gárdos_38	C19H16ClN	NC(c1ccccc1)(c1ccccc1)c1ccccc1Cl	20
Gárdos_39	C20H15F2NO	NC(=O)C(c1ccccc1)(c1ccc(F)c1)c1ccccc(F)c1	30
Gárdos_40	C23H25N2OP	O=P(c1ccccc1)(c1ccccc1)C(c1ccnc1)N1CCCC1	1800
Gárdos_41	C18H13NO3S2	O=C1CN(S(=O)(=O)c2cccs2)c2ccccc2-c2ccccc21	2400
Gárdos_42	C20H14F3NO	NC(=O)C(c1ccc(F)c1)(c1ccccc(F)c1)c1ccc(F)c1	13
Gárdos_43	C20H15F2NO	NC(=O)C(c1ccccc1)(c1ccc(F)cc1)c1ccccc1F	9
Gárdos_44	C21H17FN3OP	O=P(Nc1cc(F)ccc1-n1ccn1)(c1ccccc1)c1ccccc1	7800
Gárdos_45	C21H20N3OP	N#CCCN(c1ccnc1)P(=O)(c1ccccc1)c1ccccc1	31000
Gárdos_46	C21H23N2OP	CCCN(c1ccnc1)P(=O)(c1ccccc1)c1ccccc1	14000
Gárdos_47	C18H19N2O2P	CCCN(c1ccn1)P(=O)(c1ccccc1)c1ccccc1	18000

Gárdos_48	C23H20N3OP	O=P(c1ccccc1)(c1ccccc1)N(Cc1cccn1)c1cccn1	10000
Gárdos_49	C20H14F3NO	NC(=O)C(c1ccc(F)cc1)(c1ccc(F)cc1)c1ccc(F)c1	17
Gárdos_50	C14H10F4N2O 2S2	CC(c1ccc(F)c(OC(F)(F)F)c1)N1C(=O)CSc2ncsc21	60
Gárdos_51	C23H19N2OP	O=P(c1ccccc1)(c1ccccc1)C(c1cccn1)c1cccn1	1000